Copyright Warning & Restrictions

The copyright law of the United States (Title 17, United States Code) governs the making of photocopies or other reproductions of copyrighted material.

Under certain conditions specified in the law, libraries and archives are authorized to furnish a photocopy or other reproduction. One of these specified conditions is that the photocopy or reproduction is not to be "used for any purpose other than private study, scholarship, or research." If a, user makes a request for, or later uses, a photocopy or reproduction for purposes in excess of "fair use" that user may be liable for copyright infringement,

This institution reserves the right to refuse to accept a copying order if, in its judgment, fulfillment of the order would involve violation of copyright law.

Please Note: The author retains the copyright while the New Jersey Institute of Technology reserves the right to distribute this thesis or dissertation

Printing note: If you do not wish to print this page, then select "Pages from: first page # to: last page #" on the print dialog screen

ABSTRACT

DRIVER BEHAVIOR CLASSIFICATION AND LATERAL CONTROL FOR AUTOMOBILE SAFETY SYSTEMS

by
Jing Yang

Advanced driver assistance systems (ADAS) have been developed to help drivers maintain stability, improve road safety, and avoid potential collision. The data acquisition equipment that can be used to measure the state and parameter information of the vehicle may not be available for a standard passenger car due to economical and technical limitations. This work focuses on developing three technologies (longitudinal tire force estimation, driver behavior classification and lateral control) using low-cost sensors that can be utilized in ADAS.

For the longitudinal tire force estimation, a low cost 1Hz positioning global system (GPS) and a steering angle sensor are used as the vehicle data acquisition equipment. A nonlinear extended two-wheel vehicle dynamic model is employed. The sideslip angle and the yaw rate are estimated by discrete Kalman Filter. A time independent piecewise optimization scheme is proposed to provide time-continuous estimates of longitude tire force, which can be transferred to the throttle/brake pedal position. The proposed method can be validated by the estimation results.

Driver behavior classification systems can detect unsafe driver behavior and avoid potentially dangerous situations. To realize this strategy, a machine learning classification method, Gaussian Mixture model (GMM), is applied to classify driver behavior. In this application, a low cost 1Hz GPS receiver is considered as the vehicle data acquisition

equipment instead of other more costly sensors (such as steering angle sensor, throttle/brake position sensor, and etc.). Since the driving information is limited, the nonlinear extended two-wheel vehicle dynamic model is adopted to reconstruct the driver behavior. Firstly, the sideslip angle and the yaw rate are calculated since they are not available from the GPS measurements. Secondly, a piecewise optimization scheme is proposed to reproduce the steering angle and the longitudinal force. Finally, a GMM classifier is trained to identify abnormal driver behavior. The simulation results demonstrated that the proposed scenario can detect the unsafe driver behavior effectively.

The lateral control system developed in this study is a look-down reference system which uses a magnetic sensor at the front bumper to measure the front lateral displacement and a GPS to measure the vehicle's heading orientation. Firstly, the steering angles can be estimated by using the data provided by the front magnetic sensor and GPS. The estimation algorithm is an observer for a new extended single-track model, in which the steering angle and its derivative are viewed as two state variables. Secondly, the road curvature is determined based on the linear relationship with respect to the steering angle. Thirdly, an accurate and real-time estimation of the vehicle's lateral displacements can be accomplished according to a state observer. Finally, the closed loop controller is used as a compensator for automated steering. The proposed estimation and control algorithms are validated by simulation results. The results showed that this lateral steering control system achieved a good and robust performance for vehicles following or tracking a reference path.

DRIVER BEHAVIOR CLASSIFICATION AND LATERAL CONTROL FOR AUTOMOBILE SAFETY SYSTEMS

by
Jing Yang

A Dissertation
Submitted to the Faculty of
New Jersey Institute of Technology
in Partial Fulfillment of the Requirements for the Degree of
Doctor of Philosophy in Electrical Engineering

Department of Electrical and Computer Engineering

May 2012

APPROVAL PAGE

DRIVER BEHAVIOR CLASSIFICATION AND LATERAL CONTROL FOR AUTOMOBILE SAFETY SYSTEMS

Jing Yang

Dr. Edwin Hou, Dissertation Co-Advisor Associate Professor of Electrical and Computer Engineering, NJIT	Date
Dr. Mengchu Zhou, Dissertation Co-Advisor Professor of Electrical and Computer Engineering, NJIT	Date
Dr. Nirwan Ansari, Committee Member Professor of Electrical and Computer Engineering, NJIT	Date
Dr. Richard A. Haddad, Committee Member Professor of Electrical and Computer Engineering, NJIT	Date
Dr. Janice R. Daniel, Committee Member Associate Professor of Civil and Environmental Engineering, NJIT	Date

BIOGRAPHICAL SKETCH

Author: Jing Yang

Degree: Doctor of Philosophy

Date: May 2012

Undergraduate and Graduate Education:

- Doctor of Philosophy in Electrical Engineering,
  New Jersey Institute of Technology, Newark, NJ, May, 2012

- Master of Science in Automation,
  Tsinghua University, Beijing, P. R. China, 2006

- Bachelor of Science in Electrical and Computer Engineering,
  East China University of Science and Technology, Shanghai, P. R. China, 2003

Major: Electrical Engineering

Publications:

J. Yang, E. Hou and M. C. Zhou,
"Front Sensor and GPS-based Lateral Control of Automated Vehicles,"
Accepted for publication, IEEE Transactions on Intelligent Transportation Systems, 2012.

J. Yang, E. Hou,
"Kalman Filter and GPS-based Longitudinal Tire Force Estimation,"
International Journal of Intelligent Control and Systems, Vol. 16, No. 3, pp. 199-206, Sept. 2011.

J. Yang, T. N. Chang, E. Hou, and N. Ansari
"Longitude Force Estimation for Bandwidth Conservative Communication and Vehicular Monitoring," *in Proc. of the IEEE Conference on Automation Science and Engineering,* Toronto, Canada, pp.668- 673, 21-24 Aug. 2010.

J. Yang, T. N. Chang, and E. Hou,
"Lateral Control for Vehicles' Automatic Steering with Front Sensor and GPS,"

in Proc. of the International Conference on Control Automation and Systems, Seoul, Korea, pp. 928-932, Oct. 2010.

J. Yang, T. N. Chang, E. Hou,
"Driver Distraction Detection for Vehicular Monitoring,"
*in Proc. of the 36th Annual Conference on IEEE Industrial Electronics Societ*y, Glendale, AZ, USA, pp. 108-113, Nov. 2010.

J. Yang, E. Hou,
"Classification of Driving Behavior using a Gaussian Mixture Model Classifier,"
Under second round review, Proceedings of the Institution of Mechanical Engineers, Part D, Journal of Automobile Engineering.

J. Yang, E. Hou, and M. C. Zhou,
"Driver Distraction Detection System: A Survey,"
Submitted to the IEEE Transactions on Intelligent Transportation Systems.

Dedicated to my beloved parents, husband and daughter

ACKNOWLEDGMENT

This dissertation would not have been possible without support, motivation and encouragement of Dr. Timothy N. Chang. I learned many things from him and I will miss him deeply. I especially would like to thank my advisor Dr. Edwin Hou for his guidance and patience during my study. In particular, I want to thank my co-advisor Dr. Mengchu Zhou for his supervision and those kind discussions with him, helping me clear my mind.

Special thanks are given to Dr. Nirwan Ansari, Dr. Richard A. Haddad, and Dr. Janice R Daniel, for actively participating in my committee.

I would like to acknowledge the financial support provided by NJIT and National Science Foundation Grant ECS-0823960.

Also, I want to thank all my colleagues, Biao Cheng, Lan Yu, and Wei Shi, in the Real-time Control Laboratory for their help over the years.

Finally, I would like to thank my husband and parents for supporting and encouraging me in everything I do.

TABLE OF CONTENTS

TABLE OF CONTENTS
(Continued)

Chapter **Page**

TABLE OF CONTENTS
(Continued)

Chapter **Page**

LIST OF TABLES

LIST OF FIGURES

LIST OF FIGURES
(Continued)

CHAPTER 1

INTRODUCTION

1.1 Objective

Automobiles are ubiquitous in modern societies and they are indispensable in our daily life. Consequently, one of the most important aspects in vehicle design by the automobile industry is improving car safety. In the past few decades, automobile safety systems have been developed to reduce, prevent or avoid driver error and therefore, enhanced the safety of vehicles. These active vehicle safety systems are called advanced driver assistance systems (ADAS).

Most applications in driver safety systems adopt multimodal sensors as the data acquisition equipment, which may be costly and inconvenient to install for general uses. This study aims at designing driver safety systems with low cost data acquisition equipment to measure vehicle states (sideslip angle, yaw rate, vehicle velocity, heading angle, and etc.), driving behavior information (steering angle and throttle/brake pedal position), and environment data (road condition, weather condition, and other environment conditions).

The objective of this dissertation is concentrated on developments of advanced driver assistance systems in the following applications:

- Longitudinal tire force estimation
- Driver behavior classification
- Lateral steering control

1.2 Background Information

Driving safety is an important issue since driving is a common activity for many people in everyday life. Based on the traffic statistics and analysis available from the US Department of Transportation, Federal Highway Administration, Office of Highway Information, during the thirty-eight years from 1970 to 2008, the number of licensed drivers in the U.S. increased 86.82%, from about 111.5.0 million to 208.3 million. 57% of the driving-age population was licensed to drive a motor vehicle in 1950. That number has increased to 87% of the driving-age population in 2008. Americans drove over 3 trillion miles in 2007. From 1980 to 2005, the average annual vehicle miles traveled (VMT) per licensed driver have increased 42.1%, from 10,043 miles to 14,273 miles [1]. Despite the safety improvements in road and vehicle design, the total number of fatal crashes still increased. Motor vehicle-related fatalities increased from 33,186 in 1950 to 43,510 in 2005, while the fatality rate per 100 million vehicle miles of travel (VMT) increased from 1.46 to 7.24 [2-3]. The 2005 mortality data from the National Center for Health Statistics (NCHS) shows the 10 leading causes of death by age group. According to the statistics, motor vehicle traffic crashes were the leading cause of death for every group from age 3 to 34. The motor vehicle traffic crashes ranked third overall in terms of the year of lost, behind only to malignant neoplasms and diseases of heart [4]. The increasing number of fatalities demonstrates that driving safety represents a persistent and important issue. Developing advanced driver assistance systems to reduce crash involvements would benefit millions of people across the world.

Motor-vehicle crashes can be attributed to multiple causes: driver error, road design, vehicle design and maintenance. A 1985 study, using British and American crash

reports as data, found that 57% of crashes were only due to driver factors, 27% to combined roadway and driver factors, 6% to combined vehicle and driver factors, 3% solely to roadway factors, 3% to combined roadway, driver, and vehicle factors, 2% solely to vehicle factors and 1% to combined roadway and vehicle factors [5]. It is obvious that driver error represents a dominant cause of crashes. For example, driver error includes speeding and driver impairment. On the one hand, the official British road casualty statistics show that "traveling too fast for conditions" was a contributory factor in 11% of all casualty-crashes [6]. On the other hand, most of the crashes are due to the impairments of the driver's attention. There are six major categories of attention impairments: alcohol, fatigue, aging, physical impairment, drug use and distraction. Alcohol contributes to approximately 40% of fatalities in US highway [7] and 33.8% of motor vehicle deaths in Canada [8]. Accidents due to fatigues often involve young drivers and truck drivers because they tend to adopt risky strategies such as driving at night and/or lack good-quality sleep [7]. Old age drivers have low reaction speed and narrow field of attention [9-10]. Drivers who have poor eyesight or other physical impairment may cause fatal crashes if the vehicle modifications are not appropriate or they are not qualified to drive. When a person drives after using drugs (including some prescription drugs, over the counter drugs, and illegal drugs), the potential drug impairments may create a hazardous situation to themselves and other road uses, like pedestrians or cyclists. The last impairment is distraction, which has become increasingly important with the introduction of in-vehicle technologies (e.g., navigation systems, mobile phones, smart phones, and internet). Driver distraction diverts the driver's attention away from the activities critical for safe driving towards a competing activity [11]. It contributes to 13-50% of all crashes, resulting in as

many as 10,000 fatalities and $40 billion in damages each year [7]. These statistics have motivated research in the development of advanced driver assistance systems (ADAS).

Many ADAS have been investigated in the last decade to reduce driver error and avoid potentially dangerous situations. The advanced driver assistance system will enhance car safety and more generally road safety. This research is concentrated on three applications that are the key technologies used to design advanced driver assistance systems: longitudinal tire force estimation, driver behavior classification, and lateral control system. Until now, most of the research and development efforts have been dedicated to the development of these three individual technologies. For many approaches, the vehicle and driving related information, such as steering angle, throttle/brake pedal position, vehicle states (vehicle speed, acceleration, yaw angle, yaw rate, sideslip angle, and etc.), distance between the ahead/flowing vehicle, are directly obtained from the controller area network bus (CAN-bus) or multimodal sensors (GPS, steering angle sensor, throttle/brake pedal position sensors, cameras, microphones, etc.). These data acquisition equipment and methods are cost prohibitive and inconvenient to use for the general drivers. This research focuses in designing three strategies: estimating longitudinal tire force, detecting abnormal driver behavior, and automatic lateral control, by using as little measurement devices as possible, and will therefore reduces the design cost for advanced driver assistance systems.

1.3 Dissertation Contributions

The key contributions of this dissertation are:

1) For the vehicle state estimation, a task to estimate the longitudinal tire force which can be transferred to the corresponding throttle/brake positions has been addressed.

A low cost 1Hz GPS receiver and a steering angle sensor are used as the vehicle data acquisition equipment. A longitude force estimation scenario is developed for the nonlinear extended two-wheel vehicle dynamic model using only the GPS information.

2) For the driver behavior classification scenario, a Gaussian Mixture model (GMM) classifier has been developed to assign the driving behavior into normal or abnormal category. The vehicle states and the driver inputs are estimated according to the GPS data and the vehicle dynamic models. GMM is used to capture the sequence of driving characteristics based on the reconstructed driver's inputs. This application can enhance the safety of the drivers by warning drivers in potentially dangerous traffic situations.

3) For vehicle lateral steering control, a GPS and front sensor based approach is adopted to estimate in real time the necessary states and model parameters (the steering angle, road curvature, and lateral displacements). The control strategy used is a look-down reference system which uses a sensor at the front bumper to measure the lateral displacement and a GPS to measure the heading orientation. An accurate and real-time estimation of the lateral displacements with respect to the road can be accomplished in such a control system. The simulation results show that the system provides a good and robust performance for path tracking.

1.4 Dissertation Organization

The rest of this dissertation is organized as follows: Chapter 2 presents the currently available technology and offers a review of the relevant literature. It begins with introduction of the advanced driver assistance system. Then, data acquisition equipment used in driver safety systems is investigated, followed by a discussion on the vehicle states estimation and longitudinal tire force estimation. The concepts of driver behavior

classification approaches are also presented. Finally, the current lateral control systems are discussed. Chapter 3 introduces two types of vehicle dynamics used in this thesis: single-track linear model and two-wheel extended nonlinear model. Chapter 4 is dedicated to the proposed a novel strategy to estimate longitudinal tire force for two-wheel extended vehicle model. The state estimator is studied. In order to estimate the longitudinal tire force, an optimizer is then developed. Chapter 5 discusses a scenario to detect the abnormal driver behavior. The driver behavior is reconstructed and a Gaussian mixture model classifier is used to determine whether the driver behavior is normal or abnormal. A novel lateral steering control system with a GPS and a front sensor is presented in Chapter 6. The entire system is a look-down system which has three parts: a road curvature and steering angle estimator, a lateral states observer, and a feedback controller. Chapter 7 concludes this dissertation.

CHAPTER 2

LITERATURE REVIEW

2.1 Advanced Driver Assistance System

In the past few decades, advanced automobile safety systems have been studied and developed mostly in research laboratories. Only until recently, automobile manufacturers are beginning to deploy them in the production of consumer vehicles. Automobile safety systems can be grouped into two categories: Passive safety systems and Active safety system.

Passive safety systems are only deployed or effective in response to an automobile crash. These systems protect drivers and passengers from injuries or reduce severity of injuries during the collision. Passive systems include seat belts, air bags, headrests, and the passenger-safety cage. For example, air bags are now mandatory in every new automobile sold in the United States. Vehicle crashworthiness is another regulated passive system. The regulation of crashworthiness began in the late 1960s and today all vehicles in the U.S. are required to pass mandated crashworthiness tests before they are sold to the public.

Advanced Driver Assistance Systems (ADAS) are active safety systems that can reduce the possibility of crashes. They aim at providing assistance to the driver by informing them about the condition of the car, the condition of the road, any potential hazards, or by providing active assistance to the driver. An ADAS may include many types of practical systems, for example, lateral control systems, longitudinal control systems, automated highway system (AHS), driver distraction detection system, reversing or parking aids, vision enhancements systems, and intelligent speed adaptation, in-vehicle

navigation system, antilock brake system, electronic stability program, collision avoidance system, intelligent cruise control, lane departure warning system, lane change assistance, automatic parking, intelligent speed adaptation, night vision, adaptive light control, pedestrian protection system, traffic sign recognition, blind spot detection, driver drowsiness detection, vehicular communication system, hill descent control, electrical vehicle warning sounds used in hybrids and plug-in electric vehicles [12]. An overview of longitudinal tire force estimation, driver behavior classification system and lateral control system, which is the focuses of this study, is presented in the following sections.

2.2 Data Acquisition Equipment

An ADAS needs to measure or estimate vehicle and driving related information and process them to automatically control the vehicle or provide feedback to the driver. These data include steering angle, throttle/brake pedal position, vehicle states (vehicle speed, acceleration, yaw angle, yaw rate, sideslip angle, and etc.), distance between the ahead/flowing vehicles, and lateral displacement. The information can be obtained from multimodal data acquisition sensors and equipment installed in the vehicle. The commonly utilized data acquisition devices in ADAS include:

- Controller area network bus (CAN-bus)

CAN-bus is a vehicle bus standard designed to allow microcontrollers and devices to communicate with each other. The CAN-bus is a serial, asynchronous, multi-master communications protocol suited for networking a vehicle's electronic control systems, sensors, and actuators. The CAN-bus signal contains real-time vehicle information in the form of messages integrating many modules. Usually, the open connector to the CAN-bus is the On-Board Diagnostics (OBD-II) port. The driving parameters provided by the

CAN-bus usually include Revolutions per minute (RPM), Acceleration pedal position, Wheel speeds, Steering angle, Lateral acceleration and yaw rate. Different vehicle models may provide all or part of the above data. One of the limitations of the CAN-bus signals is that they are not available for every vehicle models. Besides, the CAN-bus signals are coded with standards that differ from one manufacture to another. Thus, the database used to decode the CAN-bus signal may not be available to the general public or the cost for the database and data acquisition software maybe prohibitive.

- Global Position System (GPS)

A GPS is used to measure the position of the vehicle, its heading orientation, and even its vehicle velocity. Currently, a low-cost vehicle GPS has an updating rate of 1Hz or 5Hz. In research projects conducted by various vehicle research programs (such as DARPA Grand challenge, California PATH, Department of Transportation, and so on), more accurate GPS (for example, absolute GPS, differential GPS, or GPS with a higher updating rate) were employed. In order to obtain the rate up to 100 Hz, a GPS/INS is usually adopted, where INS stands for Inertial Navigation System. It refers to the use of GPS satellite signals to correct or calibrate a solution from an INS. INS usually can continuously provide accurate measurements of a vehicle's position, orientation, or velocity.

- Steering angle sensor

The overall steering wheel angle is measured by the steering angle sensor which is mounted on the steering shaft.

- Throttle/brake pedal position sensors

Throttle pedal position sensor and brake pedal position sensor are used to measure the positions of the acceleration and brake pedal respectively.

- Yaw rate sensor

A yaw rate sensor is a gyroscopic device that measures a vehicle's angular velocity around its vertical axis.

- Magnetic sensor

A magnetic sensor is a distance sensor, which can be used to measure the lateral displacement or longitudinal distance between two vehicles.

- Cameras

Video cameras can be used to record the driver's eye, head movements, face features, vehicle's motions or road condition.

- Microphones

Microphones can be used to record a driver's speech.

- Body sensors

Body sensors can provide the information about a driver's body movements, e.g., hand and neck movements.

- faceLAB

faceLAB is an eye and facial tracking system developed by Seeing Machines, Inc. [95]. It consists of a separate computer, Sony stereo cameras and loud-speakers. The computer is used for image processing. Cameras are positioned to the left and right of the screen above the dashboard for image capturing. It can capture the data on eye movement, head position and rotation, eyelid aperture, lip and eyebrow.

2.3 Vehicle States Estimation

Knowledge of the vehicle variables is essential for advanced driver assistance systems. However, some of the fundamental variables (such as sideslip angle, vehicle velocity, yaw angle, yaw rate) are not measurable in a standard car due to both technical and economical reasons. Consequently, these variables must be observed or estimated. Among those fundamental variables, the sideslip angle and the yaw rate are of most critical.

The vehicle sideslip angle can be calculated if the orientation (attitude) and velocity of the vehicle are known because the sideslip angle is the difference between the yaw angle and the direction of the velocity. For most cases when the orientation (attitude) and velocity are not available, a number of methods have been proposed to estimate the sideslip angle. Existing common methods can be based on dynamic handling models [21-22], estimators that are designed according to the kinematic relationships [23], the combined measurements of the yaw rate gyro and lateral accelerometer [24-25]. The sideslip angle can be also estimated by the integration of the yaw rate and the lateral acceleration because the derivative of the sideslip angle can be expressed in terms of these measurements [26-27].

2.4 Tire Force Estimation

The tire force determines the vehicle's motion in both lateral and longitudinal directions. Figure 2.1 illustrates the wheel dynamic variables [13] which can be used to model the tire force. Based on the tire model, tire force can be directly calculated by the wheel cornering stiffness and sideslip angle. The wheel cornering stiffness is a parameter closely related to the tire-road friction. Large amount of research have been reported in

the field of tire force estimation and many systems use model-based estimators to estimate the states. To improve the accuracy of the vehicle parameters estimation, one researcher used estimates of the tire cornering stiffness to improve estimation of the vehicle states using a model-based estimator [14]. Tire-road forces and sideslip angle observers are designed in vehicle-road system, which is modeled by combining a vehicle model with a tire-force model [15]. The tire cornering stiffness can be also estimated from the lateral vehicle models [16-17] and with the addition of non-linear tire models, the cornering stiffness and tire road friction can be estimated simultaneously [18-19]. A method to estimate both the lateral and longitudinal tire stiffness has been developed by using a non-linear tire model, which takes into account both the lateral and longitudinal tire models [20].

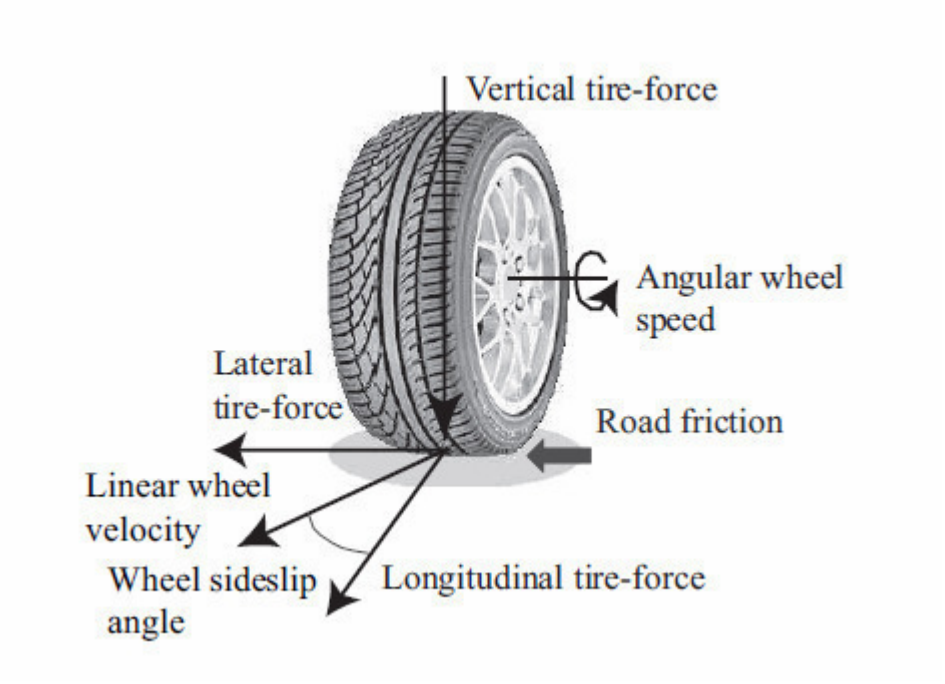

Figure 2.1. Wheel dynamic variables [13].

This study will be concentrated on the longitudinal tire force estimation. The longitudinal tire force determines the vehicle's longitudinal motion, such as velocity and

acceleration. Since longitudinal tire force can be transferred to the corresponding throttle/brake positions, the driver behavior could be reconstructed.

2.5 Driver Behavior Classification

Driver behavior can be classified into either normal or abnormal behavior. Numerous research studies have conducted to detect abnormal driver behavior. This section begins by discussing abnormal driver behavior and then driver behavior classification systems are introduced. Finally, currently existing abnormal driver behavior detection approaches are discussed.

2.5.1 Abnormal Driver Behavior

Abnormal driving behavior is defined as the behavior that is influenced by either mental or physical impairments. Six major categories of impairments are defined and they are: alcohol, fatigue, aging, physical impairment, drug use and distraction. It has been found that distraction represent the dominant cause of crashes [11].

The International Standards Organization developed the following definition for distraction: Distraction is “attention given to non-driving-related activity, typically to the detriment of driving performance” [28]. The comprehensive definition of driver distraction is presented by the Australian Road Safety Board in 2006 [29]: “Driver distraction is the voluntary or involuntary diversion of attention from the primary driving tasks not related to impairment (from alcohol, drugs, fatigue, or a medical condition) where the diversion occurs because the driver is performing an additional task (or tasks) and temporarily focusing on an object, event, or person not related to the primary driving tasks.” The diversion reduces a driver’s situational awareness, decision making and/or

performance resulting, in some instances, in a collision or near-miss or corrective action by the driver and/or other road user.

There are three types of driver distraction when considering the different sources that cause the driver's inattention.

Firstly, there is a general agreement that the existence of a triggering activity is a critical part of the definition. The triggering activity means a secondary task which diverts the driver's attention away from the driving task. The triggering activity can be classified into three categories: purposeful activity (e.g., inserting a CD, texting on a cell phone, or inputting information into navigation systems); incidental activity (e.g., answering a phone, interacting with passengers or eating); and uncontrolled activity (e.g., movement of animal and child inside the vehicle, sneezing, coughing or itching) [30].

Secondly, there is also a growing realization that "cognitive distraction" is a significant component of driver distraction. Cognitive distraction refers to the mental workload associated with a task (e.g., being lost in thought, emotionally upset or emotionally preoccupied). Cognitive distraction is generally not observable [30-31] in most situations.

Finally, external distractions are also involved in the categorizations of driver distraction. The external distractions include unusual or unexpected events or activities (e.g., wild animals crossing), inclusion of relatively common driving situations (e.g., driver blinded by sun or by oncoming headlines, sirens of police emergency vehicles), and external objects (e.g., advertising signage, outside person objects or events) [32].

When considering the different ways that distracting tasks affect drivers, the driver distraction can be categorized into three types [33]:

- Visual distraction: Tasks that require the driver to look away from the roadway to visually obtain information;
- Manual distraction: Tasks that require the driver to take a hand off the steering wheel and manipulate a device;
- Cognitive distraction: Tasks that require mental workload so that the driver will be thinking about something other than the driving task.

Each type of distractions can lead to hazardous behaviors such as large lane variation, abrupt steering control, slow response to hazards, and less efficient visual perception than attentive driving. Moreover, these types of distractions can occur in combination and interact with each other. Table 2.1 summarizes the effects of visual, cognitive and combined distractions on eye activities, lane position and steering control [36].

Table 2.1 Summary of Driver Distraction Effects [36]

	Visual Distraction	Cognitive Distraction	Combined Distraction
Eye Activities	High frequency of off-road glances, long total eye-off road time, and low percentage of road center	Gaze concentration in the center of the road	High frequency of off-road glances and long total eye-off-road time gaze concentration when drivers look at the road
Lane Position	Large lane variation	Unchanged or small lane variation	Large lane variation
Steering Control	Discrete steering correction and large correct magnitude (large steering error)	Small correction magnitude (small steering error)	Discrete steering correction and both large and small correction magnitude

2.5.2 Driver Behavior Classification System

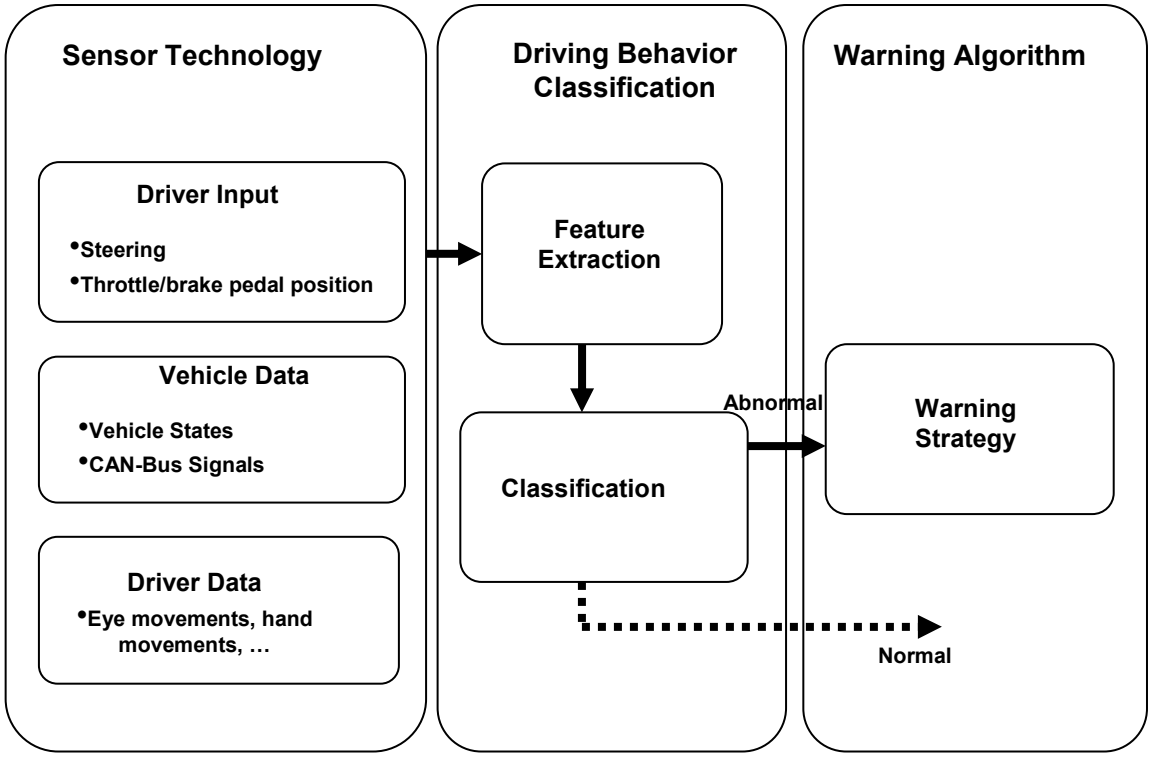

Figure. 2.2 A general structure of driving behavior classification systems.

Figure 2.2 illustrates the general structure of a driving behavior classification system. The operation of this system can be summarized with the following three steps.

1) The raw data are measured using multiple sensors/devices and CAN-bus. There are mainly three types of raw data:

- Driver input:

They refer to steering operation and throttle/brake pedal operation.

- Vehicle data:

They refer to the kinematic state variables of a vehicle, e.g., vehicle speed, yaw angle, yaw rate, sideslip angle, acceleration and lateral position.

- Driver data:

They refer to the driver behaviors and reactions, like eye movement, head movement, hand movement, body movement or physiological response.

2) Certain features of the data are extracted and used to represent the driving behavior. These features are then used to classify the driver's state. For most system, there are two states: normal driving behavior and abnormal driving behavior. The decision whether a driver behavior is abnormal or not can be determined according to some rules (e.g., a classification approach or a classifier) based on these features.

Prior studies have reported various features that can be used to measure the level of driver's abnormality. They indicated the effects of distraction on the driver's inputs, vehicle state information and driver's behavior.

- Driver control input features:

Some researchers have adopted statistics of a driver's operation signals to measure the driving performance. It was found that the mean, variance, root mean square (RMS) and entropy of steering angles are suitable to reflect a driver's steering maneuvers [89, 92-93]. It was pointed out in [90] and [91] that driver distractions may cause a delayed accelerator release reaction time. This delayed accelerator release reaction time is defined as the time when the lead vehicle starts to brake until the driver releases the accelerator. In the UMTRI research in the SAVE-IT project, it was found that when drivers are performing an in-vehicle task, they control their speed by intermittently adjusting the throttle as shown in Figure 2.3 [94].

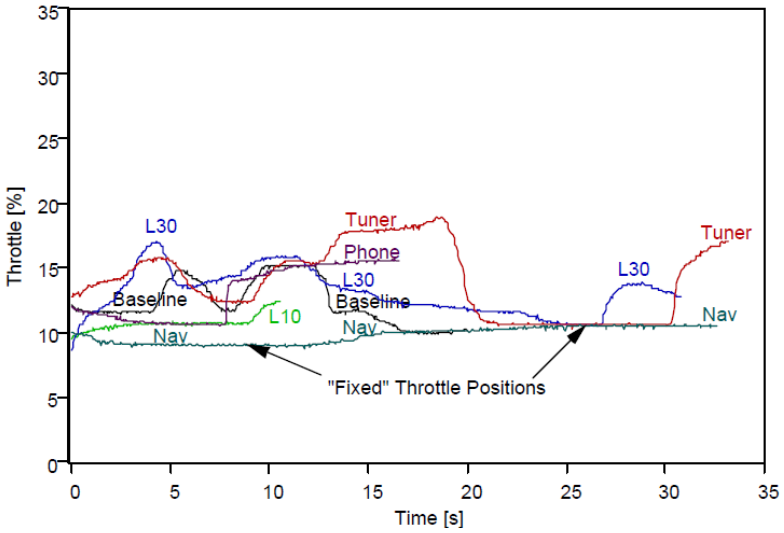

Figure 2.3 Throttle position when drivers are performing different in-vehicle tasks [94].

- Vehicle kinematic state features*:*

Driver abnormal behavior is associated with unintended changes of a vehicle's state resulting in unsafe driving performance. The vehicle state includes forward speed, lane position, sideslip angle, yaw angle, and yaw rate. Ranney [96] found that distraction may result in speed changes or allowing the vehicle to drift outside the lane boundaries. Zylstra et al. [97] point out that distracted driving does affect the mean lateral position. It was shown in [98] that the standard deviation of lane position was a good measure of visual distraction. Generally speaking, visual distraction affects lateral vehicle control, whereas cognitive distraction affects longitudinal vehicle control [99-100]. In summary, the driver's abnormal behavior affects the lateral displacement, sideslip angle, yaw angle, yaw rate and vehicle speed.

- Driver's behavior and reaction features:

Human factor professionals have indicated that eye movements (glance, gaze, and smooth pursuit), head movements and physiological responses are the ideal measures of the driver's state.

a) Eye Movements: The eye glance (eye-off-road) is highly related to visual distraction. For example, the visual distraction causes long off-road glance duration [98, 101-104]. Smooth pursuit occurs when the driver is tracking a moving object (e.g., a passing vehicle) [99]. SAVE-IT program uses eye glance behaviors to determine visual distraction in real time. Examples of statistical measures of eye glance include [105]:

- Peak glance duration: It is defined as the time of the longest glance at a target area.
- Mean glance duration: It is defined as the mean amount of time of all glances at a target area.
- Glance frequency: It is defined as the number of glances at a target area during the performance of a task.
- Total glance duration: It is defined as the cumulative time elapsed for all glances at a target area during the performance of a task.
- Mean time between glances: It is defined as the cumulative time elapsed looking away from a target area, divided by the number of glances away from the target area.

Prior studies in [106] showed that a driver's visual field narrows both vertically and horizontally. This means that drivers who are under cognitive distraction spend less time checking mirrors for hazards. According to [107] and [108], cognitive distraction changes the pattern of the eye gaze distribution: Drivers spend longer time concentrating on the road but their mind is off the driving task. Increased cognitive load is associated with less frequent glances to the mirrors, speedometer, and traffic signals. Hence, the mean time

between glances for distracting driving is longer compared to the value for normal driving.

b) Head movements: Miyaji et al. [109] found that the standard deviation of the head movement is suitable for measuring driver distraction. Distraction levels can be measured by the changes of the head position. It was found that changes of the head position depend on different face orientations (i.e., frontal, left, right, up and down) [110].

c) Physiological Responses: It was reported in [109] that pupil dilation occurs when a driver is talking, which results in cognitive distraction. The pupil diameter, vertical rotation "pitch angle" component and a lateral rotation "yaw angle" component are shown in Figure 2.4.

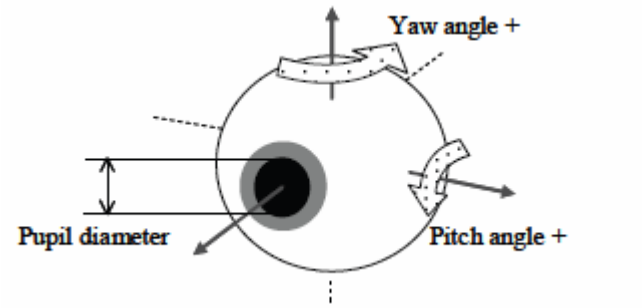

Figure 2.4 Pupil diameter and gaze angles [109].

The average value of the heart rate R-to-R interval (RRI) obtained from electrocardiograph (ECG) decreases when the drivers' cognitive loads are imposed [109, 111]. RRI is the distance between an R-wave and a consecutive one and is extracted from ECG signal. An example of the RRI in ECG waveform is shown in Figure 2.5. The temperature at the tip of the nose decreases when a driver is performing a cognitively distracting secondary activity, e.g., thinking about something or talking [112]. Wesley et al. [113] point out that skin temperature of supraorbital region increases when visual or

cognitive distraction occurs. A short film commissioned by DARPA and directed by Singer shows that electroencephalography (EEG) signals can be used to assess the cognitive workload [111].

Figure 2.5 Heart Rate RRI in ECG wave [109].

3) A warning strategy determines when and in which way the driver will be warned if abnormal driving behavior is detected. If certain criteria are met, the driver should not be warned. These criteria are introduced in [114]:

- Vehicle speed: The driver's gaze is often off the road but the driver is not being distracted when the vehicle speed is less than 50km/h .
- Direction indicators: No warning should be given while the driver is changing lanes and turning.
- Reverse gear: The driver should look over the shoulder.
- Brake pedal: The driver should not be warned if he or she is braking in order to not interfere with driving maneuvers.
- Steering angle: The driver makes large changes of wheel direction, in order not to interfere with the main driving task.
- Lateral acceleration: When the vehicle has to make strong movements in order not to interfere with a driving task, no warning should be given.

On the contrast, the warnings should be triggered while the driver distraction is detected and a driver is not at one of the above situations [115]. Basically, there are three main types of warnings:

- Visual warning, e.g., lights, icons, or text warning.
- Auditory warning, e.g., sounds or voice.
- Vibration warning, e.g., seat vibration or steering wheel vibration.

2.5.3 Driver Behavior Classification Algorithms

There have been many research studies on developing algorithms that can effectively detect a driver's abnormality in advanced driver assistance systems (e.g., crash warning systems, lane keeping systems, and etc.). In order to determine whether a driver behavior is normal or not, the extracted features need to be mapped to a decision. Basically, a driver's behavior is considered as being abnormal when a threshold is reached. This can be viewed as direct matching method. However, abnormal driver behavior can hardly be represented by a linear model and cannot be classified only by a simple matching method. Therefore, the machine learning technology is often employed. Different nonlinear classifiers are designed and tested in the prior research activities:

1) K-nearest neighbor (K-NN):

K-NN is a classification method based on closest training examples in the feature space. It is the simplest of all machine learning algorithms: an object is classified by a majority vote of its *k* nearest neighbors [116]. Sathyanarayana et al. [117] propose a system for detecting driver distractions using K-Nearest Neighbors (K-NN) classifier (K=1). The accuracies of distraction detection (classification) using K-NN, principal

component analysis (PCA) with K-NN and Linear Discriminate Analysis (LDA) with K-NN are 77.77%, 94.44%, and 88.30% respectively.

2) Bayesian Networks (BNs):

BN is a probabilistic model that represents a set of random variables. The nodes in it depict random variables and arrows depict conditional relationship between variables. There are two main types of BNs: static and dynamic. The former describes the situations that are not affected by previous states. The latter includes two Static BNs at successive time steps and the current state of variable depends on the state at the previous time step. It can modeled as a time-series signals according to a Markov process. BNs have been used for human behavior modeling, document classification, information retrieval, image processing, and data fusion. One advantage of BNs is that they provide an easier form of knowledge representation rather than a complete joint distribution. Another one is that they can handle situations with missing data. Their effectiveness has been demonstrated in the application of detecting cognitive distraction [118-119].

3) Decision tree:

A decision tree is a decision support tool that uses a tree-like graph or model of decisions and their possible consequences. It is commonly used in operations research to help identify a strategy most likely to reach a goal. Another use is to calculate conditional probabilities. It has two advantages: simple to understand and interpret, and easy to combine with other decision techniques. In [120], it is used to estimate the level of drivers' cognitive workload from the information of eye glances and driving performance. A decision tree is used to estimate the driver's cognitive workload from eye glances and driving performance [44].

4) Support Vector Machines (SVMs):

SVMs original proposed by Vapnik in 1995 are based on statistical learning theory. In the case of SVMs, a data point is viewed as a p-dimensional vector (a list of p numbers), and SVMs can find the best hyperplane that represents the largest separation, or margin, between two classes. SVMs can be used to represent nonlinear relationship between variables and classifying data [121]. SVMs have been applied to face recognition, speech recognition, image recognition, and information retrieval. They enjoy several advantages: they can generate both linear and nonlinear models with the same efficiency; provide more robust models compared to linear-regression algorithms; and can extract information from noisy data. Because of these advantages, they are suitable for measuring the level of cognitive distraction [122-123]. In [124], they successfully detect cognitive distraction with an accuracy of 81.1% from eye movements and driving data. There are detailed discussions about Support Vector Machines (SVMs) used to detect distractions in the SAVE-IT project's final report [125]. The distraction mitigation system used in the SAVE-IT project is depicted in Figure 2.6.

5) Artificial neural networks (ANNs):

An ANN consists of an interconnected group of artificial neurons. Modern neural networks are non-linear statistical data modeling tools. They are usually used to model complex relationships between inputs and outputs or to find patterns in data. It has been successfully utilized in pattern recognition fields (classification and face identification), data processing (filtering, clustering and blind source separation); function approximation, or regression analysis (time series prediction and fitness approximation); and system identification and control (vehicle control and process control), and financial

applications (automated trading systems). One of its main advantages is its ability to be used as an arbitrary function to approximate the relationship between inputs and outputs from observed data. It does not need prior knowledge of the patterns in the data. Waard et al. [126] investigate the feasibility of detecting driver distraction by using ANNs. Wollmer et al. [127] uses long short-term memory recurrent ANNs to detect driver distraction and they significantly outperforms approaches such as SVM.

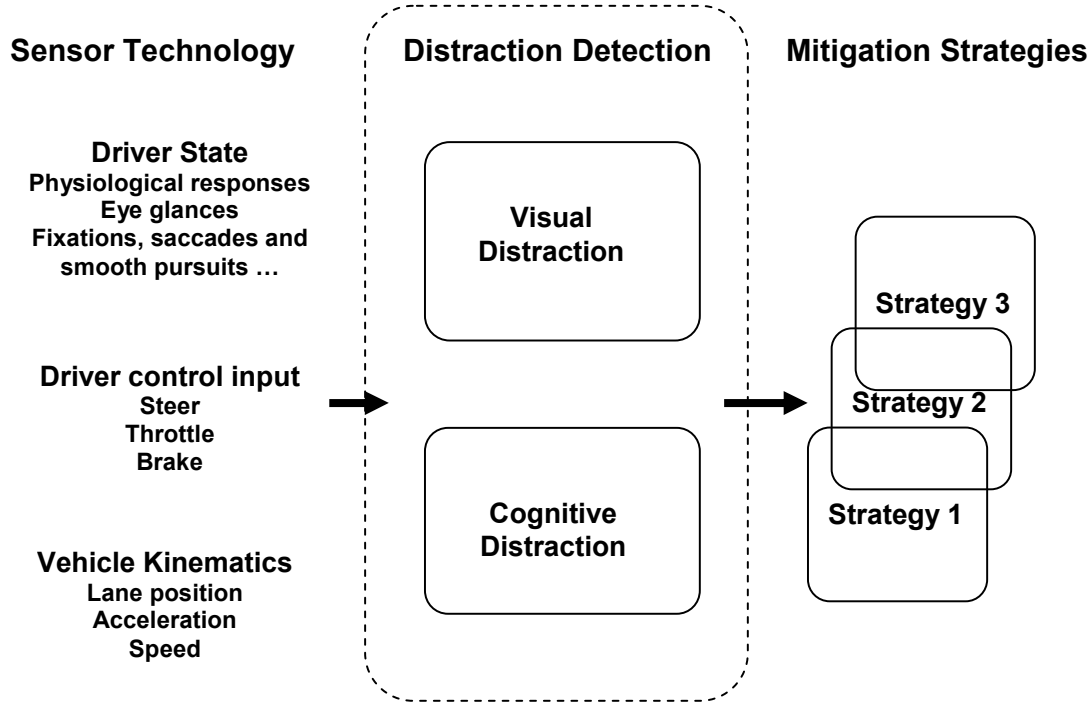

Figure 2.6 The structure of distraction mitigation system used in SAVE-IT [125].

6) AdaBoost:

Adaboost is a machine learning algorithm. Its advantages include: it has short recognition process time and high classification performance; it is sensitive to noisy data and outliers; it has no parameters to tune; it requires no prior knowledge about the weak learner and so can be flexibly combined with any other methods; it can be used for text

categorization, face detection and object detection [128-129]. Miyaji et al. [109] employed Adaboost to detect driver's cognitive distraction using physiological features.

7) Hidden Markov Model (HMM):

An HMM is a statistical Markov model in which the system being modeled is assumed to be a Markov process with hidden states. It consists of a number of states and transition probabilities and can be considered as the simplest dynamic Bayesian network. It has been applied in many fields, for example, speech, handwriting, gesture recognition; machine translation; and gene prediction. It is suitable to recover a data sequence that is not directly observable and could provide a better performance than conventional statistical approaches to model human factors and human behaviors. In [130], it was utilized to construct a framework to deal with the driver distraction detection and driving maneuver recognition.

2.6 Lateral Control System

The Automated Highway System (AHS) is a type of advanced driver assistance system. The research on AHS is supported by U.S. Department of Transportation from late 1994. AHS has been investigated by a number of research groups, such as National Automated Highway System Consortium in the United States, Intelligent Transport Systems (ITS) Japan, California PATH in the United States, etc [131-134]. The AHS concept defines a relationship between vehicles and the highway infrastructure. It uses vehicle and highway control technologies to shift driving functions from the driver/operator to the vehicle [51].

The two basic tasks for the AHS are vehicle longitudinal control and vehicle lateral control. Longitude control includes vehicle speed regulation to maintain adequate

spacing between vehicles. This type of control is suitable for preview-based and anticipatory control. Lateral control mainly refers to automatic vehicle steering to follow a track reference [52]. This type of control prevents vehicles deviating from the road. This dissertation focuses on the steering lateral control for the purpose of enhancing driving safety.

The lateral control strategies can be categorized into two groups: look-ahead and look-down reference systems. The former measures the lateral displacement from the lane reference ahead of the vehicle to do the preview-based control. Radar and machine vision based systems belong to this category and examples of successful projects using look-ahead reference system include VaMoRs-P, VITA-I and II, Carnegie Mellon University's PANS, and California PATH's stereo-vision based system [133, 135-137]. The latter measures the lateral displacement within or very close to the boundaries of the vehicle (e.g., straight down from the front bumper of the vehicle). For example, magnetic markers reference system and electric wire are its examples [54-55,138-139]. Magnetic markers use different encoding techniques to achieve the preview of road geometry. Electric wire is used to measure a vehicle's lateral state via the sensing of a magnetic field. Compared with the look-ahead reference system, a look-down reference system has some advantages [58, 79]:

1) It is reliable, yielding accuracy and good performance under any weather or light condition.

2) Other vehicles will not block the lateral displacement sensing signal.

Some steering control systems based on look-down reference system have been proposed in the literature [53-56]. More specifically, a general structure of the lateral

steering control system based on look-down reference system for lane keeping is shown in Figure 2.7 [57].

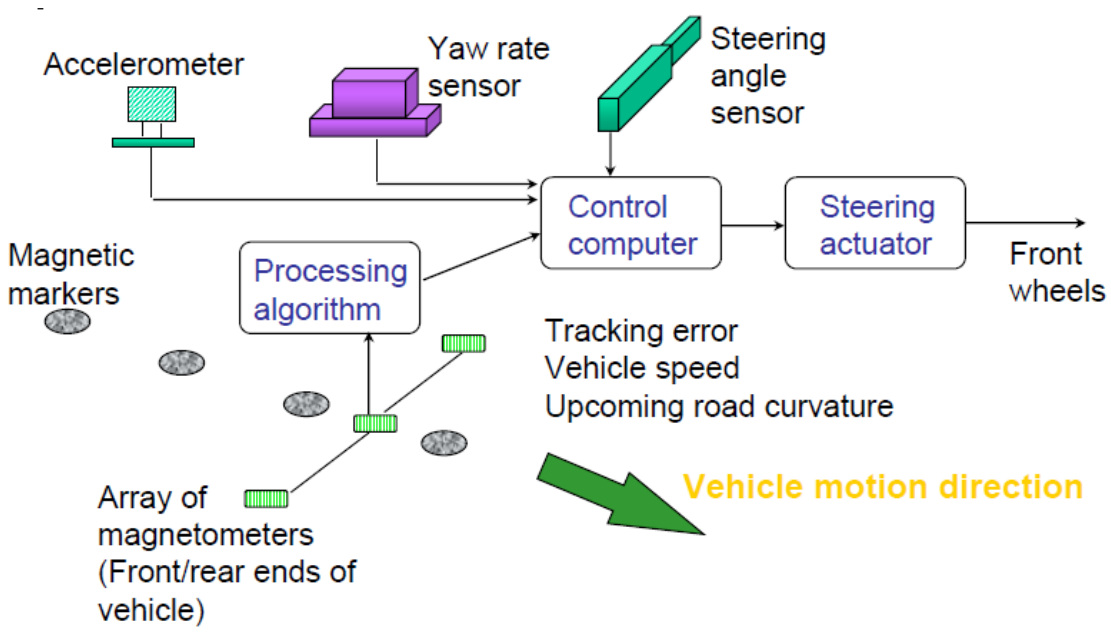

Figure 2.7 Structure of lateral steering control system [57].

Most look-down reference steering control system reported in the literature can achieve only low speed of less than $20\,\mathrm{m/s}$, i.e. 45mph [53-55, 56]. To extend the look-down reference systems to practical conditions of an automated highway system environment with speeds above $30\,\mathrm{m/s}\left(\simeq 67.5\mathrm{mph}\right)$, [58] and [79] proposed two new systems respectively. Both can achieve high speed levels while still keeping a comfortable ride. In [58], an absolute GPS is introduced to obtain road geometry. However, the information of road curvature values are based on pre-recording GPS coordinates rather than real-time GPS readings, which means higher implementation costs and is not very flexible to situations like changes of road geometry. Another disadvantage of curvature estimation in [58] is that large sudden changes are introduced into the control loop resulting in poor ride comfort to the car passengers. In [79], a robust

automatic steering control system is investigated based on the road geometry information encoded in magnetic markers and lateral displacements from front and rear sensors. However, this approach utilizes a gyroscope to record the steering angles of the vehicle and requires a large amount of magnetic markers installed on a highway, which means higher costs. In addition, the encoding of the road information needs to be implemented in advance in this system. This is not flexible to changes of road geometry. Moreover, binary polarity coding technique used in this approach is susceptible to errors.

CHAPTER 3

VEHICLE DYNAMICS

This chapter explains fundamental concepts of vehicle dynamics by introducing single-track model and two-wheel extended nonlinear model which are used in this research work. The introduced models will help to form the basic idea of a vehicle's states and parameters that are related to the driving behaviors and vehicle motions.

3.1 Single-track Model

The four-wheel car steering model featured in the horizontal plane is described by the "single-track model", which is also named as "bicycle model". The bicycle model is a standard representation in the area of ground vehicle dynamic. This model is obtained by lumping the front wheels into one wheel in the center line of the car. The same is done with the two rear wheels. The assumptions for the model are that slip angles on the inside and outside wheels are approximately the same and the effect of the suspension roll is small. These assumptions hold well for most typical driving situations. Besides, the roll, pitch and heave dynamics are not modeled. This model in this dissertation is used for lateral steering control [58].

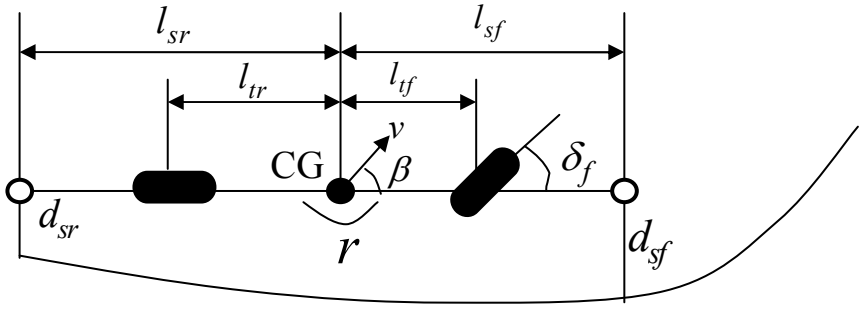

Figure 3.1 Single-track Model.

In Figure 3.1, δ_f is the steering angle, v is the vehicle velocity at center of gravity (CG) , β represents the side slip angle between center line and velocity, ψ is the heading angle, and $\dot{\psi}\,(r)$denotes the yaw rate. d_{sf} and d_{sr} are the lateral displacements of vehicle from the track reference with the front and rear sensors placed at distances l_{sf} and l_{sr} from the CG. ρ_{ref} is the curvature of the track, which is the inverse of the track radius. The state space representation of the vehicle dynamics then follows from the following fourth order model:

$$\begin{bmatrix} \dot{\beta} \\ \dot{r} \\ \dot{\psi} \\ \dot{d}_{sf} \end{bmatrix} = \begin{bmatrix} a_{11} & a_{12} & 0 & 0 \\ a_{21} & a_{22} & 0 & 0 \\ 0 & 1 & 0 & 0 \\ v & l_s & v & 0 \end{bmatrix} \begin{bmatrix} \beta \\ r \\ \psi \\ d_{sf} \end{bmatrix} + \begin{bmatrix} b_{11} \\ b_{21} \\ 0 \\ 0 \end{bmatrix} \delta_f - \begin{bmatrix} 0 \\ 0 \\ v \\ 0 \end{bmatrix} \rho_{ref} \tag{3.1}$$

The matrix elements a_{ij} and b_{ij} are defined as:

$$a_{11} = -\left(c_r + c_f\right)/\tilde{m}v$$

$$a_{12} = -1 + \left(c_r l_{tr} + c_f l_{tf}\right)/\tilde{m}v^2$$

$$a_{21} = \left(c_r l_{tr} + c_f l_{tf}\right)/\tilde{J}$$

$$a_{22} = -\left(c_r l_{tr}^2 - c_f l_{tf}^2\right)/\tilde{J}v$$

$$b_{11} = c_f/\tilde{m}v$$

$$b_{21} = c_f l_{tf}/\tilde{J}$$

$$\tilde{m} = m/\mu$$

$$\tilde{J} = I/\mu$$

where, μ is common road adhesion factor with $\mu = 1$ for dry road and $\mu = 0.5$ for wet road. The vehicle mass m is normalized by μ, i.e., $\tilde{m} = m/\mu$ is a "virtual mass". Similarly, the moment of inertia I is normalized as $\tilde{J} = I/\mu$.

If considering the lateral displacements as state variables (d_{sf} and d_{sr}), the vehicle model state-space function can be represented in equation (3.2) by applying a transformation from equation (3.1).

$$\begin{bmatrix} \dot{d}_{sf} \\ \ddot{d}_{sf} \\ \dot{d}_{sr} \\ \ddot{d}_{sr} \end{bmatrix} = \begin{bmatrix} 0 & 1 & 0 & 0 \\ \underline{a}_{21} & \underline{a}_{22} & -\underline{a}_{21} & \underline{a}_{24} \\ 0 & 0 & 0 & 1 \\ \underline{a}_{41} & \underline{a}_{42} & -\underline{a}_{41} & \underline{a}_{44} \end{bmatrix} \begin{bmatrix} d_{sf} \\ \dot{d}_{sf} \\ d_{sr} \\ \dot{d}_{sr} \end{bmatrix} - \begin{bmatrix} 0 & 0 \\ \underline{b}_{21} & -v^2 \\ 0 & g_4 v \\ \underline{b}_{41} & -v^2 \end{bmatrix} \begin{bmatrix} \delta_f \\ \rho_{ref} \end{bmatrix} \tag{3.2}$$

The entries of the matrices are given by

$$\underline{a}_{21} = \frac{g_2}{m g_4} - \frac{l_{sf} g_1}{I g_4}$$

$$\underline{a}_{22} = \frac{g_1 - l_{sr} g_2}{m v g_4} + \frac{l_{sf}\left(l_{sr} g_1 - g_3\right)}{I v g_4}$$

$$\underline{a}_{24} = -\frac{g_1 + l_{sf} g_2}{m v g_4} + \frac{l_{sf}\left(l_{sf} g_1 + g_3\right)}{I v g_4}$$

$$\underline{a}_{41} = \frac{g_2}{m g_4} + \frac{l_{sr} g_1}{I g_4}$$

$$\underline{a}_{42} = \frac{g_1 - l_{sr} g_2}{m v g_4} - \frac{l_{sr}\left(l_{sr} g_1 - g_3\right)}{I v g_4}$$

$$\underline{a}_{44} = -\frac{g_1 + l_{sf} g_2}{m v g_4} - \frac{l_{sr}\left(l_{sf} g_1 + g_3\right)}{I v g_4}$$

$$\underline{b}_{21} = \mu c_f \left(\frac{1}{m} + \frac{l_{sf} l_{tf}}{I}\right)$$

$$\underline{b}_{41} = \mu c_f \left(\frac{1}{m} - \frac{l_{sr} l_{tf}}{I} \right)$$

where,

$$g_1 = \mu \left(c_f l_{tf} - c_f l_{tf} \right)$$

$$g_2 = \mu \left(c_f + c_r \right)$$

$$g_3 = \mu \left(c_r l_{tr}^2 + c_f l_{tf}^2 \right)$$

$$g_4 = l_{sf} + l_{sr}$$

3.2 Two-wheel Extended Nonlinear Model

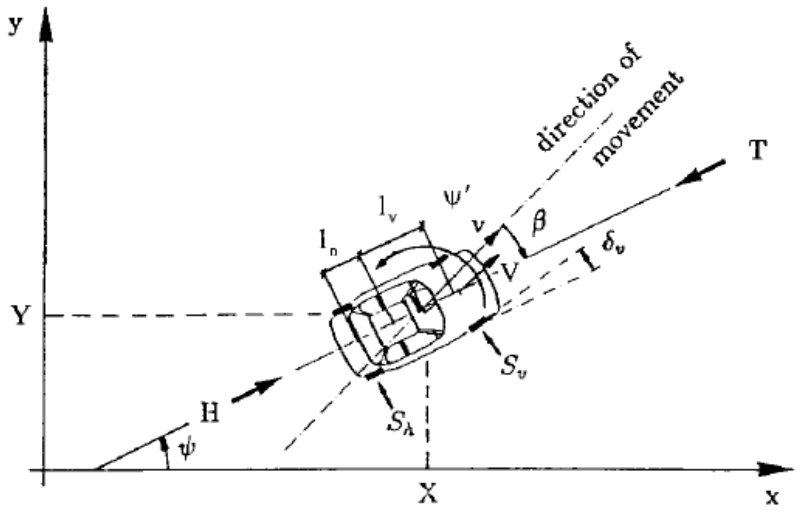

Figure 3.2 Nonlinear extended two-wheel vehicle model [61].

The extended two-wheel model is selected for two main reasons:

1) The longitudinal tire force can be directly evaluated instead of being modeled based on tire cornering stiffness and sideslip angle.

2) It is a simplified model by neglecting roll angle, pitch angle, and the lateral motion, and groups the front and rear wheels as a single wheel.

This model has also been applied to represent the driver model in the commercial car simulation software veDYNA [59-60]. The nonlinear extended two-wheel vehicle dynamic model is represented in Figure 3.2. Table 3.1 summarizes the notations used to describe the dynamic variables of the nonlinear model and vehicle characteristics [61].

Table 3.1 Notations of Two-wheel Vehicle Model

Symbol	Definition
δ_v	steering angle
$\dot{\psi}$	yaw rate
β	sideslip angle
ψ	yaw angle (heading angle)
v	longitudinal velocity
S_v	front lateral force
S_h	rear lateral force
H	rear longitudinal tire force
V	front longitudinal tire force
T	air resistance force
X	X-coordinate of the center of gravity (CG)
Y	Y-coordinate of the CG
l_v	distance from front axel to CG
l_h	distance from rear axel to CG
m	vehicle mass
I	moment of inertia

In order to derive the state space equations for the simplified vehicle model, the angles δ_v and β are assumed to be small and the front longitudinal force V is neglected. Then, the nonlinear mode can be described by equation (3.3).

$$\dot{\underline{x}} = \begin{bmatrix} x_3 + \frac{1}{m}\frac{T(\underline{x})x_1}{x_4} - \frac{1}{m}\frac{S_h(\underline{x})}{x_4} \\ x_3 \\ -\frac{l_h}{I}S_h(\underline{x}) \\ -\frac{1}{m}T(\underline{x}) \\ x_4\cos(x_2 - x_1) \\ x_4\sin(x_2 - x_1) \end{bmatrix} + \begin{bmatrix} -\frac{1}{mx_4} & -\frac{1}{m}\frac{x_1}{x_4} \\ 0 & 0 \\ \frac{l_v}{I} & 0 \\ 0 & \frac{1}{m} \\ 0 & 0 \\ 0 & 0 \end{bmatrix} w \tag{3.3}$$

The six-dimensional state vector is:

$$x = [x_1, x_2, x_3, x_4, x_5, x_6]' = [\beta, \psi, \dot{\psi}, v, X, Y]'.$$

The two-dimensional input vector w includes the front lateral force $S_v(\underline{x})$ and longitudinal force H:

$$w = [w_1 \quad w_2]' = [S_v(\underline{x}) \quad H]'.$$

The lateral force $S_v(\underline{x})$ generated by the front tire is dependent on the steering angle δ_v. More specifically,

$$S_v(\underline{x}) = \Gamma_v\left(x_1 - \frac{l_v}{x_4}x_3 + \delta_v\right) \tag{3.4}$$

The rear force $S_h(\underline{x})$ and the air resistance $T(\underline{x})$ can be respectively described by equations (3.5) and (3.6):

$$S_h(\underline{x}) = \Gamma_h\left(x_1 + \frac{l_h}{x_4}x_3\right) \tag{3.5}$$

$$T\left(\underline{x}\right) = c_w \frac{\ell_L}{2} A x_4^2 . \tag{3.6}$$

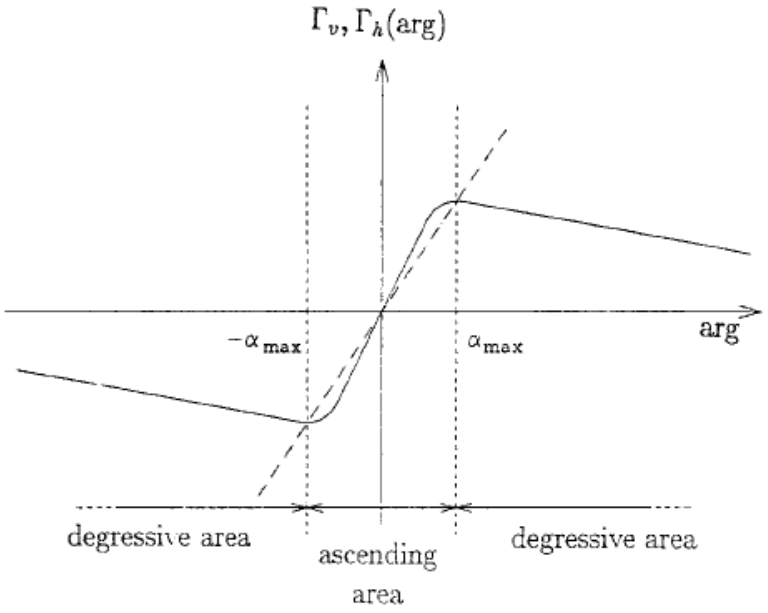

Figure 3.3 Characteristic curve of the tires [61].

The air resistance $T\left(\underline{x}\right)$ depends on the aerodynamic resistance coefficient c_w, the atmospheric density ℓ_L, and the surface of the vehicle's cross section A. The functions Γ_v and Γ_h represent the characteristic curves of the tires, and they are plotted in Figure 3.3. They are determined by the same characteristic line, which describes the lateral force values depending on the argument. For small values of argument, smaller that $\alpha_{\max}$, a linear relation of the side force can be recognized and when values of argument are greater than $\alpha_{\max}$, the side force decreases. Furthermore, at $\alpha_{\max}$ the side force value reaches its maximum value. The area between the $\alpha_{\max}$ values is described as the ascending part and

the area outside this area is the descending part of the characteristic line [61]. The maximum value of α_{max} is approximated to 6.5 deg [60].

CHAPTER 4

LONGITUDINAL TIRE FORCE ESTIMAITON

4.1 Introduction

In this chapter, a driver behavior reconstruction problem is addressed. More specifically, the task in this study is to estimate the longitudinal tire force which can be transferred to the corresponding throttle/brake positions under the assumption that the steering angles are known.

An advanced driver assistance system, utilizing information about the driving operation behavior (steering angle and throttle/brake positions) and/or vehicle states (velocity, acceleration, yaw angle, yaw rate, sideslip angle, etc.) can determine potentially dangerous situations and alert the driver. These critical vehicle parameters can be directly obtained from the controller area network bus (CAN-bus) in some cars. Although the parameters can also be collected by installing additional multimodal sensors (such as GPS receiver, steering angle sensors, throttle/brake pedal position sensors, cameras, microphones, and etc.), it is inconvenient and costly for the general drivers. Therefore, in this research, a low cost GPS receiver is used to acquire four types of signals (longitudinal velocity, yaw angle, lateral and longitudinal positions of the vehicle) instead of using the high cost vehicle data acquisition equipment. A low cost 1Hz GPS receiver is used as the vehicle data acquisition equipment. It is obvious that the values of the measurements are discrete and it is assumed that the steering angles are already known. The aim is to answer the question on how the longitudinal tire force can be deduced from the partly discrete knowledge. In this work, a longitudinal force estimation scenario is developed for the nonlinear extended two-wheel vehicle dynamic model only according to the GPS

information. Firstly, two states, i.e. the sideslip angle and the yaw rate are estimated since they are not available from GPS measurements. Secondly, an optimization scheme is proposed to estimate the longitudinal tire force. Finally, the estimation results can validate the proposed methods by comparing to the reference longitudinal tire force command.

For the driver assistance system, the wireless communications technology includes vehicle data communication from vehicle to vehicle and from vehicle to infrastructure (e.g., road side station) [63]. The technology enables a number of vehicle safety applications that mainly focus on improving crash prevention performance and driving comfort. The Society of Automotive Engineers' (SAE) common vehicle-to-vehicle safety message set includes warnings (such as post-crash warning, lane change warning, wrong way driver warning, etc.) that are transmitted between vehicles to enhance the safety of driving [64-65]. However, a vehicle-to-vehicle or vehicle-to-station communication infrastructure is not well established at this point and with the volume of vehicular flow, communication bandwidth conservation is an important concern. A vehicle-to-station scenario is considered, in which, the GPS data are transmitted from a vehicle to a road side station when the vehicle is moving along a certain section of the road. The station implements vehicle states estimation and the longitudinal tire force estimation tasks, and reproduces the vehicle's interpolation motion every second. The station can also determine the driver behaviors and send the decision back to the vehicle and/or other interested vehicles that would help other drivers avoid the potential dangerous situation.

Note that the sideslip angle and yaw rate cannot be measured by the GPS receiver. Since the whole vehicle states are necessary to reconstruct the longitudinal tire force, the sideslip angle and yaw rate have to be estimated based on the known discrete GPS data

points. This is precisely the vehicle state estimation problem. Many methods have been developed to solve the problem [66]. For example, Extended Kalman Filter (EKF) has been employed to estimate the dynamic states [67] and most of the EKF methods are designed based on the four wheel vehicle model. In this research, an estimation methodology for nonlinear extended two-wheel vehicle model [61] is derived by implementing an Kalman Filter estimation method. Then, the vehicle states estimation results together with the GPS signals are further used to calculate the longitudinal tire force. Since the vehicle states obtained by the GPS receiver and estimated by the Kalman Filter are both discrete, the procedure to estimate the longitudinal tire force can be viewed as a piecewise time-independent optimization problem. In the optimization scheme, the optimal longitudinal tire force is calculated by considering the kinematic constraints.

4.2 Approximated Two-wheel Vehicle Dynamics

The vehicle model used here is the nonlinear two-wheel vehicle model described in equation (3.3), Section 3.2. Since the tire forces are determined by a characteristic curve shown in Figure 3.3. The function of Γ_v and Γ_h defined in equations (3.4) and (3.5) have to be approximated.

The assumptions adopted are that the angles δ_v and β are small. Besides, the actual values of $\frac{l_h}{x_4}x_3$ and $\frac{l_v}{x_4}x_3$ are also small because the value of vehicle's velocity is large as compared to that of $l_h x_3$ and $l_v x_3$. Assume that the arguments of Γ_v and Γ_h belong to the ascending area, i.e., $\left|x_1 - \frac{l_h}{x_4}x_3 + \delta_v\right| < 6.5\deg$ and $\left|x_1 + \frac{l_h}{x_4}x_3\right| < 6.5\deg$. Then,

both the functions Γ_v and Γ_h can be approximated by linear functions, which are described in the following.

$$S_v\left(\underline{x}\right) = \gamma_v\left(x_1 - \frac{l_v}{x_4}x_3 + \delta_v\right) \tag{4.1}$$

$$S_h\left(\underline{x}\right) = \gamma_h\left(x_1 + \frac{l_h}{x_4}x_3\right) \tag{4.2}$$

where the constants γ_v and γ_h are the slope coefficients for the two linear functions, respectively. Under the above approximation, the steering angle δ_v and the longitudinal tire force H can be used as the new input vector for the vehicle model. The vehicle model described in equation (3.3) can be rewritten as

$$\dot{\underline{x}} = A\left(\underline{x}\right) + B\left(\underline{x}\right)u \tag{4.3}$$

where,

$$u = \begin{bmatrix} \delta_v \\ H \end{bmatrix}$$

$$A\left(\underline{x}\right) = \begin{bmatrix} x_3 + \dfrac{c_w \ell_L A x_4 x_1}{2m} - \dfrac{\gamma_h\left(x_1 + l_h x_3/x_4\right)}{mx_4} - \dfrac{\gamma_v\left(x_1 - l_v x_3/x_4\right)}{mx_4} \\ x_3 \\ -\dfrac{l_h}{I}\left(x_1 + \dfrac{l_h}{x_4}x_3\right) + \dfrac{\gamma_v l_v}{I}\left(x_1 - \dfrac{l_v}{x_4}x_3\right) \\ -\dfrac{1}{2m}c_w \ell_L A x_4^2 \\ x_4\cos\left(x_2 - x_1\right) \\ x_4\sin\left(x_2 - x_1\right) \end{bmatrix}$$

$$B(\underline{x}) = \begin{bmatrix} -\gamma_v / m x_4 & -x_1 / m x_4 \\ 0 & 0 \\ \gamma_v l_v / I & 0 \\ 0 & 1/m \\ 0 & 0 \\ 0 & 0 \end{bmatrix}$$

4.3 Sideslip Angle and Yaw Rate Estimation

In order to estimate the longitudinal force, it is necessary to measure the values of all the variables. The GPS receiver is used to measure the velocity, yaw angle, X-position and Y-position. The sideslip angle β and the yaw rate $\dot{\psi}$ are not available and the vehicle state observer needs to be designed. The continuous observer used in [61] cannot be used in this case because the data collected by the GPS is not continuous. In addition, other discrete EKF methods based on four-wheel model [66-67] are also not suitable for this study. Therefore, the discrete-time Kalman Filter [68-69] is developed to estimate the sideslip angle and the yaw rate in this case.

To simplify the estimation problem, a subsystem is considered in which the state vector is composed of the sideslip angle, the yaw angle, and the yaw rate. It is also assumed that the fourth variable, vehicle velocity, is constant. This subsystem model can be simplified to the following time varying nonlinear model from equation (4.3).

$$\begin{aligned} \dot{x} &= \begin{bmatrix} \frac{c_w \ell_L A v}{2m} - \frac{\gamma_h + \gamma_v}{mv} & 0 & 1 - \frac{\gamma_h l_h - \gamma_v l_v}{mv^2} \\ 0 & 0 & 1 \\ \frac{\gamma_v l_v - l_h}{I} & 0 & -\frac{l_h^2 + \gamma_v l_v^2}{Iv} \end{bmatrix} x + \begin{bmatrix} -\frac{\gamma_v}{mv} & -\frac{x_1}{mv} \\ 0 & 0 \\ \frac{\gamma_v l_v}{I} & 0 \end{bmatrix} u \\ y &= x \end{aligned} \tag{4.4}$$

where $u = [\delta_v, H]'$ and $x = [x_1, x_2, x_3]' = [\beta, \psi, \dot{\psi}]'$.

In order to develop a discrete-time KF, the dynamic model of equation (3.4) has to be discretized. The discretization is performed by a forward Euler approximation. The step size is $\Delta T = 1s$, because the receiver updates the data every second. The nonlinear discrete-time system of the form can be obtained:

$$\begin{cases} x_{k+1} = f\left(x_k, u_k\right) \\ y_k = x_k + n_k \end{cases} \tag{4.5}$$

where n_k is the measurement noise vector, which is related to the accuracy of the GPS receiver. It is supposed to be non-intercorrelated, stationary, white and Gaussian with known covariance. The covariance of n_k is denoted as R_k.

The discretized kinematic of the vehicle velocity is

$$v_{k+1} = v_k - \frac{1}{2m} c_w \ell_L A v_k^2 + \frac{H_k}{m} \tag{4.6}$$

Then, the force at each time instant k has the form of

$$H_k = m\left(v_{k+1} - v_k\right) + \frac{1}{2} c_w \ell_L A v_k^2 . \tag{4.7}$$

There is thus only one input $\delta_{v,k}$ left if replacing H_k with the above expression. The mathematical description of discrete subsystem yields to a linear case,

$$\begin{cases} x_{k+1} = A_k x_k + B_k \delta_{v,k} \\ y_k = x_k + n_k \end{cases} \tag{4.8}$$

where,

$$x_k = \left[x_{1,k}, x_{2,k}, x_{3,k}\right]' = \left[\beta_k, \psi_k, \dot{\psi}_k\right]'$$

$$A_k = \begin{bmatrix} 2 - \frac{\gamma_h + \gamma_v}{m v_k} - \frac{v_{k+1}}{v_k} & 0 & 1 - \frac{\gamma_h l_h - \gamma_v l_v}{m v_k^2} \\ 0 & 1 & 1 \\ \frac{\gamma_v l_v - l_h}{I} & 0 & 1 - \frac{l_h^2 + \gamma_v l_v^2}{I v_k} \end{bmatrix}$$

$$B_k = \begin{bmatrix} -\frac{\gamma_v}{m v_k} & 0 & \frac{\gamma_v l_v}{I} \end{bmatrix}'$$

In real situation, the measurements are corrupted by noise. Denote $\tilde{\psi}_k = \psi_k + n_{\psi,k}$ as the measurements obtained by the GPS. $n_{\psi,k}$ is the measurement noise for the yaw angle. Combining the GPS information and the linear subsystem model of equation (4.4), the measurement vector y_k is defined by:

$$y_{1.k} = a\tilde{\psi}_{k+2} + b\tilde{\psi}_{k+1} + c\tilde{\psi}_k + d\delta_{v,k} \tag{4.9}$$

$$y_{2,k} = \tilde{\psi}_k \tag{4.10}$$

$$y_{3,k} = \tilde{\psi}_{k+1} - \tilde{\psi}_k \tag{4.11}$$

where the coefficients a, b, c, d are determined by equation (4.8).

$$a = I/\left(\gamma_v l_v - l_h\right) \tag{4.12}$$

$$b = \left(l_h^2 + \gamma_v l_v^2 - 2Iv_k\right)/v_k\left(\gamma_v l_v - l_h\right) \tag{4.13}$$

$$c = -\left(l_h^2 + \gamma_v l_v^2 - Iv_k\right)/v_k\left(\gamma_v l_v - l_h\right) \tag{4.14}$$

$$d = -\gamma_v l_v/\left(\gamma_v l_v - l_h\right). \tag{4.15}$$

Under these hypotheses, a discrete Kalman Filter can be applied to the estimation problem. The Kalman Filter algorithm is recursive and operates in two steps: a prediction step and an update step. At time step k, $\hat{x}_{k|k} = E\left\{x_k \mid y_1 \ldots y_k\right\}$ is a posteriori estimate of

the state, which is the mean of the state vector conditioned on the measurements from time step 1 to time step k. $P_{k|k} = E\left\{\left(x_k - \hat{x}_{k|k}\right)\left(x_k - \hat{x}_{k|k}\right)' \mid y_1, \ldots y_k\right\}$ is the covariance of this estimation. R_k is the measurement noise covariance. The operation of Kalman filter for the discrete model of equation (4.4) is shown in Table 4.1.

Table 4.1 The Operation of Kalman Filter

Predict (Time update)
Predict the state ahead $$\hat{x}_{k\|k-1} = A_k \hat{x}_{k-1\|k-1} + B_k \delta_{v,k-1}$$
Predict the error covariance ahead $$P_{k\|k-1} = A_k P_{k-1\|k-1} A_k'$$
Correct (Measurement update)
Compute the Kalman gain $$K_k = P_{k\|k-1}\left(P_{k\|k-1} + R_k\right)^{-1}$$
Update estimate with measurement y_k $$\hat{x}_{k\|k} = \hat{x}_{k-1\|k-1} + K_k\left[y_k - \hat{x}_{k-1\|k-1}\right]$$
Update the error covariance $$P_{k\|k} = P_{k\|k-1} A_k' - K_k P_{k\|k-1}$$

4.4 Estimation of Longitudinal Tire Force

In this section, the task is to calculate the continuous longitudinal tire force which makes the trajectory output of the nonlinear continuous model in equation (4.3) follow the actual

trajectory as accurately as possible. A piecewise time-independent optimization scheme is developed under the kinematic constraints of the vehicle.

Denote $\tilde{X}_k, \tilde{Y}_k, \tilde{v}_k, \tilde{\psi}_k, \forall k \in [1,\ldots,\ell]$ as the measurements of the GPS, and $\hat{\beta}_k, \hat{\dot{\psi}}_k$ as the estimation results from the Kalman filter. Let the vector $p_k = \left[\hat{\beta}_k, \tilde{\psi}_k, \hat{\dot{\psi}}_k, \tilde{v}_k, \tilde{X}_k, \tilde{Y}_k\right]'$ be the prior information of the vehicle states. The output of the nonlinear continuous model in equation (4.3) is $y_k = \left[y_{1,k}, y_{2,k,} y_{3,k}\right]' = \left[v_k, X_k, Y_k\right]'$ at the end of the time segment k. Firstly, the states of the vehicle are initialized with p_{k-1} at the beginning of each time segment k. Secondly, the continuous model in equation (4.3) is simulated for one second for each possible longitudinal force command, $H_k(t) = h_k,\ k\text{-}1 \le t < k$. At the end of the time segment k, a cost function is then evaluated for all the possible force commands, and the force which minimizes this cost function is chosen. Figure 4.1 shows the block diagram of proposed scheme.

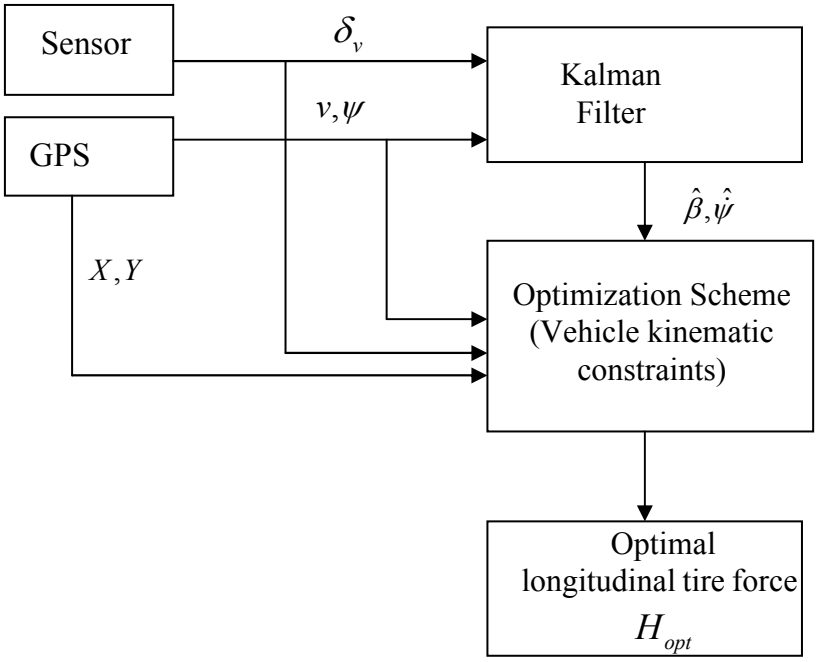

Figure 4.1. Block diagram of the proposed method.

The cost function is the error term that combines both the position offsets from the actual trajectory and the velocity error from the actual value, because the tire force has impacts on both the vehicle's position and velocity. The particular form of the cost function in time period k is as follows:

$$C_k\left(h_k\right) = E_{position,k}^2 + r_v {E_{v,k}}^2 \tag{4.16}$$

where $E_{position}$ and E_v are the position offset and the velocity error of the vehicle relative to the point measured by the GPS on the trajectory. Note that there is a length parameter r_v in the cost function which is used to scale the velocity error relative to the position error. $E_{position}$ and E_v can be obtained by the following equations:

$$E_{position,k} = \sqrt{\left(y_{2,k} - \tilde{X}_k\right)^2 + \left(y_{3,k} - \tilde{Y}_k\right)^2} \tag{4.17}$$

$$E_{v,k} = y_{1,k} - \tilde{v}_k \tag{4.18}$$

The optimization algorithm can be summarized as:

$$\min_{h_k(t)} \sum_{k=1}^{\ell} \left[\left(y_{2,k} - \tilde{X}_k\right)^2 + \left(y_{3,k} - \tilde{Y}_k\right)^2 \right] + r_v \sum_{k=1}^{\ell} \left(y_{1,k} - \tilde{v}_k\right)^2 \tag{4.19}$$

subject to the constraints:

$$\begin{cases} \dot{\underline{x}}(t) = A\left(\underline{x}(t)\right) + B\left(\underline{x}(t)\right)u(t) \\ \underline{y}(t) = \left[x_{4,}(t)x_5(t), x_6(t)\right]' \end{cases}$$
$$t_{0,k} = k-1 \qquad \forall k \in [1,\ldots,\ell]$$
$$\Delta t = 1$$
$$\underline{x}\left(t_{0,k}\right) = p_{k-1}$$

where $t_{0,k}$ is the start time at each time segment k, and Δt is the length of the time segment. Finally, the solution of the optimization problem is

$$H_{opt} = \left\{ h_k^{opt}(t), k-1 \le t < k, \forall k \in [1,\ldots,\ell] \right\}. \tag{4.20}$$

4.5 Simulation Results

4.5.1 Model Simulation

Simulations were carried out using the Matlab Simulink software. The numerical values of the vehicle characteristics and the parameters used to simulate the model are shown in Table 4.2.

Table 4.2 Values of Parameters

Symbol	Definition	Values
l_v	distance from CG to front tire	1.0065 m
l_h	distance from CG to rear tire	1.4625 m
m	vehicle mass	1550 kg
I	moment of inertia	2200 kgm^2
γ_v	slope of front lateral force function	198000 N / rad
γ_h	slope of rear lateral force function	470000 N / rad
c_w	the aerodynamic resistance coefficient	0.2
ℓ_L	atmospheric density	1.29 kg / m^3
A	vehicle's cross-section surface	1.5 m^2

Figure 4.2 shows the input commands of the model, which consists of the steering angle and the longitudinal tire force.

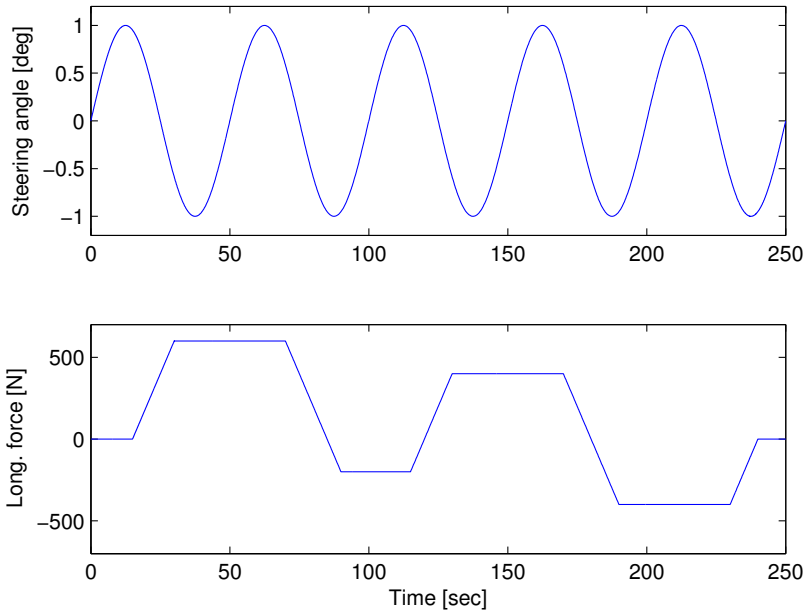

Figure 4. 2 The reference commands of model simulation.

It is assumed that a 1Hz GPS is used to measure the vehicle states: yaw angle, velocity, X-position, and Y-position. The model output states are sampled at the rate of 1 Hz. The sampled results corrupted by the additive Gaussian white noise (AWGN) can be viewed as the measurements obtained by the GPS. A typical group of accuracy values of the GPS receiver are adopted:

- The velocity accuracy is about $\pm 0.25 \text{m/s}$;
- The heading accuracy approaches $\pm 1 \text{deg}$;
- The position accuracy is around $\pm 3 \text{m}$.

The discrete vehicle states with the above random noises included are shown in Figure 4.3.

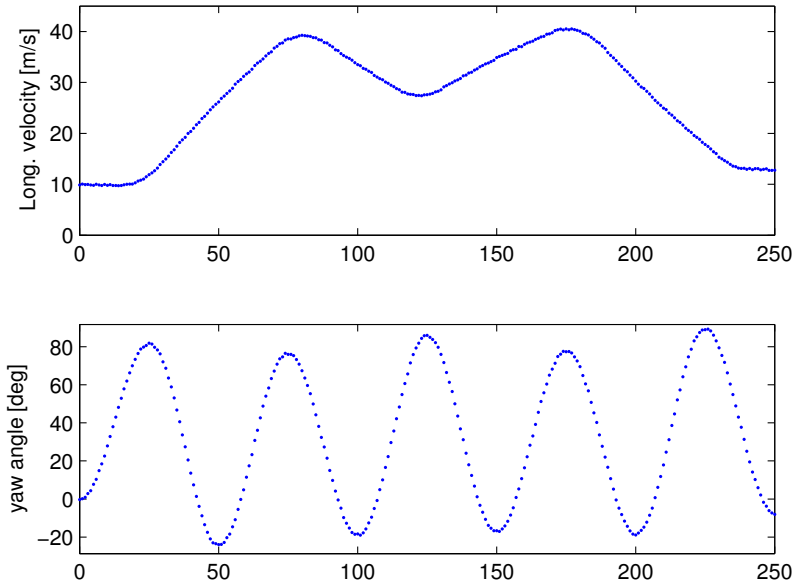

Figure 4.3 (a). Noisy sampled vehicle states (velocity and yaw rate), viewed as GPS measurements.

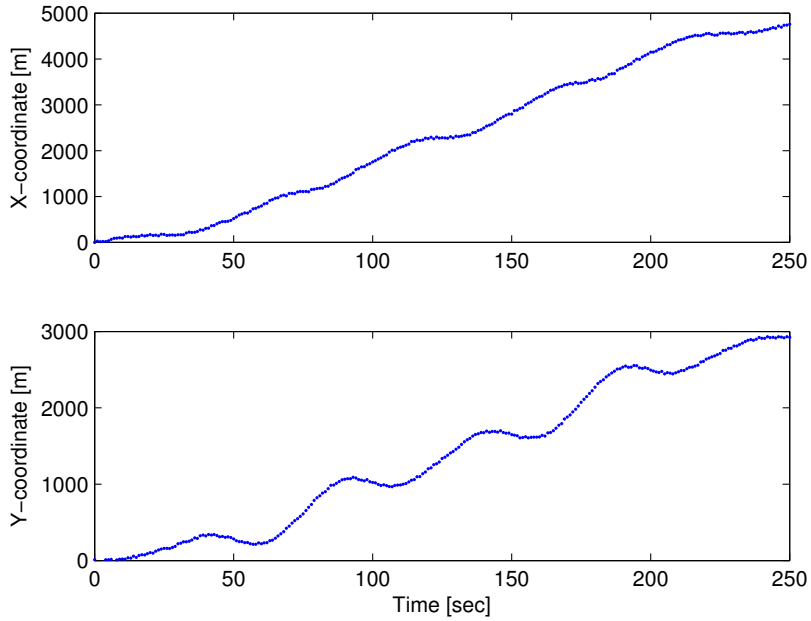

Figure 4.3 (b) Noisy sampled vehicle states (X and Y coordinates), viewed as GPS measurements.

4.5.2 Sideslip Angle and Yaw Rate Estimation

Using Kalman estimator provided in Section 4.3, the sideslip angle and yaw rate estimation results are given in Figure 4.4. Both these two estimates show great accuracy. The estimation errors are given in Figure 4.5.

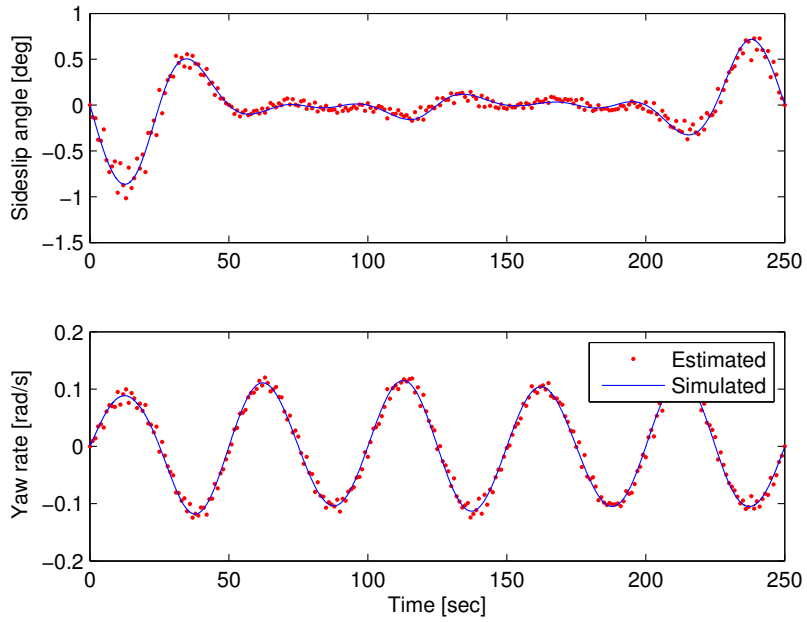

Figure 4.4 Sideslip angle and yaw rate estimation results.

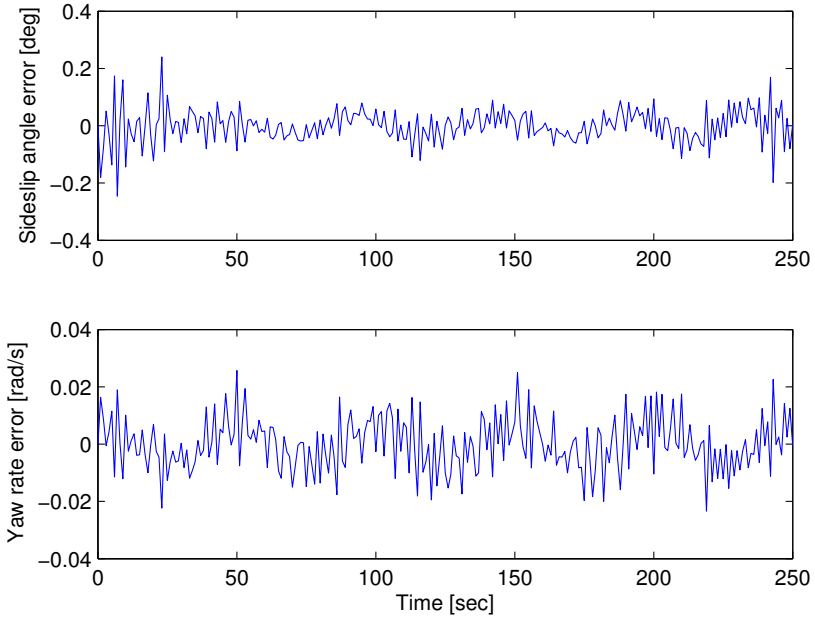

Figure 4.5 Sideslip angle and yaw rate estimation error.

4.5.3 Longitudinal Tire Force Estimation

To evaluate the performance of the piecewise optimization strategy described in Section 4.4, Figure 4.6 compares the optimal longitudinal tire force estimation results with the reference input command.

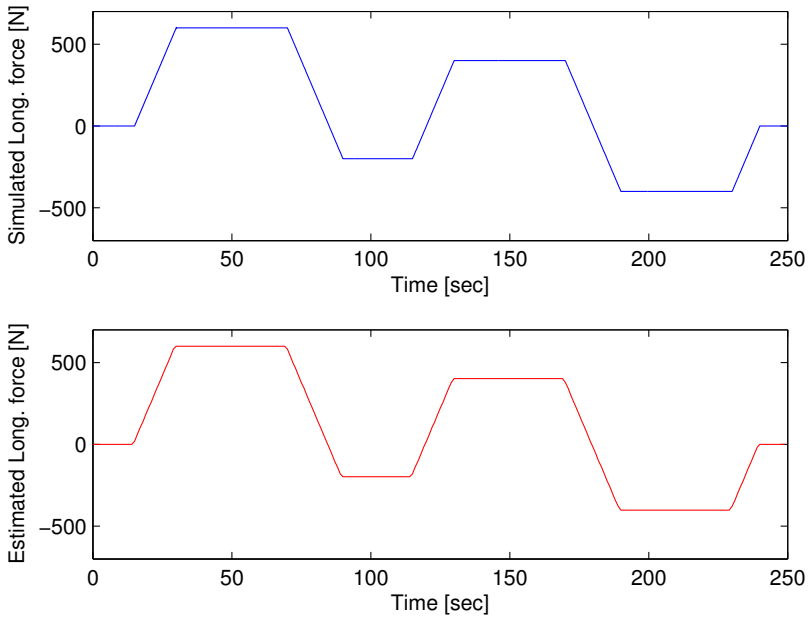

Figure 4.6 Longitudinal tire force estimation.

Based on the longitudinal tire force estimation result, the trajectory of the car can be reconstructed. In another word, the inner points of each time segment can be reproduced by using the estimated tire force as input. This procedure is carried out in the road side station. Thus, the continuous information about the driver behaviors and vehicle status are known during each second. Figure 4.7 shows the vehicle position error between simulated and reconstructed trajectory. During each second, one hundred inner points are reconstructed.

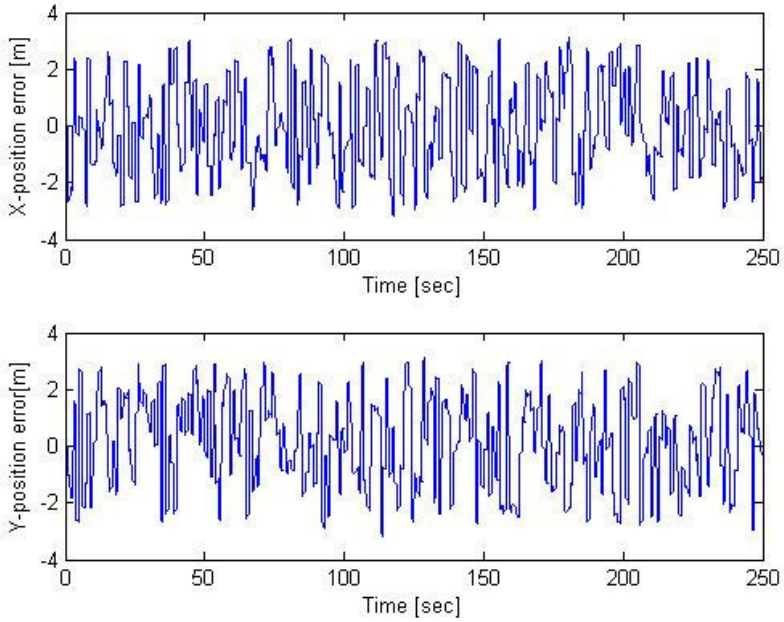

Figure 4.7 Vehicle trajectory error on the X and Y directions.

4.6 Summary

In this chapter, the effort is to develop a novel framework to derive the driver behavioral information from GPS information and vehicle model. The estimation framework includes two parts: vehicle states Kalman Filter estimator and a piecewise optimizer. The performance of the simulation results confirms the feasibility of the proposed approach.

CHAPTER 5

DRIVER BEHAVIOR CLASSFICATION

5.1 Introduction

This chapter describes a driver behavior classification system, which utilizes information about the driving operation behavior (steering angle and throttle/brake positions) and vehicle states (velocity, acceleration, yaw angle, yaw rate, sideslip angle, etc.) to determine whether the driving behavior is abnormal. To avoid the drawback that installing multimodal sensors which may be inconvenient and costly for the general drivers, a low cost GPS receiver is used to acquire four types of signals (longitudinal velocity, yaw angle, lateral and longitudinal positions of the vehicle) instead of using the high cost vehicle data acquisition equipment.

A vehicle-to-station scenario is considered, in which, the GPS data are transmitted from a vehicle to a roadside station when the vehicle is moving along a certain section of the road. The station implements vehicle states estimation task and reproduces the vehicle's interpolation motions every second. Then, the station can determine the driver behaviors (normal or abnormal) by using a Gaussian Mixture Models (GMM)-based classifier and send the detection result back to the vehicle and other interested vehicles that would help drivers avoid the potentially dangerous situation.

Compared with other pattern recognition methods mentioned above, GMM has the following distinct advantages when used in classifying driving behaviors:

1) A linear model can seldom represent driver behaviors. GMM can estimate the probability density distribution of nonlinear model.

2) GMM belongs to the class of "unsupervised" classifier which does not require prior knowledge. Although nobody knows exactly how the driver's error impairs driving performance, GMM method may be able to extract the features of this relationship.

3) GMM method produces more robust performance than traditional learning methods

GMM has been used to analyze the driving behavior in recent research. For example, [140] used GMM method to detect distracted driving based on in-vehicle CAN-bus data. A GMM framework was developed to model the driving behaviors with driving signals (e.g., following distance, vehicle speed) and model pedal operation with features extracted from raw pedal operation signals [141]. Authors modeled driving behavior employing GMM based on driving signals such as brake and accelerator pedal pressure, engine RPM, vehicle speed and steering wheel angle in [142]. In the above research, the critical driving information can be obtained through different methods. For instance, driving information can be directly obtained from the CAN-bus in some cars [140]. The CAN-bus signal contains real-time vehicle information in the form of messages integrating many modules. Usually, the open connector of the CAN-bus is On-Board Diagnostics (OBD-II). However, the CAN-bus signal is not available on the OBD-II connector for all cars. Furthermore, the database used to decode the CAN-bus signal may not be available to the general public or the cost for the database and data acquisition software maybe prohibitive. In addition, the driving information can also be collected by installing additional multimodal sensors, such as gyroscope, steering angle sensors, throttle/brake pedal position sensors, cameras, microphones, and other sensors [141-142]. It is inconvenient and costly for the general drivers to install these devices. In order to

lower the cost and simplify the procedures of data acquisition, this paper uses a low cost GPS receiver to acquire four types of signals (longitudinal velocity, yaw angle, lateral and longitudinal positions of the vehicle) instead of using the high cost vehicle data acquisition. The aim is to reproduce the driver's input commands from the partial discrete knowledge of the vehicle data and use that to classify the driving behavior.

Note that the sideslip angle and yaw rate cannot be measured by the GPS receiver. Since the whole vehicle states are needed to reconstruct the driver's input commands (e.g., steering angle and the longitudinal tire force), the sideslip angle and yaw rate have to be estimated based on the known discrete GPS data points. This is precisely the vehicle state estimation problem. In this paper, the nonlinear extended two-wheel vehicle model is discretized firstly. The sideslip angle and yaw rate can be directly calculated according to the difference equations from the discrete GPS data. Next, the vehicle states estimation results together with the GPS signals are further used to estimate the driver's input commands (the steering angle and longitudinal tire force). Since the vehicle states are discrete, the procedure can be viewed as a piecewise time-independent optimization problem. The length of the time-segment is the same as the period during which the GPS signal is updated. For example, the time-segment is 1s when using GPS receiver with 1Hz updating rate. In the optimization scheme, the optimal steering angle command and longitudinal tire force are calculated by considering the kinematic constraints of the vehicle. Certain features are extracted from the estimated steering and longitudinal tire force. Based on these features, the driving behaviors are divided into two classes by a GMM-based classifier: normal or abnormal.

5.2 Vehicle Model Simulation

The vehicle model and the numerical values of the vehicle characteristics used here are the same as those in Section 4.2.

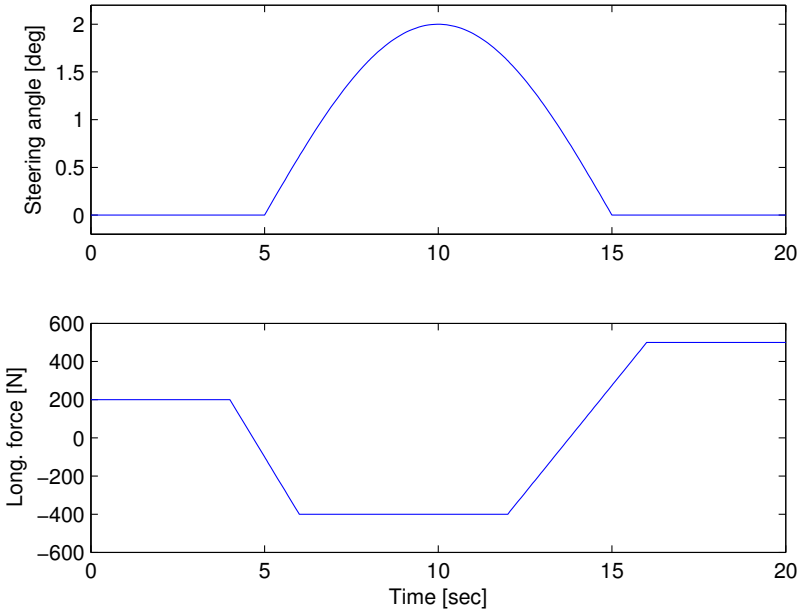

Figure 5.1 The reference commands of model simulation.

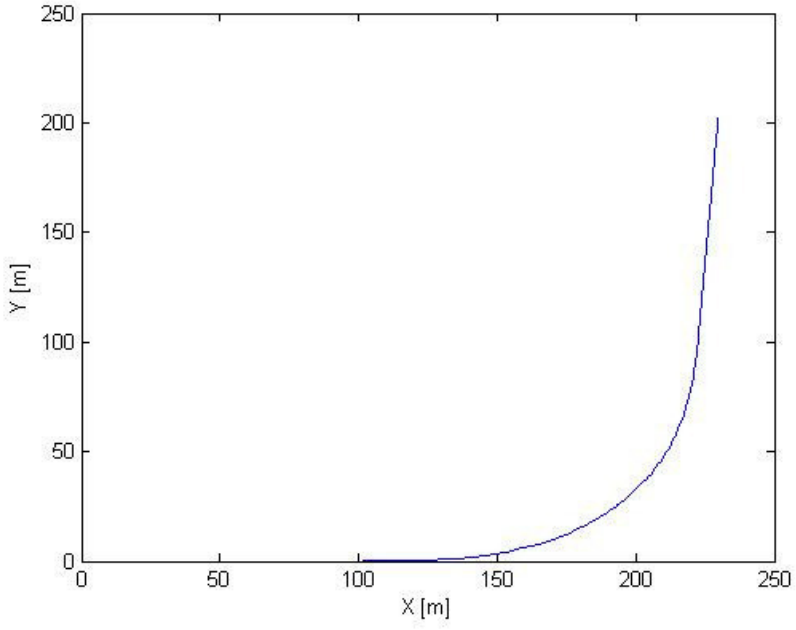

Figure 5.2 The trajectory of a left turn.

Consider the situation when the vehicle makes a left turn, the driver turns the steering wheel to make a left angle and presses the brake pedal to reduce the speed. The reference input commands can be found in Figure 5.1. Using the vehicle model and the vehicle characteristic, a left turn trajectory is simulated, which is shown in Figure 5.2.

In real situation, it is assumed that a low cost 1Hz GPS receiver is used to obtain the information: yaw angle, velocity, X-position, and Y-position. As we know, GPS can provide the measurements of the vehicle's heading angle, velocity, the latitude, and longitude of the location of the vehicle. In order to obtain the driving data for the vehicle coordinate system (ψ, X, Y), the GSP measurements for initial point of a vehicle (origin of the vehicle's coordinate plane) should be used as a reference. It is assumed that the GPS measurements of the vehicle's origin are (ψ_0, X_0, Y_0) and the GPS measurements of the vehicle's current position are (ψ_c, X_c, Y_c). Then, the yaw angle ψ is the difference of the GPS measurements of the heading angle between the current position and the origin of the vehicle, e.g., $\psi = \psi_c - \psi_0$; the vehicle's position for the vehicle coordinate system (X, Y) can be obtained by converting the geographical coordinates (latitude and longitude) of the initial position and the current position into the geographical distance [83].

For computer simulation, the plant outputs for the vehicle coordinate system are simulated. The model outputs are sampled at the rate of 1 Hz. The sampled results are corrupted with additive Gaussian white noise (AWGN) which can be viewed as the errors in the GPS measurements (expressed in the vehicle coordinates system). Denote $\tilde{\psi}_k, \tilde{v}_k, \tilde{X}_k, \tilde{Y}_k \forall k \in [1, \ldots, \ell]$ as the outputs of the vehicle model at the k th second.

$$\tilde{\psi}_k = \psi_k + n_{\psi,k}$$

$$\tilde{v}_k = v_k + n_{v,k}$$

$$\tilde{X}_k = X_k + n_{X,k}$$

$$\tilde{Y}_k = Y_k + n_{Y,k}$$

where $n_{\psi,k}$, $n_{v,k}$, $n_{X,k}$, and $n_{Y,k}$ are the measurement noise for the velocity, yaw angle, X coordinate and Y coordinate, respectively, which are related to the accuracy of the GPS receiver. The measurement noise is assumed to be non-intercorrelated, stationary, white and Gaussian with known covariance. Here, a typical group of accuracy values of the GPS receiver are adopted:

- The velocity accuracy is about $\pm 0.25\text{m/s}$;
- The heading accuracy approaches $\pm 1\text{deg}$;
- The position accuracy is around $\pm 3\text{m}$.

The discrete vehicle states with the random noises included are shown in Figure 5.3.

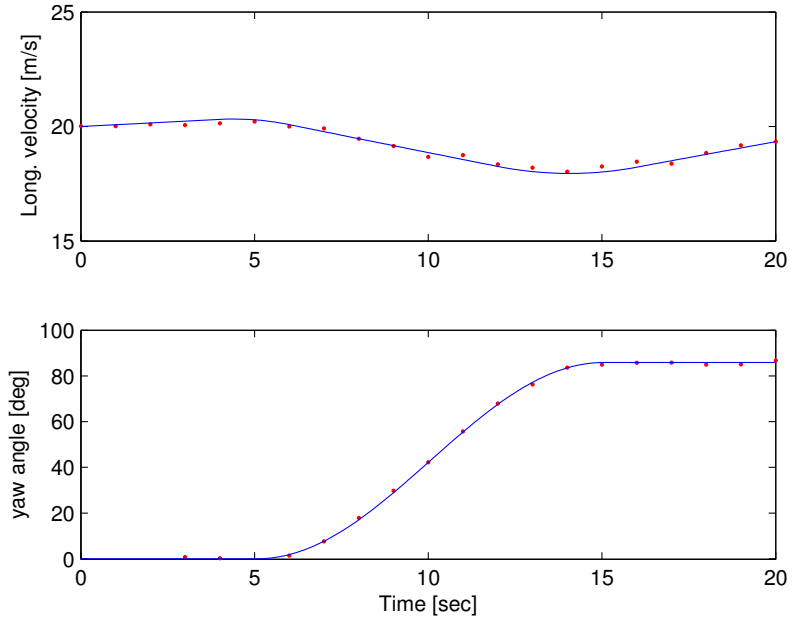

Figure 5.3(a) Noisy sampled vehicle states (velocity and yaw rate).

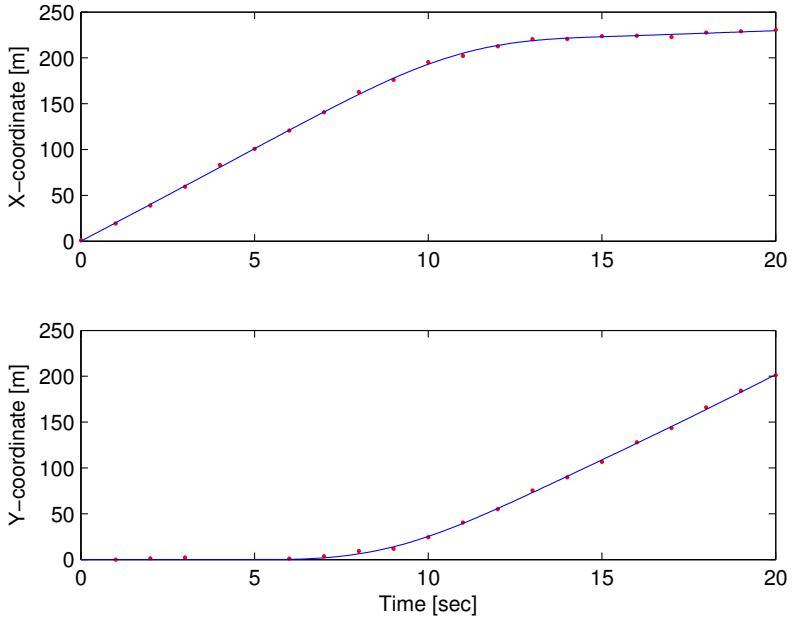

Figure 5.3(b) Noisy sampled vehicle states (X and Y coordinates).

5.3 Sideslip Angle and Yaw Rate

In order to determine the sideslip angle and the yaw rate, the dynamic model of equation (4.3) has to be discretized. The discretization is performed by a forward Euler approximation. The forward Euler method discretizes the continuous system $\dot{x}(t) = f(t, x(t)), x(t_0) = x_0$ by using the first two terms of the Taylor expansion of x, which represents the linear approximation around the point $(t_0, y(t_0))$. One step of the Euler method from t_k to $t_{k+1} = t_k + \Delta t$ is $x_{k+1} = x_k + \Delta t f(t_k, x_k)$. In this case, the step size is $\Delta t = 1s$ because the GPS receiver updates the data every second (sampling rate is 1 Hz). Then, the nonlinear discrete-time system is obtained in the form of

$$\begin{aligned} x_{k+1} &= x_k + A(x_k) + B(x_k)u_k \\ y_k &= \left[y_{1,k}, y_{2,k}, y_{3,k}, y_{4,k}\right]' = \left[\psi_k, v_k, X_k, Y_k\right]' \end{aligned} \tag{5.1}$$

According to the discretized model above, the yaw rate can be calculated by using

$$\dot{\psi}_k = \psi_{k+1} - \psi_k \tag{5.2}$$

The sideslip angle is determined from the expression

$$\beta_k = \psi_k - \arctan\left(\frac{y_{k+1} - y_k}{x_{k+1} - x_k}\right) \tag{5.3}$$

In real situation, the measurements are corrupted by noise. Denote that discrete estimations of the sideslip angle is $\hat{\beta}_k$ and the yaw rate is $\hat{\dot{\psi}}_k$. Therefore, the estimation results will be obtained from the following two estimators:

$$\hat{\beta}_k = \tilde{\psi}_k - \arctan\left(\frac{\tilde{y}_{k+1} - \tilde{y}_k}{\tilde{x}_{k+1} - \tilde{x}_k}\right) \tag{5.4}$$

$$\hat{\dot{\psi}}_k = \tilde{\psi}_{k+1} - \tilde{\psi}_k \tag{5.5}$$

Consider the measurements shown in Figure 5.3. Using the estimators provided in equations (5.4) and (5.5), the sideslip angle and yaw rate estimation results are given in Figure 5.4. The solid lines mark the simulated results from simulation of the continuous nonlinear model. The dots represent the estimated results. It is noted that both of these two estimates are quite accurate.

As mentioned before, this estimation procedure is carried out in the roadside station. When the measurements of two consecutive seconds (say k and $k+1$ second) are obtained, the state estimates at the previous second (k second) are calculated. Therefore, the state estimators are real time.

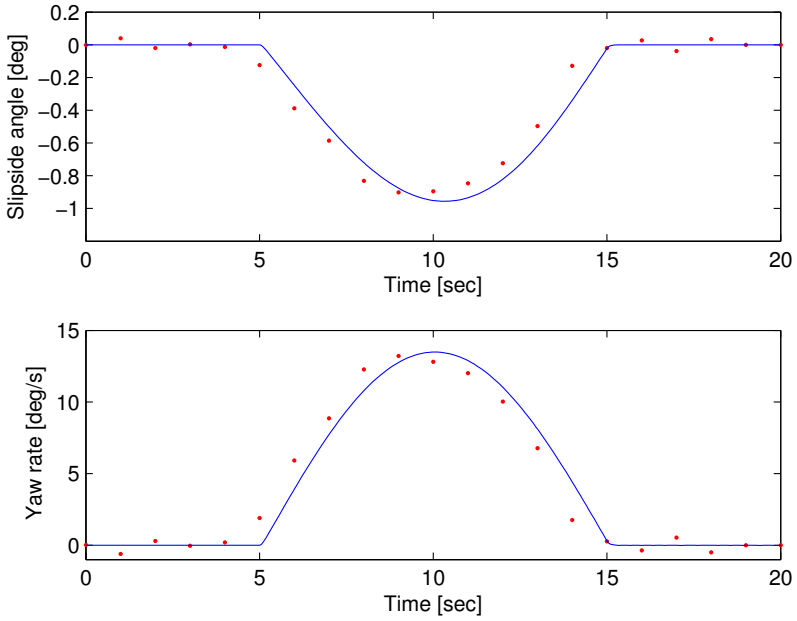

Fig 5.4 Sideslip angle and yaw rate estimation.

5.4 Piecewise Optimization Scheme

In this section, the task is to estimate the continuous driver's input commands which include steering angle and longitudinal tire force. The goal is to find an optimal solution of input commands which makes the trajectory output follows the simulated trajectory as accurately as possible. These are the kinematic constraints of the vehicle. A real time piecewise optimization scheme under such constraints is developed to solve this estimation problem.

At the end of the time segment k , $\tilde{X}_k, \tilde{Y}_k, \tilde{v}_k, \tilde{\psi}_k, \forall k \in [1,\ldots,\ell]$ are the measurements of the GPS receiver, and $\hat{\beta}_k, \hat{\dot{\psi}}_k$ as the estimation results. Let the vector $p_k = \left[\hat{\beta}_k, \tilde{\psi}_k, \hat{\dot{\psi}}_k, \tilde{v}_k, \tilde{X}_k, \tilde{Y}_k\right]'$ be the prior information of the vehicle states. At the end of the time segment k, the output of the discrete model in equation (5.1) is

$y_k = \left[y_{1,k}, y_{2,k,} y_{3,k}, y_{4,k} \right]' = \left[\psi_k, v_k, X_k, Y_k \right]'$. Firstly, the states of the vehicle are initialized with p_{k-1} at the beginning of each time segment k. Secondly, the continuous model in equation (4.3) is simulated for one second for each possible steering angle command $\Delta_{v,k}(t) = \delta_{v,k}, k\text{-}1 \le t < k$ and longitudinal force command, $H_k(t) = h_k, k\text{-}1 \le t < k$. At the end of the time segment k, a cost function is then evaluated for all of the possible input commands, and the input commands that minimize this cost function are chosen.

The cost function is the error term that combines both the position offsets from the actual trajectory and the velocity error from the actual value. The particular form of the cost function in time period k is as follows:

$$C_k\left(\Delta_{v,k}(t), H_k(t)\right) = E_{position,k}^2 + r_v E_{v,k}{}^2 \tag{5.6}$$

where $E_{position}$ and E_v are the position offset and the velocity error of the vehicle relative to the data point k measured by the GPS receiver on the trajectory. Note that there is a length parameter r_v in the cost function which is used to scale the velocity error relative to the position error. $E_{position}$ and E_v can be obtained by the following equations:

$$E_{position,k} = \sqrt{\left(y_{3,k} - \tilde{X}_k\right)^2 + \left(y_{4,k} - \tilde{Y}_k\right)^2} \tag{5.7}$$

$$E_{v,k} = y_{2,k} - \tilde{v}_k \tag{5.8}$$

The optimization algorithm can be summarized as:

$$\min_{\Delta_{v,k}(t), H_k(t)} \sum_{k=1}^{\ell} \left[\left(y_{3,k} - \tilde{X}_k\right)^2 + \left(y_{4,k} - \tilde{Y}_k\right)^2 \right] + r_v \sum_{k=1}^{\ell} \left(y_{2,k} - \tilde{v}_k\right)^2 \tag{5.9}$$

subject to the constraints:

$$
\begin{cases}
\dot{\underline{x}}(t) = A\left(\underline{x}(t)\right) + B\left(\underline{x}(t)\right)u(t) \\
\underline{y}(t) = \left[x_2(t), x_4(t), x_5(t), x_6(t)\right]'
\end{cases}
$$

$$t_{0,k} = k-1 \qquad \forall k \in [1,\ldots,\ell]$$

$$\Delta t = 1$$

$$\underline{x}\left(t_{0,k}\right) = p_{k-1}$$

where $t_{0,k}$ is the start time at each time segment k, and Δt is the length of the time segment. Finally, the solution of the optimization problem is

$$\delta_v^{opt} = \left\{\Delta_{v,k}^{opt}(t), k-1 \le t < k, \forall k \in [1,\ldots,\ell]\right\} \tag{5.10}$$

$$H^{opt} = \left\{H_k^{opt}(t), k-1 \le t < k, \forall k \in [1,\ldots,\ell]\right\}. \tag{5.11}$$

The global search method is employed to solve the above optimization problem. In order to simply the searching procedure, the search range can be determined using discrete kinematics of the vehicle in equation (5.1). The longitudinal force at each time instant k has the approximate form of

$$\hat{H}_k = m\left(\tilde{v}_{k+1} - \tilde{v}_k\right) + \frac{1}{2}c_w \ell_L A \tilde{v}_k^2. \tag{5.12}$$

The steering angle's approximation at each time instant k can be obtained by the expression

$$\hat{\delta}_{v,k} = a\tilde{\psi}_{k+2} + b\tilde{\psi}_{k+1} + c\tilde{\psi}_k + d\hat{\beta}_k \tag{5.13}$$

where the coefficients a, b, c, d are

$$a = \frac{I}{\gamma_v l_v},$$

$$b = \frac{l_h^2 + \gamma_v l_v^2 - 2Iv_k}{v_k \gamma_v l_v}$$

$$c = -\frac{l_h^2 + \gamma_v l_v^2 - Iv_k}{v_k \gamma_v l_v}$$

$$d = -\frac{\gamma_v l_v - l_h}{\gamma_v l_v}.$$

During the time segment k, the search range for the steering angle is $\left[\hat{\delta}_{v,k}, \hat{\delta}_{v,k+1}\right]$ and the search range for the longitudinal force is $\left[\hat{H}_k, \hat{H}_{k+1}\right]$. This will reduce the time needed by the search method.

To evaluate the performance of the piecewise optimization strategy, Figure 5.5 compares the optimal steering angle and the optimal longitudinal tire force estimation results with the reference input commands, respectively. Based on the steering angle and the longitudinal tire force estimation results, the trajectory of the car can be reproduced. In other words, the trajectory interpolation for each time segment can be implemented by using the optimal estimated steering angle and tire force as input commands.

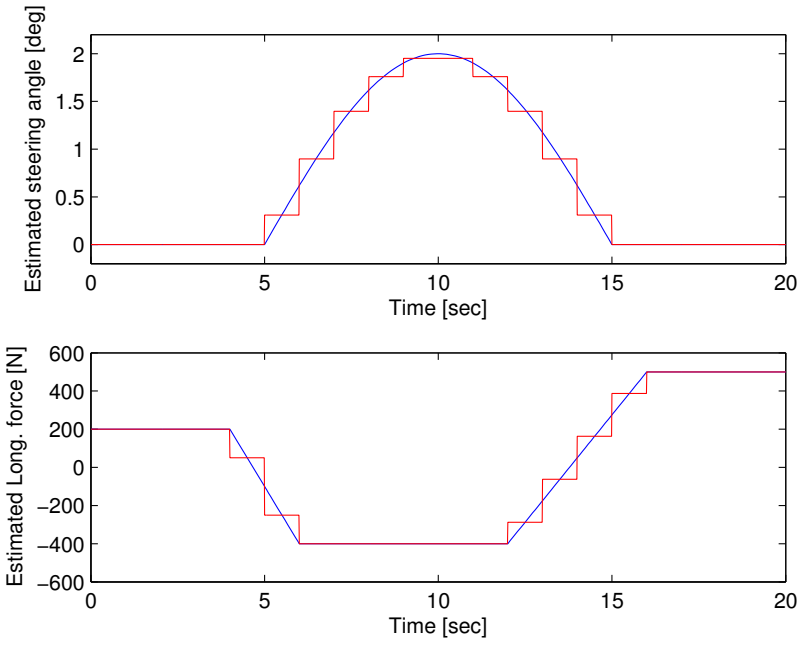

Figure 5.5 Steering angle and longitudinal tire force estimation.

5.5 Driver Behavior Classification

1) Block Diagram:

Figure 5.6 shows the block diagram of proposed scheme. The driving information acquisition and states estimation will be obtained based on the discussion in the previous sections. Feature extraction and GMM-based classifier will be discussed in the next sections

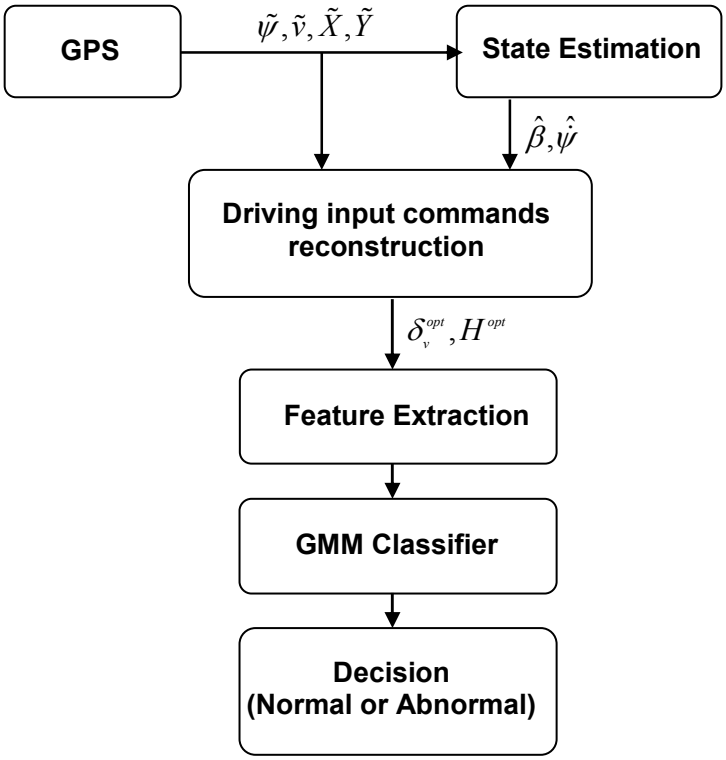

Figure 5.6 Block diagram of the proposed scheme.

2) Gaussian Mixture models as a classifier:

In order to detect whether the driver behavior is normal or not, Gaussian mixture models (GMMs) [70-71] are used as a two-class classifier. The driver's behavior will be divided into two classes which are normal or abnormal.

Gaussian mixture model is a probabilistic model for probability density function (pdf) estimation using a set of multiple Gaussian distributions. GMM have been a powerful nonlinear classification tools in many applications of pattern recognition [72-73], particularly in speech and face recognition. Gaussian mixture models are suitable for classification of driver behaviors. First, a linear model can seldom represent driver behaviors. GMM can estimate the probability density distribution of nonlinear model. Second, GMM belongs to the "unsupervised" classifier category which does not require prior knowledge before training. Third, the GMM method produces more robust performance than traditional learning methods (e.g., logistic regression, multi-layer perceptron). The GMM method may have computational difficulty if the volume of training data becomes great. However, the GMM method is a robust approach to classify the driver behavior.

GMM non-linear pattern classifier works by estimating the underlying probability density functions (pdf's) of the observations. In the GMM classifier, the conditional-pdf of the observation vector with respect to the different classes is modeled as a linear combination of multivariate Gaussian pdf's. Each of them has the following form:

$$p(\mathbf{x}) = \frac{1}{(2\pi)^{\frac{d}{2}} |\Sigma|^{2}} \exp\left(-\frac{1}{2} (\mathbf{x} - \boldsymbol{\mu})^{T} \Sigma^{-1} (\mathbf{x} - \boldsymbol{\mu}) \right) \tag{5.14}$$

where $\mathbf{x}$ is a d-component feature vector, $\boldsymbol{\mu}$ is the d-component vector containing the mean of each feature, Σ is the d-by-d covariance matrix, and $|\Sigma|$ is its determinant. It is noted that each multivariate Gaussian pdf can be completely defined if $\theta = [\boldsymbol{\mu}, \Sigma]$ is known.

In this case, each class (normal or abnormal) is modeled as a GMM based on its own features. The feature vector is denoted as $\mathbf{x}_t$. The assumptions made to build a GMM are the following [74]:

- The samples come from a known number c ($c = 2$) of classes. The two classes are denoted as C_0 (abnormal) and C_1 (normal).
- The priori probabilities $P(C_i)$ for each class C_i are known (They are taken to be all equal to $\frac{1}{c} = \frac{1}{2}$).
- The forms of the class-conditional probability densities $p(\mathbf{x} \mid C_i, \theta_i), i = 1, \ldots, c = 1, 2$ are known for all classes. It is assumed that they are a sum of K multivariate Gaussian probability density functions.
- The unknowns are the values of the parameter vectors $\theta_{i=1,2}$ (for each class, the mean vector and covariance matrix).

Assuming that the probability density function $p(\mathbf{x}_t \mid C_i)$ is a mixture of K multivariate Gaussian distributions:

$$p(\mathbf{x}_t \mid C_i) = \sum_{l=1}^{K} P(l \mid C_i)\, p(\mathbf{x}_t \mid l, C_i) \tag{5.15}$$

where $p(\mathbf{x}_t \mid l, C_i) = N(\boldsymbol{\mu}_{l,i}, \boldsymbol{\Sigma}_{l,i})$ is the probability of $\mathbf{x}_t$ being produced by the Gaussian distribution of index l in class i. $P(l \mid C_i)$ is the prior probability of having a Gaussian distribution l for class i. There are two phases for this classification problem: GMM training and the classification test.

In the training phase, the aim is to estimate the parameters of the GMMs for the two classes: $\Theta_i = \left\{ P\left(l \mid C_i\right), \boldsymbol{\mu}_{l,i}, \boldsymbol{\Sigma}_{l,i}, l = 1, \ldots K \right\}$ with $i = 1, 2$, $l = 1 \ldots K$. An optimization algorithm called Expectation Maximization (EM) [75] is used to estimate all the parameters.

The progress of EM algorithm: there are m observations of the features for each class C_i : $\mathbf{X}^{C_i} = \left[\mathbf{x}_1^{C_i}, \mathbf{x}_2^{C_i}, \ldots, \mathbf{x}_m^{C_i} \right]$. Assuming that the observations are independent and identically distributed, the likelihood that the entire set of observations has been produced by class C_i is:

$$p\left(\mathbf{X} \mid \Theta_i, C_i\right) = \prod_{t=1}^{m} p\left(\mathbf{x}_t \mid C_i\right). \tag{5.16}$$

Using the above likelihood function, EM algorithm gives the maximum likelihood estimates of all the parameters $\hat{\Theta}_{ML,i} = \arg\max \log p\left(\mathbf{X} \mid \Theta_i, C_i\right)$. Since it is hard to directly maximize the log-likelihood function, EM algorithm maximizes the lower-bound of log-likelihood function $F\left(q, \Theta\right)$. It has been proved that maximizing the lower-bound is equivalent to maximizing the expected log-likelihood [84]. EM algorithm is consisted of two steps: E-step and M-step:

E-step: $q^{(t+1)} = \arg\max_{q} F\left(q, \Theta^{(t)}\right)$

M-step: $\Theta^{(t+1)} = \arg\max_{\Theta} F\left(q^{(t+1)}, \Theta\right)$

Making a first guess on the values of the Θ_i and compute E-step and M-step. And the algorithm converges to a local optimum after conducting iterations. Note that the training

set provided to the GMM has to be well thought out in order for the model to be general enough and avoid the common problem of over-fitting the training data.

In the classification phase, the classification tests using the trained GMMs is performed. According to the Bayesian rule, a feature vector $\mathbf{x}_t$ is said to belong to class i if it maximizes

$$p(C_i \mid \mathbf{x}_t) = \frac{p(\mathbf{x}_t \mid C_i)\, p(C_i)}{p(\mathbf{x}_t)}. \tag{5.17}$$

In the case it is assumed that the two classes occur with the same probability, $p(C_0) = p(C_1) = 0.5$. It is actually only concerned with maximizing $p(\mathbf{x}_t \mid C_i)$.

The decision rule for the two-class classifier is:

- $\mathbf{x}_t$ belongs to the abnormal case if $p(\mathbf{x}_t \mid C_0) > p(\mathbf{x}_t \mid C_1)$;
- Otherwise, $\mathbf{x}_t$ belongs to the normal case.

5.6 Feature Extraction

Since the estimated steering angle and longitudinal tire force are both continuous segment signals, root mean square (RMS) statistical method is suitable to reflect the driver's input activities [85-86]. For example, RMS of the steering angle can reflect the driver's steering maneuvers; RMS of the longitudinal tire force can reflect the throttle and brake pedal operation.

RMS is a second order statistical measure of the magnitude of a continuously varying function (or waveform). The RMS formula of a continuous function $f(t)$ defined over the time interval $T_1 \le t \le T_2$ has the following form [87]:

$$f_{rms} = \sqrt{\frac{1}{T_2 - T_1}\int_{T_1}^{T_2}\left[f(t)\right]^2 dt} \tag{5.18}$$

In this study, the feature vector provided to the GMM-based classifier consists of the RMS of the reconstructed steering angle and longitudinal tire force.

$$\mathbf{x}_t = \left[\left|\delta^{opt}\right|, \left|H^{opt}\right|\right] \tag{5.19}$$

5.7 Simulation Results

The performance of abnormal driver behavior detection is verified by simulating the vehicle model for a left turn (described in section 5.2).

1) Simulating abnormal driving behavior:

Abnormal driving behaviors usually occur when the driving patterns the drivers make are not smooth, e.g., the sharp movement of the steering wheel [77]. In the UMTRI research in the SAVE-IT project, it was found that when drivers were performing an in-vehicle task, they controlled their speed by intermittently adjusting the throttle [78]. According to the above facts and experiments, some assumptions are made to simulate the abnormal driving patterns for training set:

- Large variations of the reference steering angle and the longitudinal tire force within a short period of time may reflect abnormal driving behaviors. The form of such large variations is modeled as AWGN.
- It is assumed that the driving behavior can be viewed as an abnormal case when:

$$\frac{\left|A_{\delta_v,error}\right|}{\left|A_{\delta_v,ref}\right|} > 20\% \quad \text{or} \quad \frac{\left|A_{H,error}\right|}{\left|A_{H,ref}\right|} > 20\%,$$

where $\left|A_{\delta_v,ref}\right|,\left|A_{H,ref}\right|$ are the RMS amplitude of the reference steering angle and the reference longitudinal tire force, respectively. $\left|A_{\delta_v,error}\right|,\left|A_{H,error}\right|$ are the RMS amplitude of the variations between the actual and the reference values of the steering angle and the longitudinal tire force, respectively. The values of $\left|A_{\delta_v,error}\right|$ and $\left|A_{H,error}\right|$ are generated using AWGN method.

2) GMM training:

The probability density function $p(\mathbf{x}_t \mid C_i),(i=1,2)$ is modeled by using four mixtures of Gaussian distribution $(K=4)$. The number of training data for both normal driving and abnormal driving are $M_n = M_a = 50$. EM algorithm is used to train the two GMMs. Experiments demonstrated that the EM method had an acceptable computational load with this volume of training data.

3) Testing phase:

Since the goal is detecting the abnormal driving behaviors, only classification performance for the abnormal cases is needed to test. The number of testing data for abnormal driving is $N_a = 25$. Fifty independent simulations and tests were implemented.

4) Detection Results:

Table 5.1 summarizes the classification results. The average accuracy of the abnormal driving behavior detection is 87.2%, which means that the average miss detection rate is approximately 12.8%. The reason for the miss detection is that the GPS data is sparse and somewhat inaccurate. If the GPS with a higher update rate is adopted, a more accurate detection result will be achieved.

Table 5.1 Classification Results

The number of Gaussian mixtures:	$K = 4$
The size of training set (normal):	$M_n = 50$
The size of training set (abnormal):	$M_a = 50$
The size of testing set (abnormal):	$N_a = 25$
The times of testing:	50
Average classification accuracy:	87.2%
Miss detection rate:	12.8%

5.8 Summary

In the proposed driver behavior classification system, data obtained by a GPS are employed to reproduce the driver behavior. Gaussian Mixture model (GMM) is used to capture the sequence of driving characteristics according to the reconstructed vehicle's information and it is also used as a classifier to assign the driving behavior to normal or abnormal category.

In this work, it is considered using a low cost 1Hz GPS receiver as the vehicle data acquisition equipment instead of the costly sensors (steering angle sensor, throttle/brake position sensor, etc). The nonlinear extended two-wheel vehicle dynamic model is adopted in this study. Firstly, two states, i.e., the sideslip angle and the yaw rate are calculated since they are not available from GPS measurements. Secondly, a piecewise optimization scheme is proposed to reconstruct the driving behaviors which include the steering angle and the longitudinal force. Finally, a GMM classifier is applied to identify whether the driver behavior is unsafe.

Simulation results show that the GMM based driver behavior classification scheme can effectively detect the potentially dangerous situation when the driving behavior is abnormal.

CHAPTER 6

LATERAL CONTROL FOR AUTOMATED STEERING

6.1 Introduction

To overcome the disadvantages of the two lateral control methods introduced in [58] and [79] (which are briefly described in Section 2.7), this chapter proposes a novel design of a look-down reference control system using only a GPS and front sensor. Compared to the lateral control system proposed in [58], the basic idea and general structure of the proposed control system is the same. The novelties lie in 1) utilizing a GPS and front sensor to obtain data, and 2) designing effective steering angle estimator and road curvature estimator for real-time situations. This resultant system has the advantage of low cost and can realize the real-time estimation of road curvature. In the proposed system, a front sensor is used to measure the front lateral displacement and a GPS is used to measure the heading of the vehicle. According to such measurements, the steering angle can be estimated in real-time from an extended observer instead of being measured by additional costly sensors (e.g., feedback potentiometer attached to the front wheel in [58], or gyroscope at center of gravity in [79]). Accordingly, the road curvature is estimated based on its relationship with the steering angle in real-time. This can overcome the restriction of pre-recording the road geometry in [58] and pre-encoding the road information in [79], representing a significant advance in the field. Therefore, this approach is able to handle the real-time changes of road geometry without introducing large sudden transition changes into the control loop as in [58]. It is noticed that [58] employs the parameters of test vehicle and controller in [20] to validate its control system. In [79], a lateral displacement controller is designed according to the actual experimental data in the California PATH project. Such controller

is well developed and demonstrated to be robust for practical highway environment. Similar to [58], the proposed system also employs the well developed controller in [79]. In addition, the proposed system is also validated by using the data from the California PATH test vehicle used in [79]. The vehicle dynamic and this control system are both simulated with MATLAB Simulink. The proposed estimation and control algorithms are validated by computer simulation results. The simulation results show that this lateral steering control system achieves a good and robust performance for vehicles that follow or track a reference path and therefore would enhances driver safety.

6.2 Vehicle Dynamic

6.2.1 Single Track Vehicle Dynamics

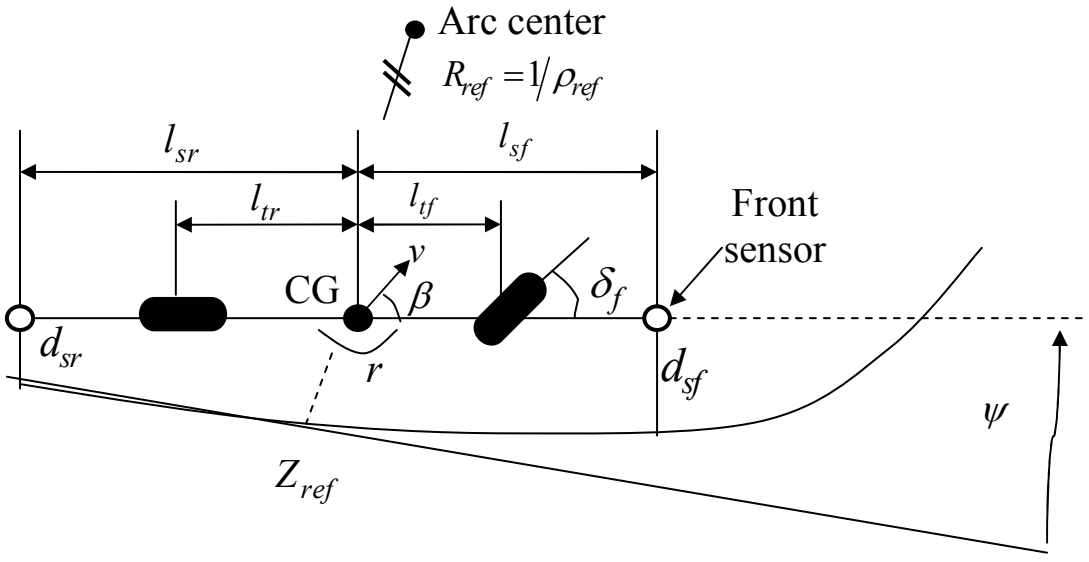

Figure 6.1 Single track model including path tracking.

This vehicle dynamic used here is the single track model described in Section 3.3. In this case, sketch of a vehicle following a lane reference (Z_{ref}) is shown in Figure 6.1. For the look-down reference system here, the front lateral displacement of the vehicle from the lane reference d_{sf} is measured by using an actual magnetic sensor at the front bumper. d_{sr} corresponds to the rear lateral displacement. Since the rear sensor does not exist at the rear bumper, d_{sr} is not available but can be viewed as a measurement by a "virtual magnetic sensor". The sensors are mounted at l_{sf} in the front of and l_{sr} behind of the center of gravity (CG). The curvature of the reference track is ρ_{ref} , which is the reciprocal of the track radius R_{ref} . δ_f is the steering angle, β represents the side slip angle, ψ is the heading orientation, r denotes the yaw rate and v is the velocity of the vehicle.

The state space representation for this model can be expressed in two ways described in Section 3.3:

$$\dot{X} = AX + B_1\delta_f - B_2\rho_{ref} \tag{6.1}$$

where,

$$X = \begin{bmatrix} \beta \\ r \\ \psi \\ d_{sf} \end{bmatrix}$$

$$A = \begin{bmatrix} a_{11} & a_{12} & 0 & 0 \\ a_{21} & a_{22} & 0 & 0 \\ 0 & 1 & 0 & 0 \\ v & l_s & v & 0 \end{bmatrix}$$

$$B_1 = \begin{bmatrix} b_{11} \\ b_{21} \\ 0 \\ 0 \end{bmatrix}$$

$$B_2 = \begin{bmatrix} 0 \\ 0 \\ v \\ 0 \end{bmatrix}$$

The other representation is:

$$\dot{\underline{X}} = \underline{A}\underline{X} - \underline{B}U \tag{6.2}$$

where,

$$\underline{X} = \begin{bmatrix} d_{sf} \\ \dot{d}_{sf} \\ d_{sr} \\ \dot{d}_{sr} \end{bmatrix}$$

$$U = \begin{bmatrix} \delta_f \\ \rho_{ref} \end{bmatrix}$$

$$\underline{A} = \begin{bmatrix} 0 & 1 & 0 & 0 \\ \underline{a}_{21} & \underline{a}_{22} & -\underline{a}_{21} & \underline{a}_{24} \\ 0 & 0 & 0 & 1 \\ \underline{a}_{41} & \underline{a}_{42} & -\underline{a}_{41} & \underline{a}_{44} \end{bmatrix}$$

$$\underline{B} = \begin{bmatrix} 0 & 0 \\ \underline{b}_{21} & -v^2 \\ 0 & g_4 v \\ \underline{b}_{41} & -v^2 \end{bmatrix}$$

The first vehicle model is used to design the steering angle observer and the second one is used to develop the lateral displacements. The values of the vehicle's parameters used for the subsequent designs of the steering angle observer, displacements estimator and controller are based on a 1986 Pontiac 6000 STE sedan, an experimental vehicle used by the California PATH program (see [58] and [79]). All parameters are constant and are

assumed to be known. The descriptions and values of the vehicle plant parameters are listed in Table 6.1.

Table 6.1 Parameters and Values for Vehicle Dynamic

Symbol	Definition	Values
m	Vehicle mass	1573 kg
I	Yaw moment of inertia	2873 kgm^2
l_{tf}	Distance from front axles to center of gravity (CG)	1.1m
l_{tr}	Distance from rear axles to CG	1.58m
l_{sf}	Distance from front sensor to CG	1.96m
l_{sr}	Distance from rear sensor to CG	2.49m
c_f	Cornering stiffness of front tire	80000 N/rad
c_r	Cornering stiffness of rear tire	80000 N/rad
μ	Road adhesion factor	1 (dry road), 0.5(wet road)

6.2.2 Actuator Dynamics

The steering actuator of the Pontiac 6000 STE sedan is formulated as a third-order low-pass model, which is used to generate the steering angle δ_f. A low-bandwidth actuator is a low-pass solution. This actuator is considered in the control design phase and it is a linearized third-order low-pass actuator model, which can avoid excitation and saturation. This actuator has a complex pole pair at 5Hz with 0.4 damping, and a third pole is at 10Hz. The transfer function [58] is:

$$A(s)=\frac{80000}{(s+62.8)(s+12.56+28.77j)(s+12.56-28.77j)} \tag{6.3}$$

This actuator can avoid excitation and saturation, with a complex pole pair at 5 Hz with 0.4 damping, and a third pole at 10 Hz.

6.3 State Estimation

6.3.1 Relationship Between Road Curvature and Steering Angle

In the situation that the speed of the car is steady, the car will trace a circle of a certain radius (R) if the steering angle is constant. The vehicle path curvature is the reciprocal of the road radius. In [80], it has been proved that the vehicle path curvature can be estimated via two methods: 1) least-squares method and 2) method based on the mathematical representation of the vehicle model. In this study, the former one "linear-squares fitting method" is adopted, in which, only information of the steering angle is needed. On the contrast, the information of yaw angle and yaw rate are needed if the second method is adopted. Generally, the estimation of yaw angle and yaw rate are more difficultly implemented than the estimation of steering angle. Therefore, "linear-squares fitting method" has the advantage of simple and fast computation.

Since the vehicle will follow the road geometry accurately in a steering control system, the vehicle path curvature can be approximately viewed as road curvature [79]. Therefore, the road curvature approximately equals to the reciprocal of the road radius ($\rho \approx \frac{1}{R}$). The relationship between the road curvature ($\rho = \frac{1}{R}$) and the steering angle (δ_f)

is nearly a straight line according to [80] and the above approximation. It can be approximated as

$$\rho = \alpha + \gamma\delta_f \tag{6.4}$$

where, parameters α and γ are the constant parameters.

α and β can be determined through repeated independent simulations repeated for .many times (say, 500 times). On the one hand, the vehicle model used in the simulation only employs the first two variables (β and r) in equation (6.1). Therefore, the steering angle δ_f is the only input. Therefore, the front wheel steering angle δ_f is the only input. The subsystem of the model of equation (6.1) is:

$$\begin{bmatrix} \dot{\beta} \\ \dot{r} \end{bmatrix} = \begin{bmatrix} a_{11} & a_{12} \\ a_{21} & a_{22} \end{bmatrix} \begin{bmatrix} \beta \\ r \end{bmatrix} + \begin{bmatrix} b_{11} \\ b_{21} \end{bmatrix} \delta_f \tag{6.5}$$

The coordinates of the vehicle position to further calculate the values of the road curvature ρ is introduced. The derivative of the vehicle position coordinates are:

$$\dot{X} = v\cos\beta \tag{6.6}$$

$$\dot{Y} = v\sin\beta \tag{6.7}$$

Therefore, the entire vehicle dynamic is formed from the combination of equations (6.5) - (6.7) with the following nonlinear state space representation:

$$\begin{bmatrix} \dot{\beta} \\ \dot{r} \\ \dot{X} \\ \dot{Y} \end{bmatrix} = \begin{bmatrix} a_{11}\beta + a_{12}r \\ a_{21}\beta + a_{22}r \\ v\cos\beta \\ v\sin\beta \end{bmatrix} + \begin{bmatrix} b_{11} \\ b_{21} \\ 0 \\ 0 \end{bmatrix} \delta_f \tag{6.8}$$

The road curvature can be calculated by the following expression:

$$\rho = \frac{1}{R} = \frac{1}{\sqrt{X^2 + Y^2}} \tag{6.9}$$

During the independent simulations, the values of the steering angle δ_f are randomly sampled. Based on the road curvature and the steering angle experimental data used or obtained in those independent simulations, the unknown parameters α and γ can be calculated by using the linear least squares estimation method [81]. Then, the linear relationship between the road curvature and the steering angle is determined. If the steering angle is already estimated ($\hat{\delta}_f$), the road curvature estimation $\hat{\rho}$ is realized according to their linear relationship:

$$\hat{\rho} = \alpha + \gamma \hat{\delta}_f \tag{6.10}$$

6.3.2 Steering Angle Estimation

Consider the front displacement d_{sf} and the heading angle ψ as the outputs of the model in equation. (6.1), the plant is described as:

$$\dot{X} = AX + B_1 \delta_f - B_2 \rho_{ref} \tag{6.11}$$

$$\mathbf{y} = CX$$

with

$$C = \begin{bmatrix} 0 & 0 & 1 & 0 \\ 0 & 0 & 0 & 1 \end{bmatrix}$$

$$\mathbf{y} = \begin{bmatrix} \psi \\ d_{sf} \end{bmatrix}.$$

It is assumed that the second-order derivative of the steering angle is zero ($\ddot{\delta}_f = 0$). The reference road curvature input adopts the linear expression

$$\rho_{ref} = \alpha + \gamma \delta_f \tag{6.12}$$

Furthermore, two additional state variables are introduced: the first-order and second-order δ_f and $\dot{\delta}_f$. The model in equation (6.1) is then extended to a new six-order system which has no input signal:

$$\mathrm{X}^E = \mathrm{A}^E \mathrm{X}^E - \mathrm{B}^E \tag{6.13}$$

$$\mathbf{y} = \mathbf{C}^E \mathrm{X}^E$$

with

$$\mathrm{X}^E = \begin{bmatrix} X \\ \delta_f \\ \dot{\delta}_f \end{bmatrix} = \begin{bmatrix} \beta \\ r \\ \psi \\ d_{sf} \\ \delta_f \\ \dot{\delta}_f \end{bmatrix}$$

$$\mathrm{A}^E = \begin{bmatrix} A & B_1 - \gamma B_2 & \mathbf{0}_{4\times1} \\ \mathbf{0}_{4\times1} & 0 & 1 \\ \mathbf{0}_{4\times1} & 0 & 0 \end{bmatrix}$$

$$\mathrm{B}^E = \begin{bmatrix} \alpha B_2 \\ 0 \\ 0 \end{bmatrix}$$

$$\mathbf{C}^E = \begin{bmatrix} C & \mathbf{0}_{2\times1} & \mathbf{0}_{2\times1} \end{bmatrix}$$

$$\mathbf{y} = \begin{bmatrix} \psi \\ d_{sf} \end{bmatrix}.$$

X, A, B_1 and B_2 defined in equation. (6.1) and C is defined in equation. (6.11).

Since the steering angle δ_f is currently one of the state variables, its value can be estimated by a state observer. Such continuous-time observer for the six-order extended model (equation (6.13)) has the following structure:

$$\dot{\hat{\mathrm{X}}}^{E} = \mathrm{A}^{E}\hat{\mathrm{X}}^{E} - \mathrm{B}^{E} + L\left(\overline{\mathbf{y}} - \mathbf{C}^{E}\hat{\mathrm{X}}^{E}\right) \tag{6.14}$$

$\hat{\mathrm{X}}^{E}$ is the estimation of the vehicle states:

$$\hat{\mathrm{X}}^{E} = \left[\hat{\beta} \quad \hat{r} \quad \hat{\psi} \quad \hat{d}_{sf} \quad \hat{\delta}_{f} \quad \dot{\hat{\delta}}_{f}\right]^{T} \tag{6.15}$$

The continuous-time vector $\overline{\mathbf{y}}$ is produced by two first-order holds used to interpolate the discrete measurement vector $\mathbf{y}^{*}$. ψ^{*} corresponds to the discrete measurement of the vehicle's heading angle from the GPS and d_{sf}^{*} is the discrete measurement of the vehicle's front lateral displacement.

$$\overline{\mathbf{y}} = \begin{bmatrix} \overline{\psi} \\ \overline{d}_{sf} \end{bmatrix} \tag{6.16}$$

$$\mathbf{y}^{*} = \begin{bmatrix} \psi^{*} \\ d_{sf}^{*} \end{bmatrix} \tag{6.17}$$

In real life situation, d_{sf}^{*} is the discrete measurement from the front sensor. However, ψ^{*} is not the direct measurement of the heading angle from the GPS since the measurements of the heading angle provided by the GPS are values in the geographic coordinate system. In order to obtain the heading angle for the vehicle coordinate system ψ^{*}, the GSP measurement of the heading angle at the initial point of a vehicle (origin of the vehicle coordinate plane) should be used as a reference. For example, ψ^{*} is the difference of the GPS measurements of the heading angle between the current position and the origin of a vehicle. During simulation, d_{sf}^{*} is a simulated discrete value of the vehicle's front lateral displacement. It is assumed that the GPS measurement of the heading angle for

the initial position of a vehicle is 0 degree. ψ^* corresponds to the simulated discrete value of the vehicle's heading angle.

In order to choose the optimal gain (L), this state observation problem is solved by by solving its dual problem. Here, the linear quadratic regulator (LQR) theory is applied [82]. The parameters for LQR are adjusted by experiments and an accurate estimation of the steering angle ($\hat{\delta}_f$) is obtained from the fifth variable of $\hat{\mathrm{X}}^E$. Correspondingly, the estimation of the actual road curvature ($\hat{\rho}_{ref}$) is given by:

$$\hat{\rho}_{ref} = \alpha + \gamma\hat{\delta}_f \tag{6.18}$$

6.3.3 Lateral Displacement Estimation

The front and rear lateral displacements (d_{sf} and d_{sr}) must be estimated in order to design the steering feedback controller. The front magnetic sensor measures the actual front lateral displacement with respect to the road (d_{sf}^*). Based on the single track vehicle model in equation (6.2), the estimator has the form of

$$\dot{\hat{\underline{X}}} = \underline{A}\hat{\underline{X}} + \underline{B}\hat{U} + \underline{L}\left(\overline{d}_{sf} - H\hat{\underline{X}}\right) \tag{6.19}$$

$\underline{A}$ and $\underline{B}$ describe the state-space vehicle dynamics in equation (6.2). $\hat{\underline{X}}$ is the estimation of the vehicle state with the following structure:

$$\hat{\underline{X}} = \begin{bmatrix} \hat{d}_{sf} \\ \dot{\hat{d}}_{sf} \\ \hat{d}_{sr} \\ \dot{\hat{d}}_{sr} \end{bmatrix} \tag{6.20}$$

The front magnetic sensor is represented by:

$$H = \begin{bmatrix} 1 & 0 & 0 & 0 \end{bmatrix} \tag{6.21}$$

$\hat{U}$ is composed of an estimation of the steering angle ($\hat{\delta}_f$) and the actual road curvature ($\hat{\rho}_{ref}$), and they are provided by the estimators in Section 6.3.2.

$$\hat{U} = \begin{bmatrix} \hat{\delta}_f \\ \hat{\rho}_{ref} \end{bmatrix} \tag{6.22}$$

$\overline{d}_{sf}$ is the output of a first-order hold used to interpolate the discrete measurements of the front lateral displacement provided by front sensor (d^*_{sf}).

The proportional gain $\underline{L}$ is defined as:

$$\underline{L} = l \begin{bmatrix} 1 & 1 & 1 & 1 \end{bmatrix} \tag{6.23}$$

and is chosen to achieve a small estimation error. The value l is gain scheduled related to the vehicle velocity [19].

The estimator in equation (6.19) allows for the estimation of the front and rear lateral displacements ($\hat{d}_{sf}$ and $\hat{d}_{sr}$). Note that the estimated $\hat{d}_{sf}$ can be viewed as the actual measurement from the front sensor, which physically exists. And, the estimated $\hat{d}_{sr}$ is the measurement from a "virtual rear sensor", which does not physically exist.

6.4 Lateral Control Design

6.4.1 System Block Diagram

A block diagram of the lateral steering control system is shown in Figure 6.2. The single track vehicle dynamic, steering actuator and feedback controller are described in Section 6.2.1, Section 6.2.2 and Section 6.4.2.

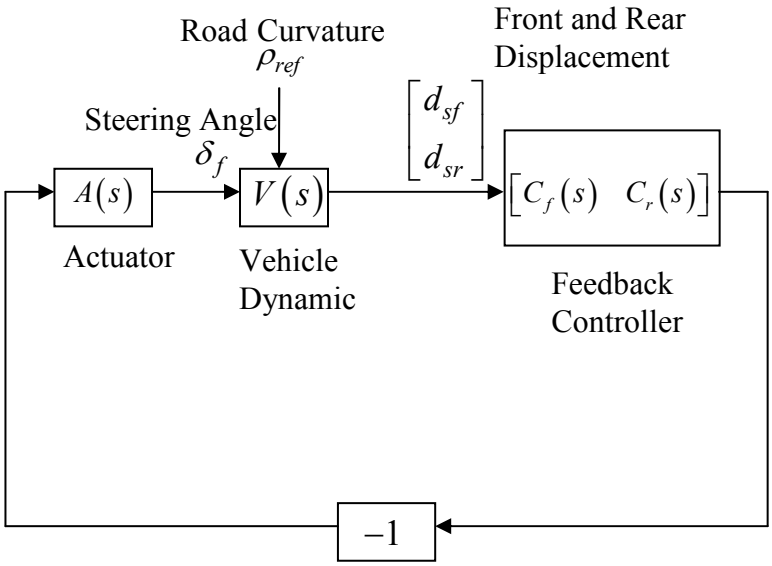

Figure 6.2 Block diagram of lateral steering control system using the estimations of front and rear lateral displacements as feedback.

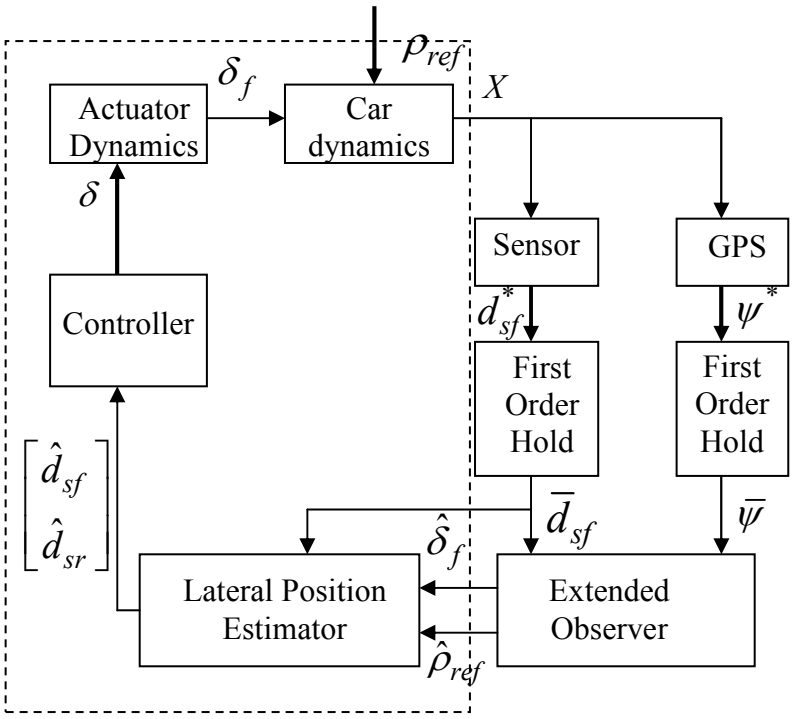

Figure 6.3 Implementation of the lateral control system.

Figure 6.3 shows the implementation of the entire closed-loop lateral steering control system. The boxed pad in Figure 6.3 shows the steering control by using the estimations of front and rear displacements ($\hat{d}_{sf}$ and $\hat{d}_{sr}$) as feedback, which is similar to the lateral control system developed in [58]. The improvement is that a GPS and a front sensor are used as the data acquisition devices. d_{sf}^{*} and ψ^{*} are the discrete measurements for the front lateral displacement and the heading angle, respectively. Continuous-time values of front lateral displacement and heading angle ($\overline{d}_{sf}$ and $\overline{\psi}$) are both provided by a first-zero hold, which is used to interpolate each discrete measurement. The proposed system only has one front magnetic sensor. The second rear sensor does not physically exist, but it could be viewed as a virtual sensor. The information of the rear sensor can be provided by the lateral displacements estimation procedure described in Section 6.3.3. The estimations of steering angle and actual road curvature are realized in Section 6.3.2. The feedback controller will be developed in the following section.

6.4.2 Feedback Controller Structure

The feedback controller structure in Figure 6.3 was developed in [79]. The controller structure has three poles, which could prevent the displacement measurements noise propagating through the closed loop system. Such controller provides good damping at all frequencies to prevent excitation of a single noise frequency and controller roll-off to protect the actuator from high frequency noise. Besides, such controller is robust with respect to changes in the road adhesion parameter (e.g., μ reduces from 1 to 0.5) and presents acceptable levels of maximum lateral displacement to step inputs [58, 79].

The structure of the controller is:

$$\begin{bmatrix} C_f(s) & C_r(s) \end{bmatrix} \tag{6.24}$$

where,

$$C_f(s) = \frac{K_{DD_f} s^2 + K_{D_f} s + K_{P_f}}{\left(s/\omega_2 + 1\right)\left(s^2/\omega_1^2 + 2D/\omega_1 s + 1\right)} + \frac{K_I}{s}$$

$$C_r(s) = \frac{K_{DD_r} s^2 + K_{D_r} s + K_{P_r}}{\left(s/\omega_2 + 1\right)\left(s^2/\omega_1^2 + 2D/\omega_1 s + 1\right)}$$

The parameters of the controller structure are chosen as:

- Denominator poles :

$$\omega_1 = \omega_2 = 4\pi\,.$$

- Damping factor:

$$D = 0.8\,.$$

- Integral gain:

$$K_I = 0.1;$$

- Zeros and the steady-state gains of $C_f(s)$:

$$K_{DD_f} = 0.0001,$$

$$K_{D_f} = 0.087,$$

$$K_{P_f} = 0.51,$$

- Zeros and the steady-state gains of $C_r(s)$:

$$K_{DDr} = 0,$$

$$K_{Dr} = -0.024,$$

$$K_{Pr} = -0.28.$$

6.5. Simulation Results

The state estimator and feedback controller design shown in Figure 6.3 is implemented and tested with the data from the Pontiac 6000 STE sedan in the MATLAB Simulink environment. The plant parameters used are listed in Table 6.1. A GPS is carried in the vehicle and it is assumed that the sampling rate is 1 second. A magnetic sensor is installed at the front bumper and the sampling rate for all simulations is 1second. In order to test the robustness of the controller for actual situations, the simulations of the GPS and the magnetic sensor signals are carried out by introducing additive white Gaussian noise (AWGN). The measuring noise of the GPS is a normal distribution with mean of 0 degree and variance of 1 degree^2 or $N(0,1)$. The measuring noise of the displacement sensor is a normal distribution with mean of 0cm and variance of 1cm^2 or $N(0,1)$.

The vehicle's reference path consists of a straight section, a right turn followed by a left turn, another right turn and finally a straight section. There are no transitions between the curves to obtain the step response. The radius of each turn is $R_{ref} = 800\text{m}$, which means that the road curvatures for each turn is $\rho_{ref} = 1.25 \times 10^{-3}$ / m. The simulation time is for 60s. This road curvature map of the reference track is shown in Figure 6.4. In the following simulations, four different test cases with speeds of $v = 45\,\text{mi/h}$ ($v = 20\,\text{m/s}$) and $v = 80\,\text{mi/h}$ ($v = 35.56\,\text{m/s}$, a highway speed) are considered, respectively, on a dry road

($\mu = 1$) and wet road ($\mu = 0.5$). The parameters used for such four test cases are listed in Table 6.2.

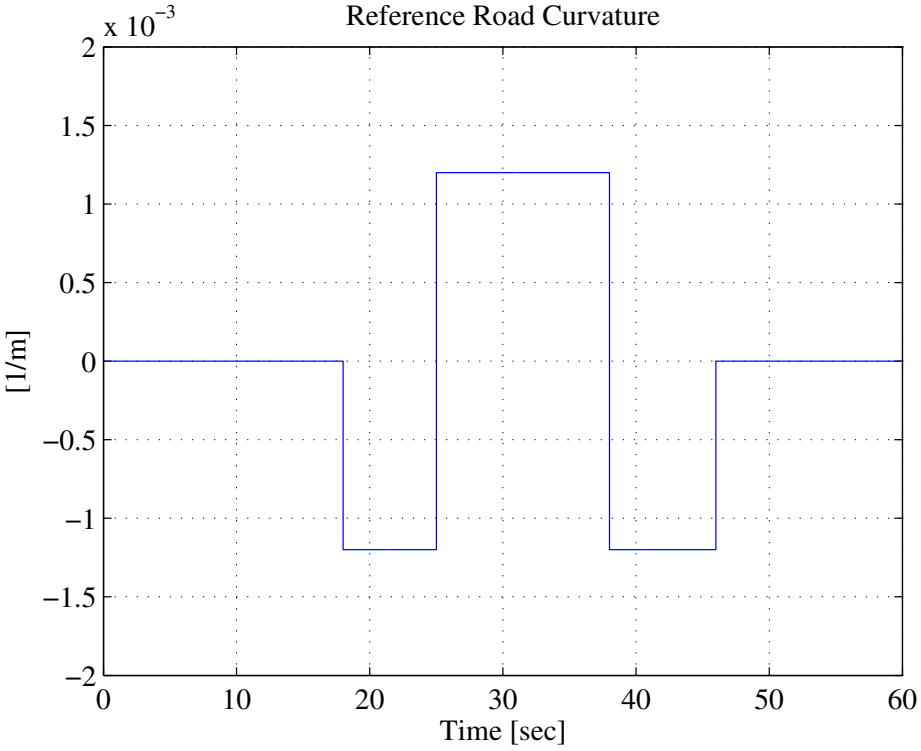

Figure 6.4 Actual road curvature of the reference track.

Table 6.2 Simulation Test Cases

Test Case	Vehicle Speed	Road Condition
1	$v = 45$ mi/h	Dry road ($\mu = 1$)
2	$v = 80$ mi/h	Dry road ($\mu = 1$)
3	$v = 45$ mi/h	Wet road ($\mu = 0.5$)
4	$v = 80$ mi/h	Wet road ($\mu = 0.5$)

Based on the mathematical representation of the vehicle models in (6.1) and (6.2), the observer is with respect to the vehicle's linear velocity and road adhesion. The observer becomes time-varying if the velocity and road adhesion are time-varying. However, the observer can be considered as time-invariant in the case that the velocity and road adhesion are constant. In this study, four cases are simulated under two different speeds and two road adhesion conditions (Table 6.2). For each simulation case, the vehicle speed and road adhesion are kept at constant values. Therefore, the observer gain can be fixed a-priori before each simulation. The realization of the observers is as follows:

1) The observer gains (L and $\underline{L}$) are properly pre-selected before each simulation case based on certain constant speed and road adhesion factor.

2) During each simulation case, the vehicle speed and road factor are kept at constant values. Then, the observer gains (L and $\underline{L}$) are fixed.

This realization method is also employed in [58].

Figure 6.5 shows the controller performance on a dry road with a speed at $v = 45\,\text{mi/h}$. The estimation results of both steering angle and road curvature are within the accuracy specifications. The RMSE value of steering angle estimation is 8.84% and the RMSE value of road curvature estimation is 9.98%. Both of these two estimates are quite accurate. The yaw rate is under an acceptable level. The lateral displacement control result has no overshoot and is well damped. This simulation result yields a very small maximum vehicle lateral displacement (steady state error is approximately $0.1\,\text{m}$), which shows an extremely accurate road tracking performance.

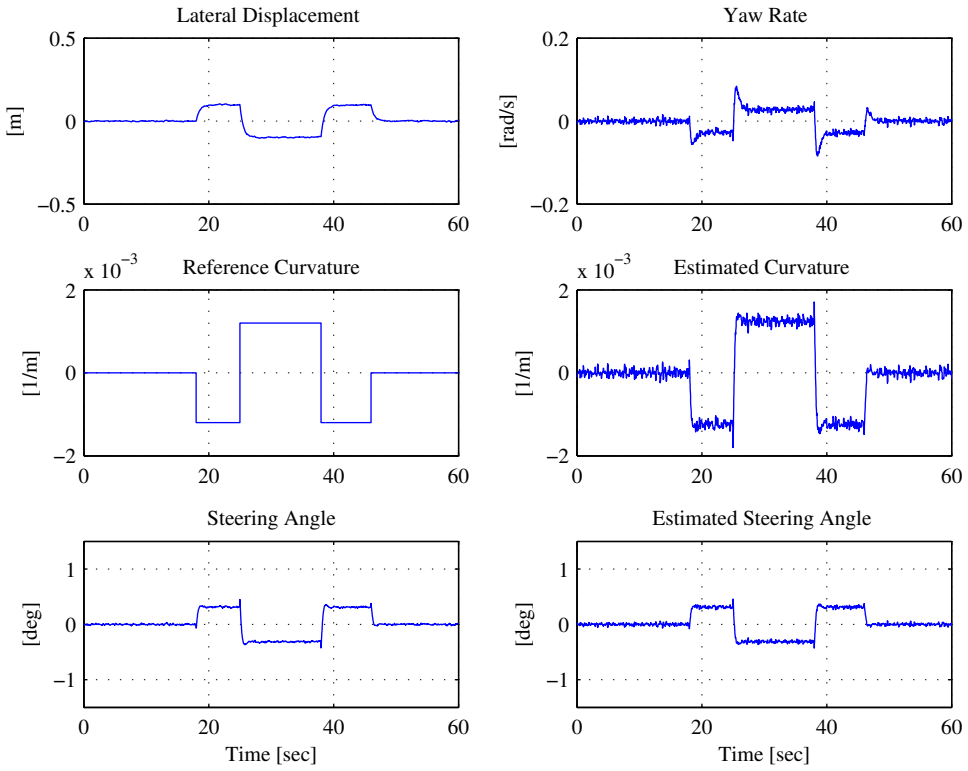

Figure 6.5 Simulation results for a speed of 45mi/h on dry road (road adhesion factor $\mu = 1$).

In order to test the performance of the control system on a highway, the simulations are implemented with a speed at $v = 80\,\text{mi/h}$. Figure 6.6 shows the controller performance on a dry road with a speed of $80\,\text{mi/h}$. The RMSE value of steering angle estimation is 9.13% and the RMSE value of road curvature estimation is 11.28%. The value of maximum lateral displacement (steady state error) for each turn is bigger that in Figure 6.5, but it is still small ($\approx 0.2\,\text{m}$). The overshoot of the yaw rate at a higher speed is larger than at a lower speed, but still at an acceptable level. This will result in an uncomfortable ride for the car passengers at each curvature transition.

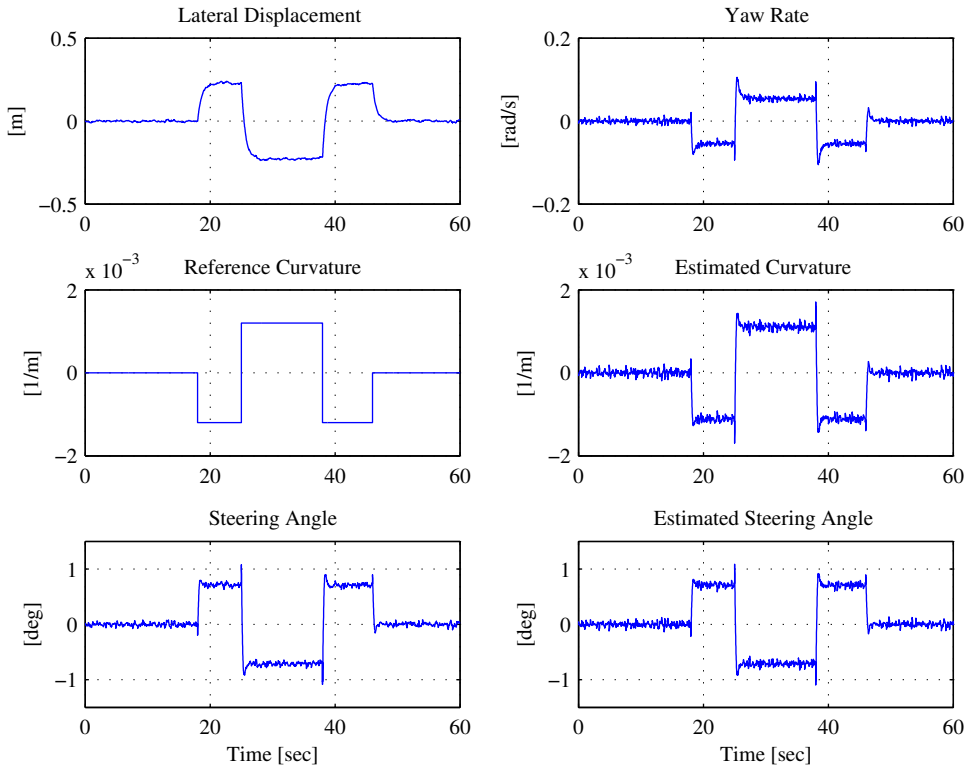

Figure 6.6 Simulation results for a speed of 80 mi/h on dry road (road adhesion factor $\mu = 1$).

To simulate a wet road (road adhesion factor is $\mu = 0.5$), all controller gains (described in Section 6.4.2) are reduced to 50% of their original values [79]. Figure 6.7 shows the simulation results for a vehicle with a speed at $v = 45\,\text{mi/h}$ on a wet road. With all controller gains halved, the lateral displacement increased accordingly compared to the result with the same speed but on a dry road as shown in Figure 6.5. The RMSE value of steering angle estimation is 10.58% and the RMSE value of road curvature estimation is 12.26%. The steady state error of lateral displacement is approximately $0.2\,\text{m}$.

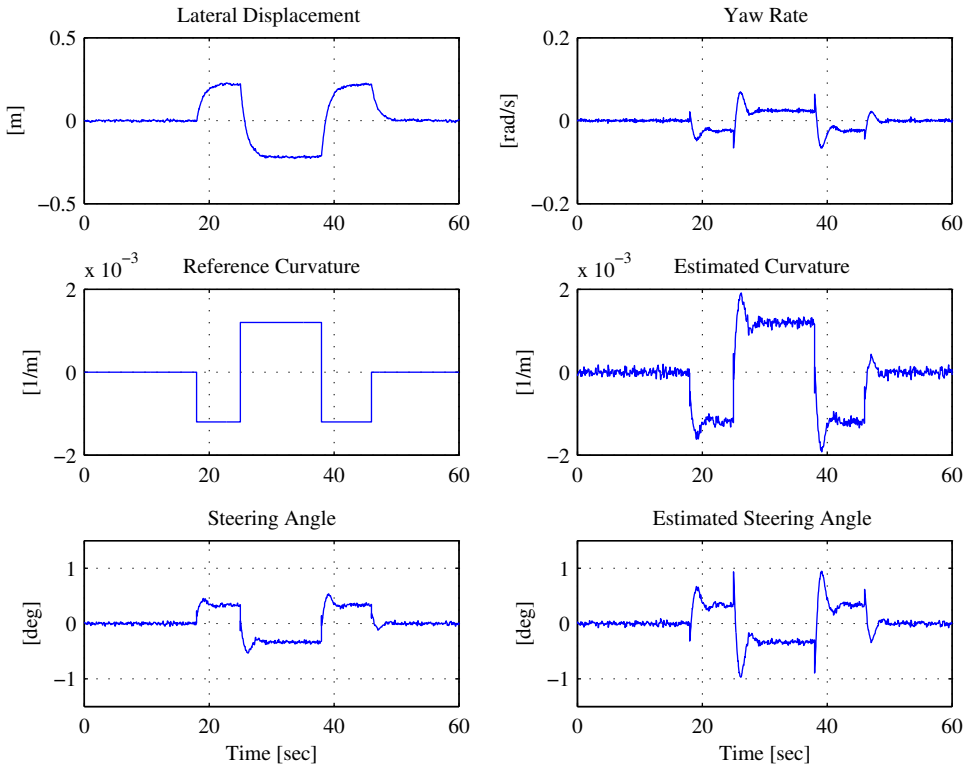

Figure 6.7 Simulation results for a speed of 45mi/h on wet road (road adhesion factor $\mu = 0.5$).

The controller performance with a highway speed at $v = 80$ mi/h on a wet road ($\mu = 0.5$) is shown in Figure 6.8. The RMSE value of steering angle estimation is 11.54% and the RMSE value of road curvature estimation is 13.37%. The steady state error of lateral displacement increases compared to those in Figure 6.6 and Figure 6.7. In this case, the yaw rate result yields a large overshoot of nearly 150% , which means it is unsafe and uncomfortable for passengers to drive on a wet road with a highway speed. This problem has been discussed in [58], in which the smooth curvature algorithm created from the off-line actual road curvature database is applied to improve the control performance. A tradeoff when applying such curvature smoothing is that the while lateral displacement

increases in over-shoot (but still at acceptable levels), and oscillations in the steering angle and yaw rate are considerably reduced in magnitude.

As mentioned before, very large sudden changes in the curvature transition are introduced into the lateral control system presented in [58]. The results, when compared to the results of [58] on the same simulation cases, clearly shown to have smaller steering angle and yaw rate overshoots. Consequently, the proposed control strategy can clearly provide more a comfortable and safer ride experience. Only for the worst case (when driving at a highway speed on a wet road), some smooth curvature algorithms to ensure the high performance need to be employed.

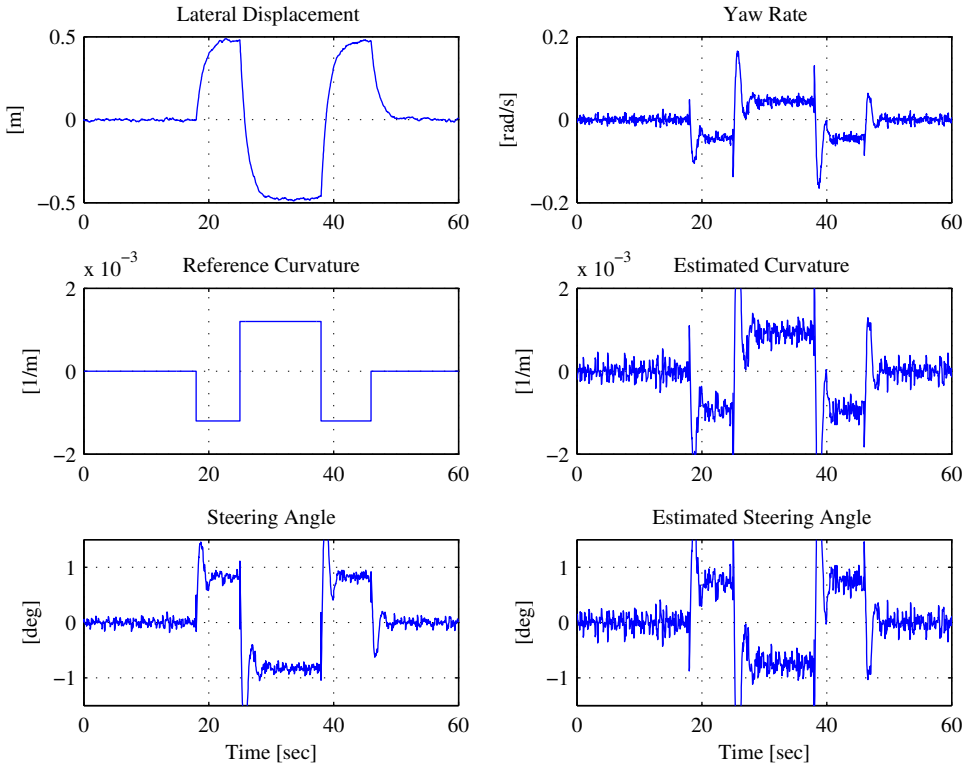

Figure 6.8 Simulation results for a speed of 80 mi/h on wet road (road adhesion factor $\mu = 0.5$).

6.6. Summary

This chapter investigates the automatic steering control for passenger vehicle. By using a GPS and a front magnetic sensor, a novel look-down reference lateral control system is developed. In such a system, accurate and real-time estimations of the steering angle, road curvature, and vehicle's front and rear lateral displacement are accomplished. The performance of the steering angle extended observer, displacement estimation module and the feedback controller is validated by simulation results. The results show that the proposed steering control system is effective enough to be used for the automated steering control both on dry and wet road under a high vehicle speed. This application could be used in advanced driver assistance systems, such as lane keeping system, path control system, collision avoidance system, and so on. This system could enhance the safety of driving.

CHAPTER 7

CONCLUSIONS AND FUTURE WORK

7.1 Conclusions

With the availability of low-cost GPS and other low cost sensors, this dissertation investigates the use of such devices to develop vehicle state estimation, driver behavior classification, and lateral control technologies which are needed in advanced driver assistance systems. Since these low cost devices can only provide limited driving information, the driver dynamics and kinemics are employed to estimate the vehicle states and the driver behaviors.

For the vehicle state estimation, a task to estimate the longitudinal tire force which can be transferred to the corresponding throttle/brake positions is addressed. A low cost 1Hz GPS receiver and a steering angle sensor are used as the vehicle data acquisition equipment. A longitude force estimation scenario is developed for the nonlinear extended two-wheel vehicle dynamic model using only the GPS information. The sideslip angle and the yaw rate are estimated and an optimization scheme is proposed to estimate the longitude tire force. The estimation results validate the proposed method by comparing with the reference longitude tire force command.

For the driver behavior classification scenario, GPS data are employed to reproduce the driver behavior. Gaussian Mixture model (GMM) is used to capture the sequence of driving characteristics according to the reconstructed vehicle's information and it is also used as a classifier to assign the driving behavior into normal or abnormal category. The nonlinear extended two-wheel vehicle dynamic model is adopted in this study. Two states,

i.e., the sideslip angle and the yaw rate are calculated, a piecewise optimization scheme is proposed to reconstruct the driving behaviors which include the steering angle and the longitude force. A GMM classifier is applied to identify whether the driver is under an abnormal driving situation. This application can enhance the safety of the drivers by warning drivers of the potentially dangerous traffic situations.

Controlling a vehicle requires the ability to measure or estimate its motion and to determine parameters such as the vehicle states and vehicle displacements. As a fundamental building block for the vehicle lateral control work, a GPS-based approach to estimate in real time the necessary states and model parameters (the steering angle, road curvature, and lateral displacements) has been developed. The control strategy used is a look-down reference system which uses a sensor at the front bumper to measure the lateral displacement and a GPS to measure the heading orientation. The road curvature estimator is designed based on the steering angle. The steering angles are estimated by using the sensor and the GPS information. The estimation algorithm employed is an observer for a new extended system model, in which the steering angle and its derivative are viewed as two state variables. Then, the lateral displacements estimation and the control algorithm are investigated. An accurate and real-time estimation of the lateral displacements with respect to the road can be accomplished in such a control system. The closed loop controller is used as a compensator to control the lateral dynamics of the vehicle. The vehicle dynamic and control system are simulated with MATLAB Simulink. The proposed estimation and control algorithms are validated by simulation results. The results show that the system provides a good and robust performance for path tracking.

7.2 Future Work

Based on the current studies, the near future work of interest would include:

1) Developing tire force estimation algorithm for four-wheel nonlinear vehicle model.

Four-wheel nonlinear vehicle model is a more accurate model since it considers both the lateral and longitudinal motions. On the one hand, the lateral tire forces are usually modeled as linear with respect to lateral sideslip angle (λ) for each axle (front and rear):

$$F_{lateral}\left(\lambda_i\right) = C_i\lambda_i, \quad i = 1, 2$$

where C_i is the wheel cornering stiffness, a parameter closely related to the tire-road friction. Therefore, effective algorithms for estimating cornering stiffness need to be developed. On the other hand, the longitudinal tire force for four-wheel nonlinear model is determined by longitudinal motion (sideslip angle, velocity and acceleration). The vehicle longitudinal motion is related to the vehicle dynamics and kinematics. The algorithm presented in this dissertation for the four-wheel model should be further considered.

2) Developing driver state detection algorithm for the proposed GMM classification method.

In this dissertation, the GMM classifier for abnormal driver behavior is investigated. However, driver state (distraction or fatigue) is difficult to assess and detect by using the driver inputs features. More driver data and features should be extracted to detect the driver's state. For instance, the distractions that are linked to the eye movements and biological signals, such as ECG or EOG, are good indicator of fatigue. Future study can include the driver's state analysis into the proposed GMM scenario.

3) Designing smooth algorithms for lateral control system.

Since the lateral control system proposed in this study is based on estimated road curvature, the sudden changes in curvature transition on the road will result in undesirable levels of fluctuations in the lateral acceleration and the yaw rate. This will result in a poor riding comfort to the passengers in the car. A smoothing algorithm could be used to decrease their overshoots by providing smoother curvature changes. In the future, a corresponding smoothing algorithm can be introduced into the control loop.

REFERENCES

1. "Our Nation's Highways," *U.S. Department of Transportation, Federal Highway Administration*, FHWA-PL-10-023, 2010.

2. J. Wang, R. Knipling, and M. J. Goodman. "The role of driver inattention in crashes: New statistics from the 1995 crashworthiness data system (CDS)," *the 40th Annual Proceedings: Association for the Advancement of Automotive Medicine,* 1995.

3. "Early Estimate of Motor Vehicle Traffic Fatalities for The First Half (January-June) of 2010," *U.S. Department of Transportation, National Highway Traffic Safety Administration (NHTSA)*, DOT HS 811 403, September 2010.

4. "Motor Vehicle Traffic Crashes As a Leading Cause of Death in the United States 2005," *U.S. Department of Transportation, National Highway Traffic Safety Administration (NHTSA)*, DOT HS 810 936, April 2008.

5. H. Lum and J. A. Reagan, "Interactive Highway Safety Design Model: Accident Predictive Module," *Public Roads Magazine*.

6. "Road Casualties Great Britain," *UK Department for Transport*. April 13, 2008.

7. J. D., Lee, "Driving safety," *In R. S. Nickerson (Ed.), Review of Human Factors*. Santa Monica, CA: Human Factors and Ergonomics Society.

8. [Online]. Available: www.en.wikipedia.org/wiki/Traffic_collision, 2012.

9. K., Ball, and C. Owsley, "The useful field of view test: A new technique for evaluating age-related declines in visual function," *Journal of the American Optometric Association*, 64, 71-79, 1993.

10. C. Owsley, K. Ball, G. McGwin, M. E. Sloane, D. L. Roenker, and M. F., White, "Visual processing impairment and risk of motor vehicle crash among older adults," *Journal of the American Medical Association*, 279(14), 1083-1088, 1998.

11. T. A. Ranney, "Driver Distraction: A Review of the Current State-of-Knowledge," *U.S. Department of Transportation, National Highway Traffic Safety Administration (NHTSA)*, DOT HS 810 704, 2008.

12. "Advanced Driver Assistance System (ADAS): Vehicle Control for the Future," *IMechE (Institution of Mechanical Engineers)*, December 1999.

13. G. Baffet, A. Charara, and D. Lechner, "Estimation of vehicle sideslip, tire force and wheel cornering stiffness," *Control Engineering Practice*, Vol 17, Issue 11, pp 1255-1264, 2009.

14. D. DeWaard, "The measurement of drivers' mental workload," *PhD thesis*, University of Gronigen, Haren, The Netherlands, 1996.

15. G. Baffet, J. Stephant, and A. Gharara, "Experimental evaluation of tire-road forces and sideslip angle observers," *Proceedings of the IEEE European Control Conference*, ECC, Kos, Greece, 2007.

16. J. Ryu, "State and Parameter Estimation for Vehicle Dynamics Using GPS," *PhD thesis*, Stanford University, 2004.

17. C. Sierra, E. Tseng, A. Jain and H. Peng, "Cornering Stiffness Estimation Based on Vehicle Lateral Dynamics," *Vehicle System Dynamics*, 44:1:24–38, 2006.

18. R. Daily, W. Travis, and D. M. Bevly, "The Use of GPS Tire Parameter Estimates in a Model Based Estimator," *International Journal of Vehicle Autonomous Vehicles*, 2006.

19. J. Hahn, R. Rajamani, and Alexander, "GPS-Based Real-Time Identification of Tire-Road Friction Coefficient," *IEEE Transaction on Control Systems Technology*, vol. 10, no. 3, pp. 331-343, 2002.

20. D. Edwards, "A Method to Estimate Critical Tire Properties Using Non-Linear Tire Models," *In Proceedings of IMECE*, 2007.

21. V. Zanten, "Bosch ESP Systems: 5 Years of Experience," *SAE Technical Paper* 2000-01-1633, 2000.

22. A. Hac and E. Bedner, "Robustness of Side Slip Angle and Control Algorithms for Vehicle Chassis Control," *ESV Conference, paper* No. 07-0353, 2007.

23. K. Koibuchi, M. Yamamoto, Y. Fukuda, and S. Inagaki, "Vehicle Stability Control in Limit Cornering by Active Brake," *SAE Technical Paper* 960487, 1996.

24. Y. Fukada, "Slip-angle estimation for vehicle stability control," *Vehicle System Dynamics*, 32(4):375–388, 1999.

25. A. Nishio, "Development of vehicle stability control system based on vehicle sideslip angle estimation," *SAE Paper* No. 2001-01-0137, 2001.

26. J. Farrelly, and P. Wellstead, "Estimation of vehicle lateral velocity," *In Proceedings of IEEE Conference on Control Applications*, pages 552–557, Dearborn, MI, 1996.

27. H. Tseng, "Development of vehicle stability control at Ford," *IEEE/ASME Transactions on Mechatronics*, 4(3):223–234, 1999.

28. M. Pettitt, G. Burnett, and A. Stevens, "Defining driver distraction," *World Congress on Intelligent Transport Systems*, San Francisco, CA, 2005.

29. T. A. Ranney, "Driver Distraction: A Review of the Current State-of-Knowledge," *U.S. Department of Transportation, Federal Highway Administration (NHTSA)*, DOT HS 810 704, 2008.

30. I. Trezise, E. G. Stoney, B. Bishop, J. Eren, A. Harkness, C. Langdon, and T. Mulder, "Report of the road safety committee on the inquiry into driver distraction," *Rep. No. 209. Melbourne, Victoria, Australia: Road Safety Committee, Parliament of Victoria*, 2006.

31. M. Pettitt, G. Burnett, and A. Stevens, "Defining driver distraction," *World Congress on Intelligent Transport Systems*, San Francisco, CA, 2005.

32. B. Wallace, "External-to-vehicle driver distraction: Research findings," *Rep. No. 168. Edinburgh, Scotland: Scottish Executive*, 2003.

33. "Overview of the National Highway Traffic Safety Administration's Driver Distraction Program," *U.S. Department of Transportation, Federal Highway Administration (NHTSA)*.

34. G. J. Witt, "SAfety VEhicle(s) using adaptive Interface Technology (SAVE-IT) Program," *U.S. Department of Transportation, Federal Highway Administration (NHTSA)*, 2003.

35. B. Donmez, L. Boyle, and J. D. Lee, "Taxonomy of mitigation strategies for driver distraction," *In Human Factors and Ergonomics Society 47th Annual Meeting,* Santa Monica, CA: Human Factors and Ergonomics Society. pp. 1865-1869, 2003.

36. Y. Liang, "Detecting Driver Distraction," *PhD Thesis*, The University of Iowa, 2009.

37. E. L. Waltz, "Information understanding: integrating data fusion and data mining processes," *Proceedings of the 1998 IEEE International Symposium on Circuits and Systems*, ISCAS '98. , Monterey, CA, 1998.

38. C. D. Wickens, "Multiple resources and performance prediction," *Theoretical Issues in Ergonomics Science*, 3(2), 159-177, 2002.

39. D. D. Salvucci, and K. L. Macuga, "Predicting the effects of cellular-phone dialing on driving performance," Congitive Systems Research, 3, 95-102, 2002.

40. T. B. Sheridan, "Driver distraction from a control theory perspective," *Human Factors*, 46(4), 587-599, 2004.

41. B. Donmez, L. N. Boyle, J. D. Lee, and G. Scott, "Assessing differences in young drivers' engagement in distractions," *the Transportation Research Board 85th Annual Meeting*, Washington DC, 2006.

42. H. Zhang, M. R. H. Smith, and G. J. Witt, "Identification of real-time diagnostic measures of visual distraction with an automatic eye-tracking system," *Human Factors*, 48(4), 805-821, 2006.

43. J. Engström, and S. Mardh, "SafeTE final report: Vägverket," 2007.

44. Y. Zhang, Y. Owechko, and J. Zhang, "Driver cognitive workload estimation: a data-driven perspective," *the IEEE Intelligent Transportation Systems Conference*, Washington, D.C., USA, 2004.

45. Y. Liang, and J. D. Lee, "Comparing Support Vector Machines (SVMs) and Bayesian Networks (BNs) in detecting driver cognitive distraction using eye movements," *In R. Hammoud (Ed.), Passive eye monitoring: Algorithms, applications and experiments*. Leipzig, Germany: Springer-Verlag Berlin Heidelberg. pp. 285-300, 2008.

46. Y. Liang, J. D. Lee, and M. L. Reyes, "Non-intrusive detection of driver cognitive distraction in real-time using Bayesian networks," *Transportation Research Record: Journal of the Transportation Research Board (TRR),* 2018, 1-8, 2007.

47. Y. Liang, M. L. Reyes, and J. D. Lee, "Real-time detection of driver cognitive distraction using Support Vector Machines," *IEEE Transactions on Intelligent Transportation Systems,* 8(2), 340-350, 2007.

48. J. Lee, M. Reyes, Y. Liang and Y. Lee, "SAfety VEhicles using adaptive interface Technology (Task 5) Final Report: Phase 2 Algorithms to Assess Cognitive Distraction," *U.S. Department of Transportation*, 2007.

49. N. Oliver, and E. Horvitz, "A comparison of HMMs and dynamic Bayesian networks for recognizing office activities," *In Lecture Notes in Computer Science,* Springer Berlin / Heidelberg, Vol. 3538/2005, pp. 199-209, 2005.

50. S. Fan, C. X. Mao, J. D. Zhang, and L. N. Chen, "Forecasting electricity demand by hybrid machine learning model," *Neural Information Processing, Pt 2, Proceedings,* Vol. 4233, pp. 952-963, 2006.

51. J. Rillings, "The National Automated Highway System: Cooperative Program. National Automated Highway System Consortium," *U.S. Department of Transportation*, 1997.

52. J. Hernandez and C. Kuo, "Steering control of automated vehicles using absolute positioning GPS and magnetic markers," *IEEE Trans. Vehicular Technology*, vol. 52, pp. 150-160, 2003.

53. C. Chen, J. Culdner, I. Kanellakopoulos, and M. Tomizuka, "Nonlinear damping in vehicle lateral control: Theory and experiment," *in Proc. American Control Conf.,* Philadelphia, PA, pp. 2243-2247, 1998.

54. S. Patwardhan, S. Tan, and J. Guldner, "A general framework for automatic steering control: System analysis," *in Proc. American Control Conf.,*Albuquerque, NM, pp. 257-280, 1997.

55. J. Guldner, S. Tan, and S. Patwardhan, "On fundamental issues of vehicle steering control for highway automation," *California PATH res. Rep., Univ. California, Berkeley, CA*, UCB-ITS-PRR-98-28, 1998.

56. M. Maurer, "VaMoRs-P: An advanced platform for visual autonomous road vehicle guidance," *in Proc. SPIE Conf. Mobile Robots IX,* Boston, MA, pp. 239-248, 1994.

57. M. Tomizuka, "Vehicle Lateral Control for Automated Highway Systems," *Presentation for PATH@Twenty*, 2006.

58. J. Hernandez and C. Kuo, "Steering control of automated vehicles using absolute positioning GPS and magnetic markers," *IEEE Trans. Vehicular Technology*, vol. 52, pp. 150-160, 2003.

59. M. Irmascher and M. Ehmann, "Driver classification using ve-Dyna advanced driver," *Society of Automotive Engineers (SAE)*, 2004.

60. W. F. Milliken, and D. L., Milliken, "*Race Car Vehicle Dynamics*," SAE International, 1995.

61. E. Freund, and R. Mayr, "Nonlinear path control in automated vehicle guidance," *IEEE Transactions on Robotics and Automation*, vol. 13, pp. 49-60, 1997.

62. E. J. Rossetter, and J. C. Gerdes, "A Study of Lateral Vehicle Control Under a 'Virtual' Force Framework," *In the proceedings of the 2002 International Symposium on Advanced Vehicle Control*, Hiroshima, Japan, 2002.

63. "Vehicle Safety Communications Project, Task 3 Final Report: Identify Intelligent Vehicle Safety Applications Enabled by DSRC," National Highway Traffic Safety Administration, Ed., March, 2005.

64. A. A. Carter, "The status of vehicle-to-vehicle communications as a means of improving crash prevention performance," National Highway Traffic Safety Administration, Ed.

65. Q. Xu, T. Mak, J. Ko and R. Sengupta, "Vehicle-to-vehicle safety messaging in DSRC," in Proceedings of the 1st ACM international workshop on Vehicular ad hoc networks, ACM, 2004.

66. H. F. Grip, L. Imsland, T. A. Johansen, J. C. Kalkkuhl, and A. Suissa, "Vehicle sideslip estimation," Control Systems Magazine, IEEE, vol. 29, pp. 36-52, 2009.

67. L. R. Ray, "Nonlinear state and tire force estimation for advanced vehicle control," Control Systems Technology, IEEE Transactions on, vol. 3, pp. 117-124, 1995.

68. M. S., Grewal and A. P. Andrews, *Kalman Filtering Theory and Practice*. Upper Saddle River, NJ: Prentice Hall, 1993.

69. J. D. Schutter, J. D. Geeter, T. Lefebvre and H. Bruyninckx, "Kalman Filters: A Tutorial," Technical report, 1999.

70. D. Titterington, A. Smith and U. Makov, "*Statistical Analysis of Finite Mixture Distributions*," John Wiley and Sons, 1985.

71. G. J. McLachlan and D. Peel, *Finite Mixture Models*, Wiley, 2000.

72. D. A. Reynolds, T. F. Quatieri, and R. B. Dunn, "Speaker verification using adapted Gaussian Mixture Models," *Digital Signal Processing*, vol. 10, pp 19–41, 2000.

73. F. Cardinaux, C. Cardinaux, and S. Marcel, "Comparison of MLP and GMM Classifiers for Face Verification on XM2VTS," *Springer-Verlag GmbH*, 2688, pp. 911-920, 2003.

74. R. O. Duda and P. E. Hart, Pattern Classification and Sceneanalysis. *John Wiley and Sons, Inc.* 1973.

75. P. Dempster, N. M. Laird and D. B. Rubin, "Maximum likelihood from incomplete data using the EM algorithm," *Journal of the Royal Society of Statistics*, vol. 39(1): pp. 1–38, 1977.

76. L. T. Lam, "Distraction and the risk of car crash injury: the effect of drivers' age," J. Saf. Res., 33, pp. 411-419, 2002.

77. P. Angkititrakul, D. Kwak, S. Choi, J. Kim, A. PhucPhan, A. Sathyanarayana and J. H. L. Hansen, "Getting Start with UTDrive: Driver-Behavior Modeling and Assessment of Distraction for In-Vehicle Speech Systems," *Interspeech*, 2007.

78. P. Green, "Driver Distraction, Telematics Design, and Workload Managers: Safety Issues and Solutions," SAE International, paper number: 2004-21-0022, 2004.

79. J. Guldner, W. Sienel, H. S. Tan, J. Ackermann, S. Patwardhan, and T. Bunte, "Robust automatic steering control for look-down reference systems with front and rear sensors," *IEEE Trans. Contr. Syst. Techno.,* vol. 7, pp. 2-11, 1999.

80. P. Mellodge, "*Feedback control for path following robotics car*," *Thesis*, Virginia Tech, 2002.

81. B. Ake, "*Numerical methods for least squares problems*," Philadelphia: SIAM, 1996.

82. J. B. Burl, "*Linear Optimal control*," Addison Wesley Longman edition, 1999.

83. Wikipedia: Geographic Distance. Web source: http://en.wikipedia.org/wiki/ Geographical_distance, 2012.

84. P. Dempster, N. M. Laird, and D. B. Rubin, "Maximum likelihood from incomplete data using the EM algorithm," *Journal of the Royal Society of Statistics*, vol. 39(1): pp. 1–38, 1977.

85. D. Karimi and D. D. Mann, "Role of visual cues from the environment in driving an agricultural vehicle," *The Ergonomics Open Journal*, pp. 54-61, 2008.

86. Y. Huang, K. B. Englehart, B. Hudgins, A. D. C. Chan, "Optimized Gaussian Mixture Model for Upper Limb Motion Classification," *Proceeding of the 26th Annual International Conference of the IEEE EMBS*, San Francisco, CA, USA, 2004.

87. Wikipedia : Root mean square, Web source : http://en.wikipedia.org/wiki/ Root_mean_square, 2012.

88. C. Ahlstrom and K. Kircher, "Review of Real-time Visual Driver Distraction Detection Algorithms," *Proceeding of Measuring Behavior*, 2010.

89. O. Nakayama, T. Futami, and T. Nakamura, "Development of a steering entropy method for evaluating driver workload," *SAE International*, 1999.

90. B. Donmez, L. N. Boyle, J. D. Lee, and G. Scott, "Assessing differences in young driver's engagement in distractions," *The Transportation Research Board 85th Annual Meeting*, Washington DC, 2006.

91. H. Zhang, M. R. H. Smith, and G. J. Witt, "Identification of real-time diagnostic measures of visual distraction with and automatic eye-tracking system," Human Factors, 48 (4), 805-821, 2006.

92. D. Karimi and D. D. Mann, "Role of visual cues from the environment in driving an agricultural vehicle," *The Ergonomics Open Journal*, pp. 54-61, 2008.

93. Y. Huang, K. B. Englehart, B. Hudgins, A. D. C. Chan, "Optimized Gaussian Mixture Model for Upper Limb Motion Classification," *Proceeding of the 26th Annual International Conference of the IEEE EMBS*, San Francisco, CA, USA, pp. 72-75, Sept. 2004.

94. P. Green, "Driver Distraction, Telematics Design, and Workload Managers: Safety Issues and Solutions," SAE International, paper number : 2004-21-0022, 2004.

95. [Online]. Available: www.seeingmachines.com/product/facelab/, 2012.

96. T. A. Ranney, "Driver Distraction: A Review of the Current State-of-Knowledge," *U.S. Department of Transportation, National Highway Traffic Safety Administration (NHTSA)*, DOT HS 810 704, Apr. 2008.

97. B. Zylstra, O. Tsimhoni, P. Green, and K. Mayer, "SAfety VEhicles using Adaptive Interface Technology (Task 3B): Driving Performance for Dialing, Radio, Tuning, and Destination Entry while Driving Straight Roads," *U.S. Department of Transportation, National Highway Traffic Safety Administration (NHTSA)*, 2004

98. H. Zhang, M. Smith, and R. Dufour, "A final report of SAFety Vehicles using adaptive interface technology (Phase II: Task 7C): Visual Distraction," *U.S. Department of Transportation, Federal Highway Administration (NHTSA)*, 2008

99. Y. Dong, Z. Hu, K. Uchimura, and N. Murayama, "Driver Inattention Monitoring System for Intelligent Vehicles: A Review," *IEEE Trans. Intelligent Transportation Systems*, vol 12, no. 2, pp. 596-614, Jun. 2011.

100. O. M. J. Carsten and K. Brookhuis, "Issues arising from the haste experiments," *Transp. Res. Part F: Traffic Psychol. Behavior*, vol. 8, no. 2, pp 191- 196, 2005.

101. T. W. Victor, "Keeping eye and mind on the road," in Dept of Psychology. *Digital Comprehensive Summaries of Uppsala Dissertation from the Faculty of Social Sciences*, Uppsala University: Uppsala, 2005.

102. L. Fletcher, and A. Zelinsky, "Driver State monitoring to mitigate distraction," *International Conference on Driver Distraction*. Sydney, Australia, 2005.

103. K. Kircher, and C. Ahlstrom, "Issues related to the driver distraction detection algorithm," *1st International Conference on Driver Distraction*, Sydney, Australia, Sept. 2009.

104. B. Donmez, L. N. Boyle, and J. D. Lee, "Safety implications of providing real-time feedback to distracted drivers," *Accident Analysis and Prevention*, 39, 3. pp. 581-590. 2007.

105. H. Zhang and M. Smith, "Safety Vehicles using adaptive Interface Technology (Task 7): A Literature Review of Visual Distraction Research," *The National Highway Traffic Safety Administration (NHTSA),*2004

106. "Overview of the National Highway Traffic Safety Administration's Driver Distraction Program," *U.S. Department of Transportation, Federal Highway Administration (NHTSA).*

107. J. L. Harbluk, Y. I. Noy, P. L. Trbovich, and M. Eizenman, "An on-road assessment of cognitive distraction: Impacts on driver's visual behavior and braking performance," *Accid, Anal. Prev*., vol. 39, no. 2, pp. 372-379, Mar. 2007.

108. E. M. Rantanen and J., Goldberg, "The effect of mental workload on the visual filed size and shape," Ergonomics, vol. 2, no. 6, pp. 816-834, 1999.

109. M. Miyaji, H. Kawanaka, and K. Oguri, "Driver's cognitive distraction detection using physiological features by the AdaBoost," *in Proc. 12th Int. IEEE Conf. Intell. Transp. Syst*. pp 1-6, St. Louis, Missouri, Oct. 2009.

110. M. C. Su, C. Y. Hsiung, and D. Y. Huang, "A simple approach to implementing a system for monitoring driver inattention," *in Proc. IEEE Int. Conf. Syst., Man, Cybern.*, vol. 1, pp 429-433, Taipei, Taiwan, 2006.

111. [Film]: A. Singer, The future of augmented cognition, DARPA, 2005

112. M. Itoh, "Individual differences in effects of secondary cognitive activity during driving on temperature at the nose tip," *in Proc. IEEE Int. Conf. Mechatronics Autom.*, pp. 7-11, Jinlin, China, Aug. 2009.

113. A. Wesley, D. Shastri, and I. Pavlidis, "A novel method to monitor driver's distractions," *in Proc. CHI*, pp. 4273-4278, 2010.

114. K. Kircher, A. Kircher, and F. Claezon, "Distraction and drowsiness," *A field study, VTI: Linkoping*, 2009.

115. B. Donmez, L. N. Boyle, and J. D. Lee, *Designing feedback to mitigate distraction, in Driver Distraction: Theory, effects and mitigation*, CRC Press London, 2009.

116. R. S. Michalski, J. G. Carboell, and T. M. Mitchell, *Machine Learning: An Artificial Intelligence Approach*, Morgan Kaufmann Publishers, Inc. 1985.

117. A. Sathyanarayana, S, Nageswaren, H. Ghasemzadeh, R. Jafari, and J. H. L. Hansen, "Body sensor networks for driver distraction identification," *IEEE International Conference on Vehicular Electronics and Safety (ICVES)*, pp. 120-125, Columbus, OH, Sept. 2008.

118. Y. Liang, and J. D. Lee, "Comparing Support Vector Machines (SVMs) and Bayesian Networks (BNs) in detecting driver cognitive distraction using eye movements," *In R. Hammoud (Ed.), Passive eye monitoring: Algorithms, applications and experiments*. Leipzig, Germany: Springer-Verlag Berlin Heidelberg. pp. 285-300, 2008.

119. Y. Liang, J. D. Lee, and M. L. Reyes, "Non-intrusive detection of driver cognitive distraction in real-time using Bayesian networks," *Transportation Research Record: Journal of the Transportation Research Board (TRR)*, 2018, 1-8. 2007.

120. Y. Zhang, Y. Owechko, and J. Zhang, "Driver cognitive workload estimation: a data-driven perspective," *IEEE Intelligent Transportation Systems Conference*, Washington, D.C., USA. October 2004.

121. V. N. Vapnik, *The nature of statistical learning theory*, New York: Springer, 1995.

122. S. Amari, and S. Wu, "Improving support vector machine classifiers by modifying kernel function," *Neural Networks*, vol 12, pp. 783-789, 1999.

123. H. Byun, and S. W. Lee, "Applications of support vector machines for pattern recognition: A survey," *the Pattern Recognition with Support Vector Machines: First International Worksho*p, pp 213-236, Niagara Falls, Canada, August, 2002

124. Y. Liang, M. L. Reyes, and J. D. Lee, "Real-time detection of driver cognitive distraction using Support Vector Machines," *IEEE Trans. on Intelligent Transportation Systems*, vol. 8, no. 2, pp. 340-350, 2007.

125. G. Weller and B. Schlag, "A robust method to detect driver distraction," *in Proceeding of European Conference Human Centred Design for Intelligent Transport. Systems*, pp 279-288, Berlin, Germany, 2010.

126. D. Waard, K. A. Brookhuis, and N. Hernandez-Gress, "The feasibility of detecting phone-use related driver distraction," *International Journal of Vehicle Design,* vol. 26, no.1, pp. 85-95, 2001.

127. M. Wollmer, C. Blaschke, T. Schindl, B. Schuller, B. Farber, S. Mayer, and B. Trefflich "Online Driver Distraction Detection Using Long Short-Term Memory," *Intelligent Transportation Systems, IEEE Transactions on* , vol.12, no.2, pp.574-582, Jun. 2011.

128. Y. Freund and R. E. Schapire, "A decision-theoretic generalization of online learning and an application to boosting," *J. Comput. Syst. Sci,,* vol. 55, no. 1, pp. 119-139, 1997.

129. Y. Freund and R. E. Schapire, "A short introduction to boosting," *Journal of Japanese Society for Artificial Intelligence*, 14(5): 771-780, 1999.

130. A. Sathyanarayana, P. Royraz, and J. H. Hansen, "Driver behavior analysis and route recognition by hidden Markov models," *in Proc. IEEE Int. Conf. Veh. Electron. Safety,* pp. 267-281, Columbus, OH, 2008.

131. W. Stevens, "The automated highway system program: A progress report," *13th IFAC World Congr,*, San Francisco, pp. 25-34, 1996.

132. S. Tsugawa, M. Aoki, A. Hosaka, and K. Seki, "A survey of present IVHS activities in Japan," in *13th IFAC World Congr,*, San Francisco, CA, pp. 147-152, 1996.

133. Q. T. Luong, J. Weber, D. Koller, and J. Malik, "An integrated stereobased approach to automatic vehicle guidance," in *Proc. 5th ICCV*, Jun. 1995.

134. S. E. Shladover, "PATH at 20-History and Major Milestones," *IEEE Trans. Intell. Transp. Syst.*, vol.8, no.4, pp.584-592, Dec. 2007.

135. B. Ulmer, "VITA - An autonomous road vehicle (ARV) for collision avoidance in traffic," in *Proc. Intell. Veh*, Detroit, pp. 36-41, 1992.

136. B. Ulmer, "VITA II – Active collision avoidance in real traffic," in *Proc. Intell. Veh.'94*, Paris, France, pp. 1-6, 1994.

137. T. Jochem, D. Pomerleau, B. Kumar, and J. Armstrong, "PANS: A portable navigation platform," *in Proc. Intell. Veh. Symp.*, Detroit, MI, pp. 107-112, 1995.

138. W. Zhang and R.E.Parsons, "An intelligent roadway reference system for vehicle lateral guidance/control," in Proc. Amer. Contro. Conf., San Diego, CA, pp. 281-286, 1990.

139. R. E. Fenton, G.C. Melocik, and K. W. Olson, "On the steering of automated vehicles: Theory and experiment," *IEEE Trans. Contr. Syst. Technol.*, vol. 5, pp. 127-134, 1997.

140. S. Choi, J. Kim, and D. Kwak, "Analysis and Classification of Driver Behavior using In-Vehicle CAN-Bus Information," *Biennial Workshop on DSP for In-Vehicle and Mobile Systems*, Istanbul, Turkey, June 17-19, 2007 .

141. C. Miyajima, Y. Nishiwaki, K. Ozawa, T. Wakita, K. Itou, K. Takeda, F. Itakura, "Driver Modeling Based on Driving Behavior and Its Evaluation in Driver Identification," *Proceedings of the IEEE* , vol.95, no.2, pp.427-437, Feb. 2007.

142. S. K. Benli, R. Duzagac and M. T. Eskill, "Driver recognition using Gaussian Mixture Models and decision fusion techniques," *Advances in Computation and Intelligence, Lecture Notes in Computer Science*, vol. 5370, pp. 803-811, 2008.